This is a preprint, the final version is subject to change, of the American Mineralogist (MSA)
Cite as Authors (Year) Title. American Mineralogist, in press.
(DOI will not work until issue is live.) DOI: http://dx.doi.org/10.2138/am-2017-5746

Hydroxyl, Cl, and F Partitioning Between High-Silica Rhyolitic Melts-Apatite-Fluid(s) at 50-200 MPa and 700-1000 °C

REVISION 2

JAMES D. WEBSTER[1], BETH A. GOLDOFF[1], RYAN N. FLESCH[2], PATRICIA A. NADEAU[3], ZACHARY W. SILBERT[4]

[1]Department of Earth and Planetary Sciences
American Museum of Natural History
Central Park West at 79th Street
New York, NY 10024-5192, USA

[2]Department of Geology
College of William and Mary
P.O. Box 8795
Williamsburg, VA 23187-8795, USA

[3]Department of Geological Sciences
Salem State University
352 Lafayette Street
Salem, MA 01970 USA

[4]2 Sutton Place
Ossining NY 10562, USA

Submitted to the **American Mineralogist** February 29, 2016

First revised version resubmitted July 5, 2016 and second revised version on 21 July 2016

Always consult and cite the final, published document. See http:/www.minsocam.org or GeoscienceWorld

This is a preprint, the final version is subject to change, of the American Mineralogist (MSA)
Cite as Authors (Year) Title. American Mineralogist, in press.
(DOI will not work until issue is live.) DOI: http://dx.doi.org/10.2138/am-2017-5746

ABSTRACT

Hydrothermal experiments were conducted with fluid- and apatite-saturated, high-silica rhyolitic melts at ca. 700 – 1000 °C and 50 and 200 MPa to determine the distribution of H_2O/OH, Cl, and F between melt, apatite, aqueous vapor, brine, or vapor plus brine. One to three micron-diameter seed grains of fluorapatite were added to starting charges to serve as apatite nucleation sites. $CaHPO_4$ and $Ca(OH)_2$ were used to stimulate apatite crystallization, and temperature was cycled daily, ± 10 to ± 15 ˚C, to promote growth of relatively equant apatite crystals large enough for electron probe microanalysis (EPMA). The experiments were conducted with gold capsules and run in cold-seal pressure vessels on a hydrothermal line and an internally heated gas pressure vessel for durations of 165 to 1149 hours.

The run-product glasses were analyzed by EPMA and Fourier Transform Infrared Spectroscopy, apatites by EPMA, and most fluid phases by chloridometer; Cl contents of fluids were also estimated by mass balance calculations. The fluids contained 0.3 to 39 wt% Cl at run conditions. Most experiments were conducted at 50 MPa, and these glasses contain 0.02 to 0.42 wt% Cl, 1.8 to 3.1 wt% H_2O, and 0.01 to 0.19 wt% F. The molar (Al_2O_3/CaO+Na_2O+K_2O = A/CNK) and molar (Na_2O/Na_2O+K_2O = N/NK) ratios of the 50 MPa glasses range from 0.88 to 1.04 and 0.48 to 0.68, respectively, and straddle the A/CNK and N/NK of the starting glass (0.99 and 0.59, respectively). The measured wt% Cl and F in the 50-MPa apatites range from 0.14 to 3.8 (X_{Cl}^{apat} of 0.02 to 0.56) and 0.32 to 2.4 (X_F^{apat} of 0.08 to 0.63), respectively. Stoichiometrically constrained X_{OH}^{apat} ranges from 0.14 to 0.7.

Partition and exchange coefficients were determined for OH, Cl, and F distribution between apatite and melt ± fluids. The distribution of these volatile components varies with pressure and melt and apatite compositions. The exchange of F and Cl between apatite and

Always consult and cite the final, published document. See http:/www.minsocam.org or GeoscienceWorld

This is a preprint, the final version is subject to change, of the American Mineralogist (MSA)
Cite as Authors (Year) Title. American Mineralogist, in press.
(DOI will not work until issue is live.) DOI: http://dx.doi.org/10.2138/am-2017-5746

melt, for example, fluctuates with the Si, P, Mg, Na, Ce, Fe, and S ± Ca contents of the apatite and with the molar A/CNK and N/NK ratios of the melts. Water and hydroxyl exchange between experimental apatite and melt was also investigated. It is determined empirically that the: $(X_{H2O}^{melt}/X_{Cl}^{melt}) = ((-19.66) + (39.13)*(X_{OH}^{apat})/(X_{Cl}^{apat}))$ for felsic melts at 50 to 200 MPa, having molar A/CNK ratios between 0.88 and 1.1, N/NK ratios > 0.55, and containing ca. 2 - 6 wt% H_2O. The apatites are characterized by per formula unit (6 > Si/Mg > 0.3). We test this relationship by comparing H_2O contents measured in melt inclusions from Augustine volcano, Alaska, with calculated H_2O concentrations of apatites from 9 samples from 7 of its felsic eruptive units. The results for both approaches are consistent within precision for 6 of the samples.

The empirical volatile exchange relationships determined for melt-apatite, melt-fluid, and apatite-fluid pairs are applicable to a variety of magmatic systems. One implication of this study is that the H_2O concentrations of felsic melts may be calculated from apatite compositions for volcanic systems involving equilibrium between these phases at 50 to 200 MPa, if estimates for the Cl contents of the melts are available. This approach, however, will require additional experimentation and testing. The compositions of igneous apatites could also provide fundamental constraints on the concentrations of H_2O and other volatiles in mineralizing plutonic systems for which melt inclusions are small, rare and/or crystallized. Magmatic apatites may also support assessment of H_2O concentrations in melts derived from melt inclusion compositions.

Keywords: apatite, melt, fluids, hydroxyl, chlorine, fluorine.

INTRODUCTION

Always consult and cite the final, published document. See http:/www.minsocam.org or GeoscienceWorld

This is a preprint, the final version is subject to change, of the American Mineralogist (MSA)
Cite as Authors (Year) Title. American Mineralogist, in press.
(DOI will not work until issue is live.) DOI: http://dx.doi.org/10.2138/am-2017-5746

Apatite is Earth's most abundant, naturally occurring phosphate mineral, but in most magmatic rocks it is present only as a trace mineral. Despite this, it follows that the ubiquitous crystallization of apatite has important bearing on trace-element behavior during magma evolution since apatite incorporates REEs and other trace metals. Apatite also incorporates F, Cl, OH, S, and C in its structure. If the concentrations of these fugitive volatile components are retained in igneous apatite as magmas crystallize and/or erupt, then analyses of apatite chemistry can provide crucial constraints on the raw concentrations, fugacities, and the overall behaviors of these volatiles in magmas and coexisting fluids. Thus, apatite has been applied as a still-developing geochemical tool to monitor magmatic volatile behavior during melt and fluid evolution and to provide constraints on how volatiles partition between apatite, fluids, and melts as magmas ascend through the crust, cool, and crystallize.

Of particular importance is that the OH contents of apatite are a function of the concentrations and thermodynamic behavior of H_2O in coexisting melts (Mathez and Webster 2005; Webster et al. 2012). These relationships have received particular attention through recent efforts to determine magmatic H_2O concentrations in terrestrial and extraterrestrial basaltic magmas (Patiño and Douce 2006; McCubbin et al. 2010a,b; Greenwood et al. 2011; Patiño et al. 2011; Vander Kaaden et al. 2012; Gross et al. 2013; Sarafian et al. 2013; Tartese et al. 2013, 2014; Barnes et al. 2014; McCubbin et al. 2014; Boyce et al. 2014; McCubbin and Jones 2015; Stock et al. 2016; McCubbin et al. 2016). As the primary magmatic volatile component, H_2O is fundamentally important because it controls melting processes in the crust and mantle, melt viscosity, the capacity of magma to ascend and flow, the explosivity of eruptions, and the deposition of a variety of metallic magmatic-hydrothermal ores. It follows

Always consult and cite the final, published document. See http:/www.minsocam.org or GeoscienceWorld

This is a preprint, the final version is subject to change, of the American Mineralogist (MSA)
Cite as Authors (Year) Title. American Mineralogist, in press.
(DOI will not work until issue is live.) DOI: http://dx.doi.org/10.2138/am-2017-5746

that improved constraints on the ranges in magmatic H_2O concentrations are crucial for interpreting magmatic, eruptive, and mineralizing processes.

Prior research on H_2O and other magmatic volatiles has been based, largely, on analyses of silicate melt (glass) inclusions (MI), but these samples of melt are subject to a host of potential complications including loss of H_2 and/or H_2O via diffusion through host crystals (Audetat and Lowenstern 2014). Magmatic apatite entrapped in other phenocrysts, on the other hand, is less susceptible to these problems. Volatile diffusion through apatite, for example, is sufficiently slow such that apatite is better at retaining accurate information on magmatic volatiles (Brenan 1994; Piccoli and Candela 2002). Moreover, MI occur only rarely in plutonic rocks. When present, they are typically crystallized so they must be rehomogenized to glass prior to analysis for H_2O and other volatile components. The rehomogenization process can pose problems regarding H_2O retention in the melt during heating. Plutons, however, do contain apatites that preserve evidence of magma volatiles. This geochemical study of felsic melts (Table 1) investigates experimental and modeling relations that are useful for estimating H_2O and Cl ± F in felsic melts. The results are useful for comparison with volatiles from MI data, and with further development may also prove beneficial for computing H_2O concentrations in granitic plutons mineralized with Cu, Mo, Au, and other metals.

METHODS

Experimental

All hydrothermal experiments were conducted at fluid(s)-saturated conditions, and the calculated fluid(s)/melt mass ratios varied from ca. 0.2 - 0.5 at run conditions. The capsules were loaded with approximately 30 to 60 mg of natural rhyolitic glass powder, ≤ 5 mg of Durango apatite seeds, ≤ 5 mg of $CaHPO_4$, < 3 mg of $Ca(OH)_2$, ≤ 8 mg of an aqueous 2 molar

Always consult and cite the final, published document. See http:/www.minsocam.org or GeoscienceWorld

This is a preprint, the final version is subject to change, of the American Mineralogist (MSA)
Cite as Authors (Year) Title. American Mineralogist, in press.
(DOI will not work until issue is live.) DOI: http://dx.doi.org/10.2138/am-2017-5746

HCl solution, ≤ 7 mg of an aqueous NaCl plus KCl plus HCl solution, ≤ 10 mg of NaCl plus KCl salts, and ≤ 10 mg of distilled deionized H_2O (Table 2). Two experimental charges also included ≤ 5 mg of aqueous H_3PO_4 solution. The component concentrations in the starting charges were varied to generate apatite grains with a range of F, Cl, and OH contents (Tables 2 and 3). In contrast, the mixtures and solutions of NaCl, KCl, and HCl were used to maintain the molar A/CNK (Al_2O_3/CaO+Na_2O+K_2O) and N/NK (Na_2O/Na_2O+K_2O) ratios of the melts within more modest ranges. The experiments were conducted in Au capsules with external diameters of 3 to 5 mm (wall thickness of 0.13 mm). The capsules were crimped shut, welded with a tungsten-tipped arc welder, weighed, and stored in a drying oven at 115 °C for a minimum of 1 hour before being reweighed to check for loss of volatile components (i.e., via open or leaking capsules).

Fine apatite seed grains were prepared from a purified mineral separate of the Durango, apatite (Durango, Mexico) (Jarosewich et al. 1980) by hand crushing to fragment sizes of 10 to 30 μm in diameter in an agate mortar and pestle. These fragments were further ground in a McCrone micronizing mill (using sintered alumina grinding elements) to generate ultra-fine 1 to 3 μm diameter seeds. The final grinding process generated shredded apatite grain exteriors with highly reactive surface areas. The Ca and P concentrations of the starting charges were supplemented by addition of $CaHPO_4$ and $Ca(OH)_2$ ± H_3PO_4 to stimulate growth of new apatite on the Durango apatite seeds.

The experiments were conducted in an internally heated pressure vessel (IHPV) and in Rene 41 cold seal (CS) pressure vessels at the American Museum of Natural History (AMNH) using the techniques of Doherty et al. (2014). Run temperatures and pressures were monitored using chromel-alumel thermocouples and factory-calibrated bourdon tube gauges. The temperatures

Always consult and cite the final, published document. See http:/www.minsocam.org or GeoscienceWorld

This is a preprint, the final version is subject to change, of the American Mineralogist (MSA)
Cite as Authors (Year) Title. American Mineralogist, in press.
(DOI will not work until issue is live.) DOI: http://dx.doi.org/10.2138/am-2017-5746

were initially held constant for ca. 72 hours, and subsequently, temperature was cycled daily within ± 10 to ± 15 °C of the reported run temperature. The runs were concluded by holding the temperature constant (at run temperatures) for the final 48 to 72 hours. This procedure was employed to assist in the growth of apatite phenocrysts large enough for analysis by EPMA. The IHPV runs were quenched from run temperature to below the predicted glass transition temperature within 20 seconds. The CS experiments were quenched to the glass transition temperwture within < 40 seconds.

Experimental f_{O2} was controlled by the intrinsic f_{H2} of the CS pressure vessels, their nickel alloy (Rene 41) filler rods, and the f_{H2} of the IHPV as well as by the water activity of each charge. We did not intentionally buffer f_{O2} with either H_2-emitting solid buffer assemblages or a Shaw membrane. The ambient f_{O2} buffering capacity of the IHPV is approximately equivalent to that of the $Mn_{1-x}O$-Mn_3O_4 solid oxygen buffer for runs with an a_{H2O} of one (Mathez and Webster 2005). As most IHPV runs had an $a_{H2O} \leq 1$ and the run temperatures are different from the IHPV test conditions, the f_{O2} of these runs was less than that of the $Mn_{1-x}O$-Mn_3O_4 buffer at run conditions. Previously, this IHPV has been demonstrated to provide a range in f_{O2} of NNO to NNO + 2 log units (Webster et al. 2009; Webster et al. 2011) for run conditions and a_{H2O} similar to those of the present study. The CS pressure vessels were controlled at an f_{O2} marginally ≥ of the NNO solid oxygen buffer with a_{H2O} near unity.

Analytical

EPMA. The glass and apatite compositions were measured with wavelength-dispersive spectrometry using a Cameca SX-100 electron microprobe (EPMA) at the AMNH (Table 3). Experimentally generated and natural apatites were analyzed for F, Cl, Na, Fe, Ti, Si, Mn, S, Mg, Ca, Al, and P ± K, Ce, Sr, and Ba, and the standard materials used include MgF_2 for F,

Always consult and cite the final, published document. See http:/www.minsocam.org or GeoscienceWorld

This is a preprint, the final version is subject to change, of the American Mineralogist (MSA)
Cite as Authors (Year) Title. American Mineralogist, in press.
(DOI will not work until issue is live.) DOI: http://dx.doi.org/10.2138/am-2017-5746

boracite for Cl, berlinite for P, wollastonite for Ca, and barite for S. All elements were analyzed using a 15 kV voltage and 20 nA cup (beam) current except for F, Cl, K, and Na for which a 10 kV and 4 nA cup current were used. Count times were 20 seconds for P, Ca, Ti, Fe, Si, Mg, Al, S, Sr, Ce, Ba, and Mn; and 30 seconds for F, Na, Cl, and K. All analyses were conducted using a 4 to 6 μm diameter beam. Four to twelve apatite grains were analyzed for each set of run products.

Most analyses involved movement of the apatite under the electron beam. Stationary analyses were avoided when possible because they can be problematic (Stormer et al. 1993; Goldoff et al. 2012; Stock et al. 2015) given that the X-ray intensities of the primary constituents of apatite (i.e., F, Cl, P, and Ca) vary with extended exposure time to an electron beam. Hence, we searched for apatite grains larger than 10 μm in small dimension and moved these samples under the defocussed electron beam during analyses. We also attempted to analyze apatite grains oriented perpendicular to their c-axis, as X-ray intensities for F and Cl have been shown to be most stable at this orientation (Goldoff et al. 2012). This analytical objective was not always achieved however. The averages reported in this study include a few analyses conducted at or near orientations of the beam parallel to the apatite axis and some stationary analyses. Goldoff et al. (2012) also determined that the measured X-ray intensities of F and Cl are comparatively more stable for OH-poor apatite for intermediate composition (non F- or Cl-end member) apatites at the analytical conditions used herein, and nearly all apatites analyzed contain sub-equal mole fractions of F, OH, and Cl.

The Durango apatite was analyzed 24 times during the course of this investigation to test analytical accuracy and monitor changes in results from analytical session to session. The EPMA analyses return 3.34±0.07 wt% F, 0.42±0.04 wt% Cl, 54.26±0.36 wt% CaO, 40.43±0.44

Always consult and cite the final, published document. See http:/www.minsocam.org or GeoscienceWorld

This is a preprint, the final version is subject to change, of the American Mineralogist (MSA)
Cite as Authors (Year) Title. American Mineralogist, in press.
(DOI will not work until issue is live.) DOI: http://dx.doi.org/10.2138/am-2017-5746

wt% P_2O_5, and 0.34±0.08 wt% SO_2. For comparison, wet-chemical analyses indicate that this apatite contains 3.53, 0.41, 54.02, 40.78, and 0.30 wt% (Jarosewich et al. 1980) of these constituents, respectively.

The glasses were analyzed for Na_2O, K_2O, FeO, SiO_2, and F in the first instrument pass using an electron beam accelerating potential of 15 kV and a 2 nA cup current. Al_2O_3, TiO_2, CaO, MgO, MnO, P_2O_5, Cl, and SO_2 ± SrO and Ce_2O_3 were analyzed in the second instrument pass using an accelerating potential of 15 kV and 10 nA cup current. Both beam conditions included use of a 5 μm, defocussed spot. The glasses were continually moved under the electron beam to minimize alkali and/or F migration or loss.

A high-silica rhyolite glass, the Big Southern Buttes obsidian, was analyzed 36 times during the course of this investigation (Table 1). EPMA returns of 0.22±0.10 wt% F and 0.199±0.01 wt% Cl compare to wet-chemical analyses of 0.31 and 0.2 wt% (Macdonald et al. 1992) for these constituents, respectively. These analyses also provide relative precisions about the mean values. The 1-σ precisions are > 150 rel% for MgO, P_2O_5, and SO_2 analyses of these trace constituents. The 1-σ precisions range from 30 - 60 rel% for F, TiO_2, and MnO. The 1-σ precisions are 15 rel% for CaO, 10 rel% for Na_2O and FeO, 6 rel% for Cl, 3 rel% for K_2O, 2 rel% for Al_2O_3, and 0.8 rel% for SiO_2.

FTIR. The H_2O concentrations of the run-product glasses, containing minimal to no crystals and/or vesicles, were measured with Fourier Transform Infrared Spectroscopy (FTIR) at the AMNH (Table 3). Glass chips were doubly polished to wafers with thicknesses of 70 to 327 μm (with a range of ≤ 5 μm in an individual wafer), that supported transmission of the IR beam between the rare crystals and vesicles while maintaining a beam size of > 5000 μm^2 (some areas

Always consult and cite the final, published document. See http:/www.minsocam.org or GeoscienceWorld

This is a preprint, the final version is subject to change, of the American Mineralogist (MSA)
Cite as Authors (Year) Title. American Mineralogist, in press.
(DOI will not work until issue is live.) DOI: http://dx.doi.org/10.2138/am-2017-5746

were 100 x 100 μm). Wafer thicknesses were determined using a Mitutoyo digitometer with a precision of ± 2 μm.

FTIR measurements to determine the total H_2O concentrations in glass wafers were made using a Thermo Nicolet Nexus 670 FTIR with a continuum microscope by Thermo Spectra-Tech at room temperature in transmittance mode. Nitrogen gas was passed at a rate of 15 L/min to minimize potential H and C contamination. Spectra were collected in both the mid- and near-IR regions (400 to 8500 cm^{-1}) at a resolution of 4 cm^{-1} using a KBr beam splitter, a MCT/A detector cooled by liquid N_2, and a globar source. Four hundred scans were performed for each spectrum, and a background spectrum was taken after each analysis. Four analyses were averaged to determine the homogeneity of the glass and to confirm that each analysis was taken without significant contribution from crystals or vesicles. The IR absorptions of the 4500 cm^{-1} and 5200 cm^{-1} (OH^- and molecular H_2O, respectively) peaks were measured and then converted to concentrations of molecular water and hydroxyl ion using the Beer-Lambert Law as modified by Nowak and Behrens (1995) (see Mandeville et al. (2002) for details). The concentrations were combined to give total H_2O contents. The extinction coefficients, ε_{5200} = 1.79 and ε_{4500} = 1.56 L/mol•cm of Nowak and Behrens (1995), were used. The 2350 cm^{-1} peak for molecular CO_2 was also monitored to determine the level of carbon contamination of these runs, and all runs save two contain < 25 ppm CO_2. The glasses of experiments CS-15-05C and CS-15-04C contain 122 ppm and 52 ppm CO_2, respectively.

Determining Cl concentrations of fluids and constraints on fluid phase equilibria. The run products include a saline aqueous liquid, variably vesicular glass, as well as salts and aluminosilicate-dominated materials that precipitated from the liquid during the quench. The terminology *fluid or fluid phase(s)* is used, generically, to describe the aqueous phase or phases

Always consult and cite the final, published document. See http:/www.minsocam.org or GeoscienceWorld

This is a preprint, the final version is subject to change, of the American Mineralogist (MSA)
Cite as Authors (Year) Title. American Mineralogist, in press.
(DOI will not work until issue is live.) DOI: http://dx.doi.org/10.2138/am-2017-5746

at run conditions. The fluids from these experiments involved low-density vapor, higher-density brine (saline liquid), or coexisting vapor and brine. We could not constrain which fluid phases were stable at our run conditions, but the analogue system NaCl-H_2O (Bodnar et al. 1985) indicates that vapor and brine coexist with as little as 1 wt% NaCl equivalent (i.e., 0.6 wt% Cl) in the bulk integrated fluids at 50 MPa and 800 – 900 °C. Application of these observations indicates that most of our 50 MPa experiments involved vapor and brine, because all but 5 of our runs contained at least 1 wt% Cl in the fluid(s) (Table 3). For experiments involving both vapor and brine, the reported Cl concentrations represent those in the bulk-integrated vapor plus brine.

The Cl concentrations of the quenched liquids of all but 10 of the run products were measured with a Buchler chloridometer. After quenching the experiments, the capsules were cleaned, weighed, and punctured. The punctured capsules were soaked in 500 to 2000 mg of distilled and deionized H_2O to dilute and dissolve all chloride salts that precipitated from the fluids during the quench. The open capsules were soaked for 4 to 28 days prior to fluid sampling and analysis, and afterward, were heated at 115 °C and reweighed. The recorded mass change (before and after the soak-and-heat process) represents the mass of run-product liquid with or without quenched salts that dissolved in the distilled, deionized H_2O during soaking. The diluted fluids were sampled with 10 µl capillary tubes and analyzed for chloride ions with a Buchler chloridometer using methods of Webster et al. (2009). The measured chloride values were corrected for the dilution factors associated with the post-run soaking of the capsules in distilled and deionized water. Based on replicate analyses of a standard aqueous NaCl solution containing 3.5 wt% Cl, conducted for the duration of this study, the chloridometer returns a 1σ precision of 3.8 rel%.

Always consult and cite the final, published document. See http:/www.minsocam.org or GeoscienceWorld

This is a preprint, the final version is subject to change, of the American Mineralogist (MSA)
Cite as Authors (Year) Title. American Mineralogist, in press.
(DOI will not work until issue is live.) DOI: http://dx.doi.org/10.2138/am-2017-5746

The masses of melt, fluid, and apatite and the Cl concentrations of all of the bulk fluids at run conditions were calculated using mass balance. The melt mass was computed by accounting for the increase in melt mass due to dissolution of H_2O, Cl, Ca, and P (from solutions and salts added at the start of each experimental run) into the molten rock powders and for the reduction in melt mass resulting from mineral crystallization. The mass of apatite was calculated from the total mass of P added which was obtained by summing the added masses of apatite seeds, $CaHPO_4$ salt, dilute phosphoric acid solution, and the trace amount in the glass powders, less the mass of P dissolved in the melt. The mass of P sequestered by the fluid(s) of our runs is negligible based on experimental results of Antignano and Manning (2008) demonstrating that the P concentrations of such fluids saturated in apatite are low. The quantity of fluid was computed from the total mass of the starting charge less the melt mass at run conditions. In order to compute the Cl contents of the fluids (Figure 1), the concentrations of Cl in and the computed masses of melt and apatite were used to estimate the masses of Cl sequestered by melt and apatite. The Cl concentrations of the fluid(s) were computed from the total mass of Cl in the starting charge of the experiment, less that contained in the melt and apatite. This approach also assumes that every two moles of Cl are chemically associated with one mole each of Na and K having an averaged cation mass of 31.

We report and apply the chloridometer data as representative of the Cl contents of most fluid(s) at run conditions (Table 3). For those 10 other run-product liquids not directly analyzed, we apply the calculated Cl concentrations. Excluding the single outlier, the computed and measured Cl concentrations are mutually consistent within the associated precision (Figure 1). The measured concentrations of Cl in the fluids vary from 0.4 to 39 wt%, and the computed Cl contents range from 0.3 to 39 wt%.

Always consult and cite the final, published document. See http:/www.minsocam.org or GeoscienceWorld

This is a preprint, the final version is subject to change, of the American Mineralogist (MSA)
Cite as Authors (Year) Title. American Mineralogist, in press.
(DOI will not work until issue is live.) DOI: http://dx.doi.org/10.2138/am-2017-5746

Error analysis. The reported precisions for the measured concentrations of components in melt, fluid (i.e., Cl by chloridometer), and apatite are simple 1 σ standard deviations about the average compositions. All other reported precisions were determined by standard error propagation methods (Table 3).

RESULTS

Observations on Run Products and Attainment of Equilibrium

All glasses are vesicular and contain apatite (Table 2). Most of the glasses also contain minor abundances of iron oxides, and a small number contain trace clinopyroxene ± plagioclase ± a wollastonite-like Ca- and Si-dominated phase. Most solid run products contain > 90 vol% glass. The glasses contain three textural varieties of apatite crystals including fine-grained acicular crystals too small for EPMA, clusters of anhedral crystals generally < 5 μm in diameter, and subhedral crystals ranging from <5 to rarely 50 μm in diameter. The first two forms of apatite occur intimately embedded in glass, and are comparable to those observed in experiments of Doherty et al. (2014). The final textural variety of apatite occurs as crystals fully or partially embedded in glass, as crystals within vesicles, or as free crystals (devoid of contact with glass). Apatites analyzed by EPMA for this study were the third (subhedral) textural variety. Specifically, these crystals are > 10 μm in diameter. All apatites were largely to fully embedded in glass. These apatites are interpreted to have grown sufficiently slowly from the P-bearing starting melt compositions and to have attained equilibrium with melt and fluid(s). This is because crystal growth was limited by the relatively slow diffusion of P (Wolf and London 1994; Baker 2008) through the highly polymerized rhyolitic melts.

Melts. The molar A/CNK and N/NK ratios of the natural starting glass are 0.99 and 0.59 (Table 1), respectively, but the components were exchanged between melt, fluid(s), and apatite during

Always consult and cite the final, published document. See http:/www.minsocam.org or GeoscienceWorld

This is a preprint, the final version is subject to change, of the American Mineralogist (MSA)
Cite as Authors (Year) Title. American Mineralogist, in press.
(DOI will not work until issue is live.) DOI: http://dx.doi.org/10.2138/am-2017-5746

the course of the runs. As a consequence, the molar A/CNK ratio of the ca. 50 MPa melts vary from 0.88 to 1.04. Most, however, range from 0.95 to 0.99. Molar N/NK ratios of these melts range from 0.48 to 0.68, but most are restricted to 0.55 to 0.6.

Run-product glass compositions indicate that the ca. 50 MPa melts dissolved 1.8 to 3.1 wt% H_2O, 0.03 to 0.48 wt% Cl, 0.01 to 0.19 wt% F, and ≤ 0.01 wt% SO_2. In several following plots, we have computed the (maximum) Cl solubility (Webster et al. 2015) for each melt (i.e., for melts saturated in brine or vapor plus brine, at equilibrium). We have also normalized the measured Cl contents to these Cl solubilities, in order to reduce dispersion in the experimental results.

Apatites. The apatites contain variable halogen and hydroxyl contents as well as differing concentrations of Na, Fe, Ce, Mg, Ca, P, and Si (Table 3). Hydroxyl concentrations range from 0.5 to 2.5 wt%, Cl from 0.14 to 3.8 wt%, and F from 0.32 to 2.2 wt%. These values correspond to X_{OH}^{apat} of 0.14 to 0.7, X_{Cl}^{apat} of 0.02 to 0.56, and X_F^{apat} of 0.08 to 0.59. The X_{OH}^{apat} was calculated with the method of Piccoli and Candela (2002) which involves the assumption that the hydroxyl site is filled dominantly by F, Cl, and OH. Thus, the molar occupancies in this site are assumed to sum to unity or near unity. Relationships involving the cations are addressed below.

DISCUSSION

Melt compositional relations

The H_2O, F, and Cl concentrations in the melts vary due to exchange of F, OH, and Cl between the F-rich Durango starting apatite, the melt, and the fluids. The H_2O and Cl contents also change as a function of the fluid phase relations in the runs.

Always consult and cite the final, published document. See http:/www.minsocam.org or GeoscienceWorld

This is a preprint, the final version is subject to change, of the American Mineralogist (MSA)
Cite as Authors (Year) Title. American Mineralogist, in press.
(DOI will not work until issue is live.) DOI: http://dx.doi.org/10.2138/am-2017-5746

The concentrations of H_2O in most fluid(s)-saturated rhyolitic melts at 50 MPa exhibit little change with increasing Cl in the melts even though the Cl contents of the accompanying fluids vary from < 1 to 39 wt% (Figure 2A,B). In fact, all but two of the ca. 50 MPa and 850 °C melts are consistent with an average H_2O content of 2.71±0.18 wt%. This value agrees well with modeled H_2O solubilities of 2.78 wt% (Ghiorso and Gualda 2015), 2.6 wt% (Newman and Lowenstern 2002), and 2.69 wt% (Moore et al. 1998) for rhyolitic melts at 50 MPa and 850 °C. It might be expected that the H_2O contents of the melts should decrease as increasing quantities of NaCl and KCl, with lesser HCl, were added to the experiments. Diluting the H_2O in the fluid(s), by addition of chlorides, decreases H_2O concentrations in fluids which might also decrease the H_2O concentrations of the coexisting melts at equilibrium. It is noteworthy that the two 50 MPa melts containing the maximum recorded Cl contents (e.g., 0.35 wt%) do exhibit reduced H_2O contents (Fig. 2A). Likewise, the H_2O contents of the four 200 MPa runs also remain relatively fixed at 5.68 ± 0.15 wt% as the Cl concentrations of these melts increase through a range of 0.2 wt% and the coexisting fluids increase from 4 to 7.6 wt%.

These observations can be interpreted by considering the solubility behavior of Cl in these melts and the relevant phase relations of vapor and brine. The relationship showing relatively fixed H_2O contents of melts with increasing Cl in the melt and fluid(s) system has been observed previously with haplogranite (Webster 1992), topaz rhyolite (Webster and Rebbert 1998), phonolite (Webster et al. 2014), and andesite (Botcharnikov et al. 2006; 2007) melts. It reflects strongly non-ideal mixing behavior between H_2O and the chloride species that are dissolved in the fluid(s) with associated effects on volatile dissolution in coexisting melts (Shinohara 1994; Lowenstern 1994; Signorelli and Carroll 2000; Webster and Mandeville 2007). In this regard, H_2O and dissolved alkali chloride species in aqueous hydrothermal

Always consult and cite the final, published document. See http:/www.minsocam.org or GeoscienceWorld

This is a preprint, the final version is subject to change, of the American Mineralogist (MSA)
Cite as Authors (Year) Title. American Mineralogist, in press.
(DOI will not work until issue is live.) DOI: http://dx.doi.org/10.2138/am-2017-5746

solutions mix non-ideally within and near the vapor-brine solvus in pressure-temperature-composition space (Bodnar et al. 1985; Dreisner and Heinrich 2007). The dissolution behavior of Cl in melt is also relevant. The abscissa of Figure 2B expresses the Cl contents of melt as the measured Cl concentration normalized to the modeled solubility of Cl for the specific temperature, pressure, and composition of each melt. With values of the (measured Cl/modeled Cl) ratio <1, the melt is saturated in a Cl-bearing vapor. However, with increasing Cl in the system, there is a break in slope at values of the (measured Cl/modeled Cl) ratio of unity where the melt is in equilibrium with either brine only (along the vertical curve in Fig. 2B) or brine plus vapor (at the intersection of the vertical and horizontal curves) and the melt contains its maximum possible Cl content. At the condition of two fluid phases, changes in the Cl or H_2O concentrations of the bulk system cause changes in the ratio of vapor to brine while the Cl or H_2O concentrations of the melt are fixed. It is only along the vertical curve that the H_2O concentration of the melt is free to vary.

Apatite compositional relations

Major and minor components, in addition to OH, F, and Cl, can vary significantly within the experimental apatites, and several of the mechanisms of trace-component incorporation within apatite involve coupled substitutions. Magnesium and Na correlate positively with Cl (Figure 3A); whereas, S, Si (Figure 3B), Ca, and F correlate negatively with Cl. Additionally, Ca, S, and Si associate positively with F and Na, Fe, and Mg correlate negatively with F. The positive Ca-F relations are consistent with the structure-based interpretations of natural apatites from Utah of Hughes et al. (2015), and the Na-Cl correlation may simply reflect the fact that NaCl was the dominant salt used in adding Cl to the experimental charges (Table 2). Some relationships shown by our experimental charges are consistent with prior studies on cation

Always consult and cite the final, published document. See http:/www.minsocam.org or GeoscienceWorld

This is a preprint, the final version is subject to change, of the American Mineralogist (MSA)
Cite as Authors (Year) Title. American Mineralogist, in press.
(DOI will not work until issue is live.) DOI: http://dx.doi.org/10.2138/am-2017-5746

sequestration by apatite and with covariations of these cations with halogen and hydroxyl substitutions in apatite. For example, the observation that the Mg contents of apatite are higher in Cl-bearing apatite and lower in apatites with relatively higher F contents is consistent with prior studies on Mg incorporation in apatite (Pan and Fleet 2002). Specifically, Ca replacement by Mg correlates with OH replacement of F as well as Cl as observed previously by (Patel 1980). Tacker (2004) reports that Mn preferentially orders with OH. Likewise, higher Mn contents in apatite correlate with increasing (Cl/F) (Pan and Fleet 2002). Fleet et al. (2000) observed previously that:

$$REE^{3+} + Na^{+} = 2Ca^{2+}. \qquad (1)$$

This geochemical association is supported by the compositions of these experimental apatites as (Ce + Na) substitute for Ca (Fig. 3C). In addition, the substitution of Ce for Ca in the apatites also correlates with changes in the halogen occupancy on the hydroxyl site:

$$2REE^{3+} + Cl^{-} = 3Ca^{2+} + F^{-}. \qquad (2)$$

The co-substitution of S and Si in apatites correlates with decreasing P (Fig. 3D), consistent with:

$$SO_4^{2-} + SiO_4^{4-} = 2\ PO_4^{3-} \qquad (3)$$

of Peng et al. (1997) and Pan and Fleet (2002). Sulfur incorporation in these apatites also correlates with increasing Na:

$$SO_4^{2-} + Na^{+} = PO_4^{3-} + Ca^{2+} \qquad (4)$$

as observed previously by Peng et al. (1997) and Pan and Fleet (2002).

Always consult and cite the final, published document. See http:/www.minsocam.org or GeoscienceWorld

This is a preprint, the final version is subject to change, of the American Mineralogist (MSA)
Cite as Authors (Year) Title. American Mineralogist, in press.
(DOI will not work until issue is live.) DOI: http://dx.doi.org/10.2138/am-2017-5746

Fluid composition relations

The concentrations of Cl, Na, Mg, and P increase and those of Si and F in apatite decrease with increasing Cl in the coexisting fluid phase(s). Moreover, the per formula unit (pfu) (S+Si) and (Ce+Si) in apatite increase with increasing Cl contents in the fluid(s). The Cl contents of the melt increase with increasing Cl in the fluid(s).

F Partitioning

Although not displayed graphically herein, the F concentrations of apatite appear to correlate positively with the F contents of coexisting melts. This observation is not statistically valid, however, because of the large errors associated with the EPMA analysis of F in the F-poor, run-product glasses.

Cl Partitioning

Fluids(s)/Melts. Chlorine partitions in favor of fluid(s) relative to melts, but Cl partitioning at 50 MPa is complicated by the non-ideal mixing and dissolution behaviors of H_2O and Cl in the pseudo-system: rhyolitic melt-apatite-vapor±brine. Figure 4A shows that the Cl concentrations of most melts increase with increasing Cl in the fluid(s), but the data indicate significant dispersion when displayed in this fashion. Consequently, the data have been recast with the Cl in fluid(s) plotted against the (measured Cl/ modeled Cl) melt ratio and with additional data for apatite-free experiments involving haplogranitic melts included in Figure 4B. Here, the partitioning behavior is more apparent. With ≤ 3 wt% Cl in the fluid(s) and for (measured Cl/ modeled Cl) melt ratios < 0.9, the Cl content of the melts rises rapidly with increasing Cl in the system whereas the Cl concentrations in the fluid(s) increase minimally. Conversely with continued addition of Cl, there is a break in slope and the (measured Cl/modeled Cl) approaches unity in the melt and remains at or near this value while the Cl in the fluid(s) increases

Always consult and cite the final, published document. See http:/www.minsocam.org or GeoscienceWorld

This is a preprint, the final version is subject to change, of the American Mineralogist (MSA)
Cite as Authors (Year) Title. American Mineralogist, in press.
(DOI will not work until issue is live.) DOI: http://dx.doi.org/10.2138/am-2017-5746

significantly because the melt has dissolved its maximum concentration of Cl. Any additional Cl added to the system is consumed by fluid(s) and coexisting apatite as discussed below. In summary, this behavior is consistent with vapor-melt-apatite-only conditions for those runs with ≤ 3 wt% Cl in the fluid(s) and (measured Cl/modeled Cl) ratios < 0.9. It is also consistent with brine-melt-apatite±vapor conditions where (measured Cl/modeled Cl) ratios of the melt are at or near unity as shown previously in the prior experimental studies of Webster (1992), Shinohara (1994), Lowenstern (1994), Webster and Rebbert (1998), Signorelli and Carroll (2000), Botcharnikov et al. (2006, 2007), Webster and Mandeville (2007), and Webster et al. (2014) at shallow crustal pressures and magmatic temperatures. It is noteworthy that the runs conducted at 1000 °C and 50 MPa and at 1000 °C and 100 MPa and are consistent, within estimated precision, with the majority of the other 50 MPa runs that were conducted at ca. 850 °C implying that pressure and temperature can vary through this range with only minimal consequences for Cl distribution between fluid(s) and melt. However, the 200 MPa data indicate that Cl partitions more strongly in favor of the fluid(s) at higher pressure. This has also been observed previously with felsic melts (Webster 1992). The (wt% Cl in fluid[s]/wt% Cl in melt) Nernstian partition coefficients vary from 1.7 to 163 at ca. 50 MPa.

Apatite/Melts. Chlorine partitions strongly in favor of apatite relative to these felsic melts, and the partitioning behavior shows higher concentrations in both phases as the Cl content of the system increases, which is consistent with prior experimental results (Doherty et al. 2014). Figure 5A displays the ($X_{Cl}^{apat}/X_{OH}^{apat}$) ratio versus the (measured Cl/modeled Cl) ratio for the melts. Here, we have marked out the two runs that experienced a slower, non-isobaric quench by labeling them as SQ in this figure.

Always consult and cite the final, published document. See http:/www.minsocam.org or GeoscienceWorld

This is a preprint, the final version is subject to change, of the American Mineralogist (MSA)
Cite as Authors (Year) Title. American Mineralogist, in press.
(DOI will not work until issue is live.) DOI: http://dx.doi.org/10.2138/am-2017-5746

Our experiments show that the ($X_{Cl}^{apat}/X_{OH}^{apat}$) ratio increases at a relatively modest rate as Cl is initially added to the system (with the lowest concentrations of Cl in apatite and melt) and as the (measured Cl/modeled Cl) ratio in the melt increases to values less than but approaching unity. With continued addition of Cl to the system, the (measured Cl/modeled Cl) ratio in melt is fixed near unity after the break in the slope, and henceforth the ($X_{Cl}^{apat}/X_{OH}^{apat}$) ratio increases dramatically because the melt has dissolved its maximum solubility of Cl. This behavior is similar, to a first order, to that observed for Cl partitioning between fluid(s) and these melts (Fig. 4B).

Our results involving the high-silica rhyolitic melt are compared (Figure 5B) with prior experiments employing a rhyodacitic melt and conducted at 50 MPa and 850 to 950 °C (Doherty et al. 2014). The two data sets are consistent, within the propagated precision, for low and high concentrations of Cl in the melt, for rhyodacitic to rhyolitic melts with a molar A/CNK ratio of 0.88 to 1.05.

Apatite/fluid(s). Chlorine partitions in favor of the fluid(s) relative to apatite with Nernstian $D_{Cl}^{apat/fluids}$ ranging from 0.05 to 1.8 for all experiments of this study with most values less than unity. For comparison, Kusebauch et al. (2015) determined $D_{Cl}^{apat/fluids}$ of ca. 2.3 for melt-absent, volatile-exchange experiments with apatite and fluid at 400 to 700 °C and 200 MPa and Webster et al. (2009) observed $D_{Cl}^{apat/fluids}$ of 0.02 to 0.11 for fluids and apatites saturated in rhyodacitic melts at ca. 900 °C and 200 MPa. Moreover, the bulk of our 50 MPa experiments are consistent with increasing ($X_{Cl}^{apat}/X_{OH}^{apat}$) with increasing $X_{Cl}^{fluid(s)}/X_{OH}^{fluid(s)}$ (Figure 6). For 50 MPa melts with molar A/CNK ratio of 0.9 to 1.05 and N/NK ratio of 0.53 to 0.68, this partitioning behavior is expressed empirically by:

Always consult and cite the final, published document. See http:/www.minsocam.org or GeoscienceWorld

$$\frac{X_{Cl}^{apat}}{X_{OH}^{apat}} = 1.701 + 0.506 \times \log \frac{X_{Cl}^{fluids}}{X_{H_2O}^{fluids}} \quad (5)$$

where the mole fractions of the volatile components in the fluid(s) are defined in the appendix.

H_2O/OH Partitioning and Exchange

Apatite/melt. All runs exhibit molar Nernstian partition coefficients for the distribution of OH and H_2O between apatite and melt that are near unity. Values of $D_{XOH}^{apat/melt}$ range from 0.7 to 1.4 for all but the two cold seal runs that quenched slowly and non-isobarically. Most of these experiments are consistent with OH and H_2O partitioning slightly in favor of apatite at 50 to 200 MPa and 850 to 1000 °C.

Recent research has shown that the use of Nernst-style partition coefficients for the essential structural components F, Cl, and OH in apatite is not optimal for calculating the volatile contents of melts because these compositionally simple partition coefficients (e.g., $D_{Cl}^{apat\text{-}melt}$ = concentration of Cl in apatite/concentration of Cl in melt) for any one of these volatiles may vary with the abundances of the others (Boyce et al. 2014; see summary in McCubbin et al. 2015). To avoid this compositional interdependence of the components in the hydroxyl site of apatite, McCubbin et al. (2015) recommend the application of two volatiles in apatite rather than one as is done with simple Nernst-style partition coefficients. Using this approach, two volatiles in apatites can be applied in exchange coefficients (i.e., K_d) such as for example:

$$K_{d_{OH-Cl}}^{apat-melt} = \frac{X_{Cl}^{melt} * X_{OH}^{apat}}{X_{OH}^{melt} * X_{Cl}^{apat}} \quad (6)$$

that are based on representative exchange equilibria like:

$$X_{OH}^{melt} + X_{Cl}^{apat} = X_{Cl}^{melt} + X_{OH}^{apat}. \quad (7)$$

This is a preprint, the final version is subject to change, of the American Mineralogist (MSA)
Cite as Authors (Year) Title. American Mineralogist, in press.
(DOI will not work until issue is live.) DOI: http://dx.doi.org/10.2138/am-2017-5746

We have adopted this approach to generate exchange coefficients for F, Cl, and OH (Fig. 7). Given that water dissolves in melts as $(OH)^-$ as well as molecular H_2O, we use $(OH)^-$ in melt to represent the OH/H_2O components in melt that participate in such exchange reactions.

The majority of the $K_{dOH\text{-}F}^{apat\text{-}felsicmelt}$, $K_{dOH\text{-}Cl}^{apat\text{-}felsicmelt}$, and $K_{dCl\text{-}F}^{apat\text{-}felsicmelt}$ values of this study are less than unity and range from ca. 0.002 to 0.08, 0.02 to 0.22, and 0.01 to 3.8, respectively. Interestingly, McCubbin et al. (2015) studied exchange equilibria involving apatite and iron-rich basaltic melt at 1 to 1.2 GPa and 950 to 1000°C, and determined $K_{dOH\text{-}F}^{apat\text{-}basalticmelt}$, $K_{dOH\text{-}Cl}^{apat\text{-}basalticmelt}$, and $K_{dCl\text{-}F}^{apat\text{-}basalticmelt}$ values that vary from 0.012 to 0.016, 0.018 to 0.09, and 0.17 to 0.3, respectively. It is remarkable that these ranges overlap reasonably well with those of our runs given the strong differences in fluid phase relations, pressure, and melt composition of the two experimental studies and that our runs involved significant non-ideal mixing behavior for H_2O and Cl.

The influence of melt composition, however, can be significant for exchange reactions like these. Prior experimental work has shown that apatite-melt and apatite-fluid volatile partitioning behavior varies with melt composition and, in particular, with changes in the molar A/CNK (Mathez and Webster 2005; Webster et al. 2009; Doherty et al. 2014). This influence is likewise shown by some of the exchange coefficients (Fig. 7). For example, the $K_{dCl\text{-}F}^{apat\text{-}melt}$ increases and the $K_{dOH\text{-}Cl}^{apat\text{-}melt}$ decreases with the molar (A/CNK)/(N/NK) ratio of these felsic melts. Here, the molar A/CNK ratio has a larger influence than the N/NK ratio in this relationship. The apparent weak increase in the $K_{dOH\text{-}F}^{apat\text{-}melt}$, however, is not statistically significant. The propagated errors associated with these exchange coefficients are quite significant (i.e., exceeding 100 rel%) due to the inherent imprecision in measuring the F contents of such low-F melts with accuracy. To this point, we have applied larger symbols for

Always consult and cite the final, published document. See http:/www.minsocam.org or GeoscienceWorld

This is a preprint, the final version is subject to change, of the American Mineralogist (MSA)
Cite as Authors (Year) Title. American Mineralogist, in press.
(DOI will not work until issue is live.) DOI: http://dx.doi.org/10.2138/am-2017-5746

those runs involving relatively lower propagated imprecisions on the K_d values (i.e., values < 100 rel%). These data points demonstrate that the relations involving $K_{dCl\text{-}F}^{apat\text{-}melt}$ and $K_{dOH\text{-}Cl}^{apat\text{-}melt}$ and melt composition are statistically valid if we consider the anomalous point for run CS-15-06 (i.e., the run with the lowest value of (A/CNK)/(N/NK)) as an outlier. More experimental data are required to confirm these apparent relations, but it does appear that the K_d values are not strictly constant for the ranges in melt composition, pressure, and temperature of this study given the strongly non-ideal mixing behavior for Cl and H_2O in vapor-brine systems. These relationships further indicate that the application of exchange coefficients must involve compositional matching of the melts for interpreting natural systems with experimental data. Moreover, given the apparent lack of constancy for $K_{dCl\text{-}F}^{apat\text{-}melt}$ and $K_{dOH\text{-}Cl}^{apat\text{-}melt}$ under the experimental conditions of this investigation, we do not use these exchange coefficients but rather we apply ratios of $(X_{OH}^{apat}/X_{Cl}^{apat})$ and $(X_F^{apat}/X_{Cl}^{apat})$ in the data interpretation that follows.

To investigate the partitioning of H_2O/OH between apatite and melts, for example, the exchange coefficients and equilibria expressed in equations (6) and (7) have been rearranged to provide equations that support the calculation of H_2O concentrations in apatite-saturated felsic melts. We plot the $(X_{H2O}^{melt}/X_{Cl}^{melt})$ versus the $(X_{OH}^{apat})/(X_{Cl}^{apat})$ in Figure 8 (A,B). This plot distinguishes apatites based on their Si and Mg contents for felsic melts with restricted compositional parameters. For apatite-saturated rhyolitic melts characterized by A/CNK ratios between 0.88 to 1.1 and N/NK ratios > 0.55, empirical fits to the data are expressed by the equation:

$$(X_{H2O}^{melt}/X_{Cl}^{melt}) = ((-2.86) + (16.18)*(X_{OH}^{apat})/(X_{Cl}^{apat})) \quad (8)$$

Always consult and cite the final, published document. See http:/www.minsocam.org or GeoscienceWorld

This is a preprint, the final version is subject to change, of the American Mineralogist (MSA)
Cite as Authors (Year) Title. American Mineralogist, in press.
(DOI will not work until issue is live.) DOI: http://dx.doi.org/10.2138/am-2017-5746

with an R^2=0.94. Equation (8) bears on apatites with pfu Si/Mg ratios > 6. For similar melts coexisting with apatites having pfu (6 > Si/Mg > 0.3) the empirically based relation is:

$$(X_{H2O}^{melt}/X_{Cl}^{melt}) = ((-21.99) + (41.48)*(X_{OH}^{apat})/(X_{Cl}^{apat})) \quad (9)$$

with an R^2=0.89. Regarding the relationships involving apatite volatile components and their trace cation contents, it has been noted previously that Si in apatite correlates positively with F and that Mg correlates positively with Cl while F and Cl are anti-correlated. This is consistent with the observation that the (Si/Mg) pfu ratio varies with the distribution of Cl and OH between apatite and melt as seen in Figure 8.

To expand the applicability of these relations in pressure-temperature-composition space, we have added results from several experiments involving apatites having pfu (6 > Si/Mg > 0.3) in equilibrium with rhyodacitic melts at 200 (Webster et al. 2009) and 50 MPa (Doherty et al. 2014) to generate:

$$(X_{H2O}^{melt}/X_{Cl}^{melt}) = ((-19.66) + (39.13)*(X_{OH}^{apat})/(X_{Cl}^{apat})) \quad (10)$$

with an R^2=0.88. One can rearrange and solve equations (9) and (10) for X_{H2O}^{melt}, but this approach requires an estimate for the X_{Cl}^{melt} which is calculated with equations provided in the appendix.

APPLICATION OF THESE DATA

Constraining the H_2O concentrations of eruptive and plutonic felsic magmas has important implications for aluminosilicate melting temperatures, melt viscosity, and bulk magma rheology as well as for their role in processes of volcanism, magmatic-hydrothermal mineralization, and magma evolution. Compositions of silicate MI have been used to estimate the concentrations

Always consult and cite the final, published document. See http:/www.minsocam.org or GeoscienceWorld

This is a preprint, the final version is subject to change, of the American Mineralogist (MSA)
Cite as Authors (Year) Title. American Mineralogist, in press.
(DOI will not work until issue is live.) DOI: http://dx.doi.org/10.2138/am-2017-5746

of H_2O and other volatile components in magmas, but some MI are fraught with complications including volatile leakage along cracks or host cleavage, diffusive loss of H_2O and H_2 through the host mineral, and/or sequestration of H_2O and CO_2 from melt or glass into the shrinkage or vapor bubbles (Audetat and Lowenstern 2014; Moore et al. 2015; Wallace et al. 2015; Esposito et al. 2016).

The compositions of igneous apatite have been employed to determine concentrations of H_2O, F, Cl, S (and CO_2) in melts and magmatic fluids at the times or stages of apatite crystallization (Candela 1986; Brenan 1993; Piccoli and Candela 1994; Marks et al. 2012). Prior apatite-based research has, for example, led to estimates of magmatic H_2O concentrations for basaltic systems (McCubbin et al. 2010a; Vander Kaaden et al. 2012, Gross et al. 2013; Boyce et al. 2014; McCubbin and Jones 2015). Regarding the use of apatite compositions as a geochemical tool, equation (5) supports the estimation of Cl contents in magmatic fluids and equations (8), (9), and (10) provide a basis for calculating the H_2O contents in felsic melts supporting plutonic and volcanic processes. It is important to bear in mind that these relations apply to specific ranges in the molar A/CNK and N/NK ratios of the experimental melts and to experimental apatites with specific ranges in F, Cl, and OH abundances (Figure 9A) and minor- to trace-element Si and Mg contents. As demonstrated below, applications of these equations should be restricted to igneous apatites and melts having compositions similar to those of this investigation.

Constraining volatile components in magmas of Augustine volcano, Alaska

Augustine volcano is located approximately 290 km southwest of Anchorage and is one of many island-arc stratovolcanoes in the Aleutian island chain of southern Alaska. Augustine was built from numerous prehistoric eruptive deposits (ash and other tephra, lava, and lahar

Always consult and cite the final, published document. See http:/www.minsocam.org or GeoscienceWorld

This is a preprint, the final version is subject to change, of the American Mineralogist (MSA)
Cite as Authors (Year) Title. American Mineralogist, in press.
(DOI will not work until issue is live.) DOI: http://dx.doi.org/10.2138/am-2017-5746

materials) and similar materials from the 7 historic eruptions of the past 200 years. Low K_2O, calc-alkaline magmas containing elevated volatile abundances (Johnston 1978) and particularly Cl-enriched gases (Symonds et al. 1990) are typical of Augustine's eruptions. Felsic to intermediate SiO_2 content MI contained by Augustine phenocrysts are volatile enriched with up to 8 wt% H_2O, 0.14 wt% CO_2, 0.78 wt% Cl, 0.1 wt% S, and 0.4 wt% F (Roman et al. 2006; Tappen et al. 2009; Webster et al. 2010; Nadeau et al. 2015; Webster unpublished data). Geochemical relationships involving these volatile components in MI and apatites (Webster et al. 2010; Nadeau et al. 2015) imply that most Augustine magmas contained Cl-bearing to Cl-enriched fluids that exsolved well prior to eruption (i.e., these magmas were fluid saturated in the shallow, and potentially, in the middle crust).

To test the relationship expressed by equation (10), we apply published data on the H_2O and Cl concentrations of MI in pyroxene, plagioclase, and/or amphibole or quartz phenocrysts from 4 prehistoric eruptions (i.e., 2100 annum before present (a.b.p.), 1700 a.b.p., 1400 a.b.p., and 1000 a.b.p.), phenocrysts erupted in the 1986 and 2006 eruptions (Tappen et al. 2009; Webster et al. 2010), and phenocrysts erupted with a massive Pleistocene pumiceous rhyolite (Nadeau et al. 2015). The averaged molar A/CNK ratios of these felsic MI range from 0.96 to 1.03 which is consistent with the range of 0.88 to 1.1 from the felsic experimental melts. The molar N/NK ratios of the MI, however, range from 0.73 to 0.82 and exceed those of the experimental melts (i.e. ranging from 0.55 to 0.61 for runs involved in the generation of equation (10)); we apply them nevertheless. We also use analytical data on the mole fractions of OH, F, and Cl in apatite grains from these same eruptive units (Fig. 9B, Table 4) to estimate the H_2O concentrations of the magmas involved in these specific eruptions. Most of the analyzed apatites occur as inclusions within pyroxene, plagioclase, iron-titanium oxide, and amphibole phenocrysts, and a

Always consult and cite the final, published document. See http:/www.minsocam.org or GeoscienceWorld

This is a preprint, the final version is subject to change, of the American Mineralogist (MSA)
Cite as Authors (Year) Title. American Mineralogist, in press.
(DOI will not work until issue is live.) DOI: http://dx.doi.org/10.2138/am-2017-5746

few occur as small individual phenocrysts in the matrix glass. The average pfu (Si/Mg) ratios of apatites from Augustine range from 0.31 to 0.88 which is consistent with the range of 6 > (Si/Mg) > 0.3 for the experimental apatites providing the empirical basis for equation (10).

The Cl concentrations of those MI which have also been analyzed for H_2O are converted to values of X_{Cl}^{melt} (see appendix), and the X_{Cl}^{melt} values are fed into equation (10) along with the averaged X_{OH}^{apat} and the X_{Cl}^{apat} values of the Augustine apatites from each sample. As detailed in the appendix, an initial estimate of the mass of H_2O in the melt is required to calculate the X_{Cl}^{melt}, and this value is subsequently changed iteratively until the calculated wt% H_2O in the melt provides a H_2O content equivalent to that of the estimated iterative value

Apparent H_2O concentrations calculated from the averaged apatite data are compared with the measured averages of the H_2O contents of the MI for the 9 samples of these 7 units in Figure 10. Before evaluation of the data, it should be kept in mind that a comparison like this assumes that the apatite grains grew and maintained equilibrium with felsic fractions of Augustine melts while the felsic MI were being entrapped in other phenocrysts. It also involves the assumption that the average Cl and H_2O contents of the melts and the average F and Cl contents of the apatites (recall that the OH contents of apatites are calculated from the measured F and Cl concentrations by difference) reflect the volatile exchange processes linking these phases during magma evolution. It is noteworthy that the 1-σ spread in the precision of the measured H_2O concentrations of MI from units erupted 1400 and 1000 years before present is ca. ± 2 wt%, because these MI represent a large range in pressures as the Augustine magmas ascended through the shallow crust (Tappen et al. 2009). For example, the measured H_2O contents of the MI erupted ca. 1000 a.b.p. range from 1.6 to 7.6 wt%, and those in MI that erupted 1400 a.b.p. range from 2 to 8 wt%. It is clear that application of data like these, for such a comparison, is

Always consult and cite the final, published document. See http:/www.minsocam.org or GeoscienceWorld

This is a preprint, the final version is subject to change, of the American Mineralogist (MSA)
Cite as Authors (Year) Title. American Mineralogist, in press.
(DOI will not work until issue is live.) DOI: http://dx.doi.org/10.2138/am-2017-5746

not ideal. Conversely, the measured range in H_2O is much smaller for MI erupted during the Pleistocene (i.e. the yellow pumice), 1700 a.b.p., in 1986 and again in 2006. Each of these samples demonstrates a strong and statistically significant agreement between measured and calculated H_2O concentrations. The cause for the lack of agreement for the two other Pleistocene samples is not known.

IMPLICATIONS

This study provides new experimental data and insights into the partitioning and exchange of F, Cl, and OH/H_2O between aqueous fluids, apatite, and felsic aluminosilicate melts at ca. 700 to 1000 °C and 50 to 200 MPa. The determined relationships bear on magma evolution, fluid exsolution, and the potential for mineralization in felsic plutons.

The experimental apatites are generally subequal in their F, OH, and Cl contents, and hence, contain a significant contribution from OH. The melts contain trace to minor concentrations of F, 1.8 to 3.1 wt% H_2O, and trace levels of Cl up to values equivalent to brine-saturated felsic melts. Volatile distribution between these phases is observed to vary with pressure and the molar A/CNK and N/NK ratios of the melts, as well as the Si, P, Mg, Ce, Na, S, Fe, and ± Ca concentrations of the apatites.

The experimental volatile exchange relationships determined for melt-apatite, melt-fluid, and apatite-fluid pairs are potentially applicable to a variety of magmatic systems. Of particular interest is that the H_2O concentrations of felsic melts may be calculated from apatite compositions for magmatic systems involving equilibrium between these phases at 50 to 200 MPa, if estimates for the Cl contents of the melts are available and if the apatites are large enough for EPMA. With further development, this approach may prove to be highly useful for verifying the H_2O concentrations of eruptive magmas as constrained from MI. For example,

Always consult and cite the final, published document. See http:/www.minsocam.org or GeoscienceWorld

This is a preprint, the final version is subject to change, of the American Mineralogist (MSA)
Cite as Authors (Year) Title. American Mineralogist, in press.
(DOI will not work until issue is live.) DOI: http://dx.doi.org/10.2138/am-2017-5746

our comparison of H_2O concentrations measured in silicate melt inclusions from 7 eruptive units of Augustine volcano, Alaska, with apparent H_2O contents calculated from apatite compositions indicates reasonable agreement for 4 of the units. This application, however, also points to the need for valid information on the timing of apatite crystallization, on the equilibration of apatite with melt with or without fluid, and on the potential for late-stage reaction and/or re-equilibration of apatite and other phases. The compositions of igneous apatites should also provide fundamental constraints on the concentrations of H_2O and other volatiles in mineralizing plutonic systems for which MI are rare and typically crystallized (i.e., MI that are difficult to locate, prepare, and analyze).

In our assessment, these initial results are promising and indicate that additional experimentation is required to expand the ranges of the experimental apatite compositions to better fill the OH-F-Cl compositional space (Fig. 9A). Additional experiments for near end-member F-, Cl-, and OH-rich apatites, for example, are needed. Moreover, future experiments should cover a broader range in crustal pressures and work to better constrain the importance of melt composition on the exchanges of these volatile components between melt and apatite. Additionally, the role of other key magmatic volatile components, including CO_2 and reduced and oxidized S species in the fluids, should be investigated. Finally with regard to equilibrium during volatile exchange, future comparative testing would best involve either MI entrapped within apatite phenocrysts and/or MI and apatites co-entrapped within the same growth zones of other phenocrysts. Presumably, equilibration of apatite and melt would be better constrained in the latter two situations.

ACKNOWLEDGEMENTS

Always consult and cite the final, published document. See http:/www.minsocam.org or GeoscienceWorld

This is a preprint, the final version is subject to change, of the American Mineralogist (MSA)
Cite as Authors (Year) Title. American Mineralogist, in press.
(DOI will not work until issue is live.) DOI: http://dx.doi.org/10.2138/am-2017-5746

We appreciate discussions on apatite-melt thermodynamic relations with Philip Piccoli, Francis McCubbin, and Jeremy Boyce, and detailed reviews by D. Harlov and two anonymous referees. This research was supported by NSF awards EAR-0836741 and EAR-1219484 to JDW. Synthetic apatites used as microprobe standards were provided by Daniel Harlov.

Always consult and cite the final, published document. See http:/www.minsocam.org or GeoscienceWorld

This is a preprint, the final version is subject to change, of the American Mineralogist (MSA)
Cite as Authors (Year) Title. American Mineralogist, in press.
(DOI will not work until issue is live.) DOI: http://dx.doi.org/10.2138/am-2017-5746

REFERENCES

Aiuppa, A., Baker, D., and Webster, J.D. (2009) Halogens in volcanic systems. Chemical Geology, 263, 1-18, doi:10.1016/j.chemgeo.2008.10.005.

Antignano, A., and Manning, C. E. (2008) Fluorapatite solubility in H_2O and H_2O–NaCl at 700 to 900 °C and 0.7 to 2.0 GPa. Chemical Geology, 251, 112-119.

Audetat, A., and Lowenstern, J.B. (2014) Melt inclusions. In Holland, H.D., Turekian, K.K. (eds.) Geochemistry of Mineral Deposits, Treatise on Geochemistry (second edition), 13, 143-173, DOI: 10.1016/B978-0-08-095975-7.01106-2.

Baker, D.R. (2008) The fidelity of melt inclusions as records of melt composition. Contributions to Mineralogy and Petrology, 156, 377-395.

Barnes, J.J., Tartese, R., Anand, M., McCubbin, F.M., Franchi, I.A., Starkey, N.A., and Russell, S.S. (2014) The origin of water in the primitive Moon as revealed by the lunar highlands samples. Earth and Planetary Science Letters, 390, 244-252.

Bodnar, R.J., Burnham, C.W., and Sterner, S.M. (1985) Synthetic fluid inclusions in natural quartz, III: determination of phase equilibrium properties in the system H_2O-NaCl to 1000°C and 1500 bars. Geochimica et Cosmochimica Acta, 49, 1861-1873.

Botcharnikov, R.E., Behrens, H., and Holtz, F. (2006) Solubility and speciation of C-O-H fluids in andesitic melt at T =1100°C and P=200 and 500 MPa. Chemical Geology, 229, 125-143.

Botcharnikov, R.E., Holtz, F., and Behrens, H. (2007) The effect of CO_2 on the solubility of H_2O-Cl fluids in andesitic melt. European Journal of Mineralogy, 19, 671-680.

Boyce, J.W., and Hervig, R. (2008) Magmatic degassing histories from apatite volatile stratigraphy. Geology, 36, 63-66, doi: 10.1130/G24184A.1.

Boyce, J.W., Tomlinson, S.M., McCubbin, F.M., Greenwood, J.P., and Treiman, A.H. (2014) The lunar apatite paradox. Science, 344, 400-402.

Boyce, J.W., Liu, Y., Rossman, G.R., Guan, Y., Eiler, J.M., Stolper, E.M., and Taylor, L.A. (2010) Lunar apatite with terrestrial volatile abundances. Nature, 466, 466-470.

Brenan, J. M. (1993) Partitioning of fluorine and chlorine between apatite and aqueous fluids at high pressure and temperature: Implications for the F and Cl content of high P-T fluids. Earth and Planetary Science Letters, 117(1–2), 251-263

Brenan, J.M. (1994) Kinetics of fluorine, chlorine and hydroxyl exchange in fluorapatite. Chemical Geology, 110, 195-210.

Candela, P.A. (1986) Toward a thermodynamic model for the halogens in magmatic systems: An application to melt-vapor-apatite equilibria. Chemical Geology, 57, 289-301.

Doherty, A., Webster, J.D. Goldoff, B., and Piccoli, P. (2014) Partitioning behavior of chlorine and fluorine in felsic melt–fluid(s)–apatite systems at 50 MPa and 850–950 °C. Chemical Geology, 384, 94-111, doi:10.1016/j.chemgeo.2014.06.023.

Dreisner, T., and Heinrich, C.A. (2007) The system H_2O-NaCl. Part I: Correlation formulae for phase relations in temperature-pressure-composition space from 0 to 1000°C, 0 to 5000 bar, and 0 to 1 X_{NaCl}. Geochimica et Cosmochimica Acta, 71, 4880-4901.

Always consult and cite the final, published document. See http:/www.minsocam.org or GeoscienceWorld

This is a preprint, the final version is subject to change, of the American Mineralogist (MSA)
Cite as Authors (Year) Title. American Mineralogist, in press.
(DOI will not work until issue is live.) DOI: http://dx.doi.org/10.2138/am-2017-5746

Esposito, R., Lamadrid, H.M., Redi, D., Steele-MacInnis, M., Bodnar, R.J., Manning, C.E., De Vivo, B., Cannatelli, C., Lima, A. (2016) Detection of liquid H_2O in vapor bubbles in reheated melt inclusions: Implications for magmatic fluid composition and volatile budgets of magmas. American Mineralogist, 101, 1691-1695.

Fleet, M.E., Liu X., and Pan Y. (2000) Site preference of rare earth elements in hydroxylapatite [$Ca_{10}(PO_4)_6(OH)_2$]. Journal of Solid State Chemistry 149, 391-398.

Ghiorso, M.S. and Gualda, G.A.R. (2015) An H_2O-CO_2 mixed fluid saturation model compatible with rhyolite-MELTS. Contributions to Mineralogy and Petrology, 169, 53-71.

Goldoff, B., Webster, J.D., and Harlov, D. (2012) Characterization of fluor-chlorapatites by electron probe microanalysis with a focus on time-dependent intensity variation of halogens. American Mineralogist, 97, 1103-1115, doi: 10.2138/am.2012.3812.

Greenwood, J.P., Itoh, S., Sakamoto, N., Warren, P., Taylor, L. and Yurimoto, H. (2011) Hydrogen isotope ratios in lunar rocks indicate delivery of cometary water to the Moon. Nature Geoscience, 4, 79-82.

Gross, J., Filiberto, J., and Bell, A.S. (2013) Water in the martian interior: Evidence for terrestrial MORB mantle-like volatile contents from hydroxyl-rich apatite in olivine-phyric shergottite NWA 62345. Earth and Planetary Science Letters, 369-370, 120-128.

Hughes, J.M., Heffernan, K.M., Goldoff, B., and Nekvasil, H. (2015) Cl-rich fluorapatite, devoid of OH, from the Three Peaks area, Utah: the first reported structure of natural Cl-rich fluorapatite. The Canadian Mineralogist, doi:10.3749/canmin.1400014.

Huppert, H., Sparks, R., and Turner, J. (1982) Effects of volatiles on mixing in calc-alkaline magma systems. Nature (London), 297, 554-557, doi:10.1038/297554a0.

Jarosewich, E., Nelen, J. A., and Norberg, J. A. (1980) Reference samples for electron microprobe analysis. Geostandards Newsletter 4(1), 43-47.

Kusebauch, C., John, T., Whitehouse, M.J., Klemme, S., and Putnis, A. (2015) Distribution of halogens between fluid and apatite during fluid-mediated replacement processes. Geochimica et Cosmochimica Acta, 170, 225-246.

Lowenstern, J.B. (1994) Chlorine, fluid immiscibility, and degassing in peralkaline magmas from Pantelleria, Italy. American Mineralogist, 79, 353-369.

Macdonald, R., Smith, R.L., and Thomas, J.E. (1992) Chemistry of the subalkalic silicic obsidians. US Geological Survey Professional Paper, 1523, 214 p.

Mandeville, C.M., Webster, J.D., Rutherford, M.J., Taylor, B.E., Timbal, A., and Faure, K. (2002) Determination of molar absorptivities for infrared absorption bands of H_2O in andesitic glasses. American Mineralogist, 87, 813-821.

Marks, M. A. W., Wenzel, T., Whitehouse, M. J., Loose, M., Zack, T., Barth, M., Worgard, L., Krasz, V., Eby, G. N., Stosnach, H., and Markl, G. (2012) The volatile inventory (F, Cl, Br, S, C) of magmatic apatite: An integrated analytical approach. Chemical Geology, 291, 241-255.

Mathez, E. A., and Webster, J. D. (2005) Partitioning behavior of chlorine and fluorine in the system apatite-silicate melt-fluid. Geochimica et Cosmochimica Acta, 69(5), 1275-1286.

Always consult and cite the final, published document. See http:/www.minsocam.org or GeoscienceWorld

This is a preprint, the final version is subject to change, of the American Mineralogist (MSA)
Cite as Authors (Year) Title. American Mineralogist, in press.
(DOI will not work until issue is live.) DOI: http://dx.doi.org/10.2138/am-2017-5746

McCubbin, F.M., and Jones, R.H. (2015) Extraterrestrial apatite: planetary geochemistry to astrobiology. Elements, 11, 183-188.

McCubbin, F.M., Steele, A., Hauri, E.H., Nekvasil, H., Yamashita, S., and Hemley, F.J. (2010a) Nominally hydrous magmatism on the Moon. Proceedings of the National Academy of Sciences, 107, 11223-11228.

McCubbin, F.M., Steele, A., Nekvasil, H., Schnieders, A., Rose, T., Fries, M., Carpenter, P.K., and Jolliff, B.L. (2010b) Detection of structurally bound hydroxyl in fluorapatite from Apollo mare basalt 15058,128 using TOF-SIMS. American Mineralogist, 95, 1141-1150.

McCubbin, F.M., Boyce, J.W., Srinivasan, P., Santos, A.R., Elardo, S.M., Filiberto, J., Steele, A., and Shearer, C.K. (2016) Heterogeneous distribution of H_2O in the martian interior: Implications for the abundance of H2O in depleted and enriched mantle sources. Meteoritics & Planetary Science, In Press.

McCubbin, F.M., Vander Kaaden, K.E., Tartese, R., Whitson, E.S., Anand, M., Franchi, I.A., Mikhail, S., Ustunisik, G., Hauri, E.H., Wang, J., and Boyce, J.W. (2014) Apatite-melt partitioning in basaltic magmas: The importance of exchange equilibria and the incompatibility of the OH component in halogen-rich apatite. 45th Lunar and Planetary Science Conference, abs. 2741.

Moore, G., Vennemann, T., and Carmichael, I.S.E. (1998) An empirical model for the solubility of H_2O in magmas to 3 kilobars. American Mineralogist, 83, 36-42.

Moore, L.R., Gazel, E., Tuohy, R., Lloyd, A.D., Esposito, R., Steele-MacInnis, M., Hauri, E.H., Wallace, P.J., Plank, T., and Bodnar, R.J . (2015) Bubbles matter: An assessment of the contribution of vapor bubbles to melt inclusion volatile budgets. American Mineralogist, 100, 806-823.

Nadeau, P.A., Webster, J.D., Mandeville, C.W., Goldoff, B.A., Shimizu, N., and Monteleone, B. (2015) A glimpse into Augustine volcano's pre-glacial past: insight from a massive rhyolite deposit. Journal of Volcanology and Geothermal Research, 304, 304-323.

Newman, S., and Lowenstern, J. B. (2002) VolatileCalc: A silicate melt–H_2O–CO_2 solution model written in visual basic for excel. Computers & Geosciences, 28, 597-604.

Nowak, M., and Behrens, H. (1995) The speciation of water in haplogranitic glasses and melts determined by in situ near-infrared spectroscopy. Geochimica et Cosmochimica Acta, 59, 3345-3450.

Pan, Y., and Fleet, M. (2002) "Compositions of apatite-group minerals: Substitution mechanisms and controlling factors." In M.J. Kohn, J. Rakovan, and J.M. Hughes, Eds., Phosphates - Geochemical, Geobiological, and Materials Importance, 48, p.13-49. Reviews in Mineralogy and Geochemistry, Mineralogical Society of America, Chantilly, Virginia.

Patel, P.N. (1980) Magnesium calcium hydroxylapatite solid solutions. Journal of Inorganic Nuclear Chemistry, 42, 1129-1132.

Patiño Douce, A.E., and Roden, M.F. (2006) Apatite as a probe of halogen and water fugacities in the terrestrial planets. Geochimica et Cosmochimica Acta, 70, 3173-3196.

Patiño Douce, A.E., Roden, M.F., Chaumba, J., Fleisher, C., and Yogodzinski, G. (2011)

Always consult and cite the final, published document. See http:/www.minsocam.org or GeoscienceWorld

This is a preprint, the final version is subject to change, of the American Mineralogist (MSA)
Cite as Authors (Year) Title. American Mineralogist, in press.
(DOI will not work until issue is live.) DOI: http://dx.doi.org/10.2138/am-2017-5746

Compositional variability of terrestrial mantle apatites, thermodynamic modeling of apatite volatile contents, and the halogen and water budgets of planetary mantles. Chemical Geology, 288, 14-31.

Peng, G.Y., Luhr, J.F., and McGee, J.J. (1997) Factors controlling sulfur concentrations in volcanic apatite. American Mineralogist, 82, 1210-1224.

Piccoli, P.M. (1992). Apatite chemistry in felsic magmatic systems." PhD dissertation, University of Maryland, College Park, Maryland.

Piccoli, P. M., and Candela, P. A. (2002) Apatite in igneous systems. In M.J. Kohn, J. Rakovan, and J.M. Hughes, Eds., Phosphates - Geochemical, Geobiological, and Materials Importance, 48, p.255-292. Reviews in Mineralogy and Geochemistry, Mineralogical Society of America, Chantilly, Virginia.

Roman, D. C., Cashman, K. V., Gardner, C. A., Wallace, P. A., and Donovan, J. J. (2006) Storage and interaction of compositionally heterogeneous magmas from the 1986 eruption of Augustine volcano, Alaska. Bulletin of Volcanology, 68, 240-254.

Sarafian, A.R., Roden, M.F. and Patino-Douce, A.E. (2013) The volatile content of Vesta: Clues from apatite in eucrites. Meteoritics & Planetary Science, 48, 2135-2154.

Schmidt, B.C., and Behrens, H. (2008) Water solubility in phonolite melts: Influence of melt composition and temperature. Chemical Geology, 256, 259-268.

Shinohara, H. (1994) Exsolution of immiscible vapor and liquid phases from a crystallizing silicate melt: implications for chlorine and metal transport. Geochimica et Cosmochimica Acta, 58, 5215-5221.

Shinohara, H., Ilyama, J.T., and Matsuo, S. (1989) Partition of chlorine compounds between silicate melt and hydrothermal solutions: Partition of NaCl-KCl. Geochimica et Cosmochimica Acta, 53, 2617-2630.

Signorelli, S., and Carroll, M.R. (2000) Solubility and fluid-melt partitioning of Cl in hydrous phonolite melts. Geochimica et Cosmochimica Acta, 64, 2851-2862.

Stock, M.J., Humphreys, M.C.S., Smith, V.C., Johnson, R.D., and Pyle, D.M. (2015) Apatite as magmatic volatile probe: quantifying the mechanisms and rates of EPMA-induced halogen migration. American Mineralogist, 100, 281-293.

Stock, M.J., Humphreys, M.C.S., Smith, V.C., Isaia, R., and Pyle, D.M. (2016) Late-stage volatile saturation as a potential trigger for explosive volcanic eruptions. Nature Geoscience, DOI: 10.1038.NGEO2639.

Stormer, J.C., Pierson, M.L., and Tacker, R.C. (1993) Variation of F and Cl X-ray intensity due to anisotropic diffusion in apatite during electron microprobe analysis. American Mineralogist, 78, 641–648.

Symonds, R.B., Rose, W.I., Gerlach, T.M., Briggs, P.H., and Harmon, R.S. (1990) Evaluation of gases, condensates, and SO_2 emissions from Augustine volcano, Alaska: the degassing of a Cl-rich volcanic system. Bulletin Volcanology, 52(5), 355–374.

Tacker, R.C. (2004) Hydroxyl ordering in igneous apatite. American Mineralogist, 89, 1411-1421.

Tappen, C., Webster, J., Mandeville, C., and Roderick, D. (2009) Petrology and geochemistry

Always consult and cite the final, published document. See http:/www.minsocam.org or GeoscienceWorld

This is a preprint, the final version is subject to change, of the American Mineralogist (MSA)
Cite as Authors (Year) Title. American Mineralogist, in press.
(DOI will not work until issue is live.) DOI: http://dx.doi.org/10.2138/am-2017-5746

of ca. 2100–1000 a.b.p. magmas of Augustine volcano, Alaska, based on analysis of prehistoric pumiceous tephra. Journal of Volcanology and Geothermal Research, 183, 42-62, doi: 10.1016/j.jvolgeores.2009.03.007.

Tartese, R., Anand, M., Barnes, J.J., Starkey, N.A., Franchi, I.A., and Sano, Y. (2013) The abundance, distribution, and isotopic composition of hydrogen in the Moon as revealed by basaltic lunar samples: implications for the volatile inventory of the Moon. Geochimica et Cosmochimica Acta, 122, 58-74.

Tartese, R., Anand, M., McCubbin, F.M., Elardo, S.M., Shearer, C.K., and Franchi, I.A. (2014) Apatites in lunar KREEP basalts: The missing link to understanding the H isotope systematics of the Moon. Geology 42, 363-366.

Vander Kaaden, K.E., McCubbin, F.M., Whitson, E.S., Hauri, E.H., and Wang, J. (2012) Partitioning of F, Cl, and H_2O between apatite and a synthetic Shergottite liquid (QUE 94201) at 1.0 GPa and 990-1000°C. 43rd Lunar and Planetary Science Conference, abs. 1247.

Wallace, P.J., Kamenetsky, V.S., and Cervantes, P. (2015) Melt inclusion CO_2 contents, pressures of olivine crystallization, and the problem of shrinkage bubbles. American Mineralogist, 100, 787-794.

Webster, J.D. (1992) Water solubility and chlorine partitioning in Cl-rich granitic systems: Effects of melt composition at 2 kbar and 800°C. Geochimica et Cosmochimica Acta, 56, 679-687.

Webster, J.D., and Mandeville, C.W. (2007) Fluid immiscibility in volcanic systems. In: A. Leibscher, C. Heinrich, eds., Fluid-Fluid Equilibria in the Crust, Reviews in Mineralogy and Geochemistry, 65, 313-362.

Webster, J.D., and Rebbert C.R. (1998) Experimental investigation of H_2O and Cl solubilities in F-enriched silicate liquids: implications for volatile saturation of topaz rhyolite magmas. Contributions to Mineralogy and Petrology, 132, 198-207.

Webster, J.D., Tappen, C., and Mandeville, C. (2009) Partitioning behavior of chlorine and fluorine in the system apatite-melt-fluid; II, Felsic silicate systems at 200 MPa. Geochimica et Cosmochimica Acta, 73, 559-581, doi:10.1016/j.gca.2008.10.034.

Webster, J.D., Mandeville, C., Goldoff, B., Coombs, M., and Tappen, C. (2010) Augustine Volcano; the influence of volatile components in magmas erupted A.D. 2006 to 2,100 years before present. U.S. Geological Survey Professional Paper, 383-423.

Webster, J.D., Goldoff, B., and Shimizu, N. (2011) COHS fluids and granitic magma: how S partitions and modifies CO_2 concentrations of fluid-saturated felsic melt at 200 MPa. Contributions to Mineralogy and Petrology, 162, 849-865.

Webster, J.D., Piccoli, P., and Goldoff, B.A. (2012) Resolving histories of magmatic volatiles in fluids and silicate melts as a function of pressure, temperature, and melt composition through apatite geochemistry (abs.). EOS, V21D-02.

Webster, J.D., Sintoni, M.F., Goldoff, B., De Vivo, B., and Shimizu, N. (2014) C-O-H-S-Cl-F volatile component solubilities and partitioning in phonolitic-trachytic melts and aqueous-carbonic vapor ± saline liquid at 200 MPa. Journal of Petrology 55(11), 2217-2248.

Webster, J.D., Vetere, F., Botcharnikov, R.E., Goldoff, B., McBirney, A., and Doherty, A.L. (2015) Experimental and modeled chlorine solubilities in aluminosilicate melts at 1 to

Always consult and cite the final, published document. See http:/www.minsocam.org or GeoscienceWorld

This is a preprint, the final version is subject to change, of the American Mineralogist (MSA)
Cite as Authors (Year) Title. American Mineralogist, in press.
(DOI will not work until issue is live.) DOI: http://dx.doi.org/10.2138/am-2017-5746

7000 bars and 700 to 1250°C: Applications to magmas of Augustine Volcano, Alaska. American Mineralogist, 100, 522-535.

Wolf, M.B., and London, D. (1994) Apatite dissolution into peraluminous haplogranitic melts: An experimental study of solubilities and mechanisms. Geochimica et Cosmochimica Acta, 58, 4127-4145.

Always consult and cite the final, published document. See http:/www.minsocam.org or GeoscienceWorld

This is a preprint, the final version is subject to change, of the American Mineralogist (MSA)
Cite as Authors (Year) Title. American Mineralogist, in press.
(DOI will not work until issue is live.) DOI: http://dx.doi.org/10.2138/am-2017-5746

FIGURE CAPTIONS

1. Plot comparing the Cl concentrations of aqueous run-product liquids measured by chloridometer with Cl concentrations of fluids (vapor, brine, or integrated vapor plus brine) calculated by mass balance for run conditions. See text for description of methods used. Solid curve is the 1:1 line. Red circles designate 200 MPa and 748 - 775 °C, green diamonds designate ca. 50 MP and 850 °C, and blue squares designate 50 MPa and 1000 °C runs. The reason for the outlier, noted with the question mark, is unknown.

2. Plots comparing the measured H_2O versus measured Cl concentrations of fluid- and apatite-saturated melts (A) and (measured Cl content/modeled Cl solubility) ratios of melts (B). At 200 MPa, the bold, solid horizontal curve displays H_2O and Cl contents where silicate melt is stable with vapor. The bold vertical curves designate melt plus brine stabilities for the maximum Cl solubility in the most primitive melt (solid curve) and the minimum Cl solubility for most felsic (most evolved) melt (dashed curve). The intersection point of the bold vertical and horizontal curves is where melt, vapor, and brine are stable. Phase relations are equivalent for 50 MPa conditions (fine curves). In (B) all of the vertical curves overlap at unity for the (measured Cl content of melts/modeled Cl solubility in melts) ratio. Chlorine solubility computed using the model of Webster et al. (2015). Symbols are the same as in Figure 1.

3. Plots comparing pfu contents of (A) Na (circles) and Mg (squares) versus Cl; (B) Si (circles) and S (diamonds) versus Cl; (C) (Ce+Na) versus (Ca+Ca); and (D) (S+Si) versus (P+P) of run product apatites for ca. 50 MPa and 850 °C experiments.

4. Plots comparing the Cl concentrations of fluid(s) versus the measured Cl concentrations of apatite-saturated melts (A) and the (measured Cl content/modeled Cl solubility) ratio of melts (B). In (A), the data show significant dispersion as a function of pressure, temperature, and subtle differences in melt composition (see text for discussion). Nevertheless the Cl concentrations of the felsic melts increase rapidly with increasing Cl contents in the fluid(s). In (B), the dispersion of Cl concentrations in the melt is reduced for all 50 MPa runs by normalizing to the computed Cl solubility of the melts accounting for differences in temperature and melt composition. These data show definitive increases in the (measured Cl content/modeled Cl solubility) ratio of the melts with increasing Cl in the fluid(s). With the (measured Cl content/modeled Cl solubility) ratio of the melts at unity, all additional excess Cl partitions in favor of the fluid(s) and apatite (see Fig. 5) as the melt contains its maximum Cl solubility. Symbols are the same as in Figure 1, except the violet triangles represent 100 MPa and 1000 °C runs of this study and the black circles designate apatite-free Cl partitioning experiments for felsic melts at 50 MPa and 910 to 930 °C of (Webster and Rebbert 1998). The 50 MPa Cl partitioning results of this study are highly consistent with those of Webster and Rebbert (1998). Chlorine solubility computed using the model of Webster et al. (2015).

5. Plots comparing the ($X_{Cl}^{apat}/X_{OH}^{apat}$) ratio versus the (measured Cl content/modeled Cl solubility) ratio of the melts for this investigation (A) and this study in comparison with similar experiments involving rhyodacitic melts of Doherty et al. (2014) (B). With increasing Cl in the system, both the ($X_{Cl}^{apat}/X_{OH}^{apat}$) and the (measured Cl content/modeled Cl solubility) ratios increase, until the (measured Cl content/modeled Cl solubility) ratio of the melts achieves unity and all additional excess Cl partitions in favor of apatites and the

Always consult and cite the final, published document. See http:/www.minsocam.org or GeoscienceWorld

This is a preprint, the final version is subject to change, of the American Mineralogist (MSA)
Cite as Authors (Year) Title. American Mineralogist, in press.
(DOI will not work until issue is live.) DOI: http://dx.doi.org/10.2138/am-2017-5746

fluid(s) because the melt contains its maximum Cl solubility. Plot (B) shows that the exchange of Cl and OH between apatite and the high-silica rhyolitic melts of this study is consistent with that involving the rhyodacitic melts of Doherty et al. (2014) – all at 50 MPa. Symbols are the same as in Figure 4, except that the green lozenge symbols designate experiments for felsic melts at 900 to 920 °C (Doherty et al. 2014). Chlorine solubility is computed using the model of Webster et al. (2015). Symbols labeled SQ represent experimental charges that experienced a slow, non-isobaric quench.

6. Plot displaying the exchange of Cl and OH (or H_2O) between apatite and fluids, expressed as the ($X_{Cl}^{apat}/X_{OH}^{apat}$) ratio versus the ($X_{Cl}^{fluid(s)}/X_{H2O}^{fluid(s)}$) ratio for runs at 50 MPa. The exchange relationship is linear and near vertical up to values of the ($X_{Cl}^{apat}/X_{OH}^{apat}$) ratio of ca. 0.8. With increasing Cl content in the system, the slope of the exchange relation decreases. Symbols are the same as in Figure 4.

7. Plots showing the $K_{dCl\text{-}F}^{apat\text{-}melt}$(circles), $K_{dOH\text{-}Cl}^{apat\text{-}melt}$(squares), and $K_{dOH\text{-}F}^{apat\text{-}melt}$ (triangles) (see text for definition of these exchange coefficients) versus the molar (A/CNK)/(N/NK) ratio for the experiments from this study. We apply larger symbols to highlight those experiments involving relatively lower propagated imprecisions on the exchange coefficients that are less than 100 rel%. These highlighted data demonstrate statistically valid increasing $K_{dCl\text{-}F}^{apat\text{-}melt}$ and decreasing $K_{dOH\text{-}Cl}^{apat\text{-}melt}$ with changing melt composition and pressure-temperature conditions. If the anomalous run with the lowest molar (A/CNK)/(N/NK) ratio (identified with a question mark) is treated as an outlier, then the statistical significance of these relations increases. See text for discussion.

8. Plots displaying the ($X_{H2O}^{melt}/X_{Cl}^{melt}$) ratio versus the ($X_{OH}^{apat}$)/($X_{Cl}^{apat}$) ratio for runs with rhyolitic melts (A) and those for rhyodacitic and rhyolitic melts at 50 to 200 MPa that empirically support equation (10) (B). All melts have 0.88 < A/CNK < 1.1 and N/NK > 0.55. The apatites are distinguished by pfu (Si/Mg) ratios > 6 (squares fit by dashed curve) and with (6 > Si/Mg > 0.3) (triangles fit by solid curve). Data for rhyolitic runs are from this study and those for rhyodacitic runs are from Webster et al. (2009) for 200 MPa and Doherty et al. (2014) for 50 MPa.

9. Plot displaying the averaged mole fractions of F, OH, and Cl for the experimental apatites of this study, Webster et al. (2009), and Doherty et al. (2014) used to generate equation (10) (A), and the averaged compositions of natural apatites from 9 samples representing 7 different eruptive units of Augustine volcano, Alaska (B). Symbols in (A) are the same as in Figure 1. The downward-pointing triangle represents 50 MPa run of Doherty et al. (2014). The upward-pointing triangles represent 200 MPa data of Webster et al. (2009). Symbols in (B) include right-pointing triangle = sample AUJW004 erupted 2006; diamond = sample from the 1986 eruption; square = prehistoric tephra erupted ca. 1000 years before present (a.b.p.); upward-pointing triangle = prehistoric tephra erupted ca. 1700 a.b.p.; downward-pointing triangle = prehistoric tephra erupted ca. 2100 a.b.p.; filled rectangle = prehistoric tephra erupted ca. 1400 a.b.p.; open rectangle = massive Pleistocene flow-banded rhyolite; open circle = massive Pleistocene white pumice; and filled circle = massive Pleistocene yellow pumice. The black curves outlining the data in (A) indicate the compositional region of applicability for equation (10) based on the error-propagated spread in mole fractions of OH, F, and Cl in the apatite data, and for (B) outline the error-propagated spread in natural apatite compositional variability.

Always consult and cite the final, published document. See http:/www.minsocam.org or GeoscienceWorld

This is a preprint, the final version is subject to change, of the American Mineralogist (MSA)
Cite as Authors (Year) Title. American Mineralogist, in press.
(DOI will not work until issue is live.) DOI: http://dx.doi.org/10.2138/am-2017-5746

10. Plot comparing the average measured concentrations of H_2O in felsic silicate melt inclusions versus the H_2O concentrations in melt calculated from averaged apatite compositions from 9 samples representing 7 eruptive units of Augustine volcano, Alaska. Accounting for the 1-σ standard deviations for the measured H_2O in the melt inclusions and the propagated errors associated with the calculated H_2O contents from the apatite compositions, the two estimates of H_2O concentrations in these melts are mutually consistent for 6 of the samples. See text for discussion. The symbols are as follows: downward-pointing triangle = sample AUJW004 erupted 2006; circle = sample of the 1986 eruption; filled diamond = prehistoric tephra erupted ca. 1000 years before present (a.b.p.); square = prehistoric tephra erupted ca. 1700 a.b.p.; lozenge-shaped symbol = prehistoric tephra erupted ca. 2100 a.b.p.; upward-pointing filled triangle = prehistoric tephra erupted ca. 1400 a.b.p.; half-filled diamond = massive Pleistocene flow-banded rhyolite; half-filled square = massive Pleistocene white pumice; and half-filled triangle = massive Pleistocene yellow pumice. Sources of the melt inclusion data include 2100 to 1000 a.b.p. tephra (Tappen et al. 2009), the 1986 and 2006 eruptions (Webster et al. 2010), and the massive Pleistocene pumices (Nadeau et al. 2015).

APPENDIX

The mole fraction of H_2O in the fluid(s) is calculated with the equation:

$$X_{H_2O}^{fluids} = \frac{\dfrac{mass_{H_2O}^{fluids}}{18}}{\dfrac{mass_{H_2O}^{fluids}}{18} + \dfrac{mass_{Cl}^{fluids}}{35.453} + \dfrac{mass_{NaK}^{fluids}}{31}} \qquad \text{(I)}$$

and the mole fraction of Cl in the fluid(s) is calculated with the equation:

$$X_{Cl}^{fluid} = \frac{\dfrac{mass_{Cl}^{fluids}}{35.453}}{\dfrac{mass_{H2O}^{fluids}}{18} + \dfrac{mass_{Cl}^{fluids}}{35.453} + \dfrac{mass_{NaK}^{fluids}}{31}} \qquad \text{(II)}$$

recalling that the mass of 31 accounts for the moles of Cl that are chemically associated with an assumed equimolar quantity of Na and K (i.e., their averaged mass). Similarly, the X_{H2O}^{melt} and X_{Cl}^{melt} are calculated, respectively, with the equations:

Always consult and cite the final, published document. See http:/www.minsocam.org or GeoscienceWorld

This is a preprint, the final version is subject to change, of the American Mineralogist (MSA)
Cite as Authors (Year) Title. American Mineralogist, in press.
(DOI will not work until issue is live.) DOI: http://dx.doi.org/10.2138/am-2017-5746

$$X_{H_2O}^{melt} = \frac{\frac{mass_{H_2O}^{melt}}{18}}{\frac{mass_{H_2O}^{melt}}{18} + \frac{mass_{Cl}^{melt}}{35.453} + \frac{mass_{volatile-freemelt}^{melt}}{265}} \qquad \text{(III)}$$

and:

$$X_{Cl}^{melt} = \frac{\frac{mass_{Cl}^{melt}}{35.453}}{\frac{mass_{Cl}^{melt}}{35.453} + \frac{mass_{H_2O}^{melt}}{18} + \frac{mass_{volatile-freemelt}^{melt}}{265}} \qquad \text{(IV)}$$

Rearranging allows one to calculate the wt% H_2O in the melt with equation (V):

$$wt\%\ H_2O \text{ in melt} = \frac{18 * X_{H_2O}^{melt} * \left[\left(\frac{wt\%\ \text{Cl in melt}}{35.45}\right) + \left(\frac{(100 - inputwt\%\ H_2O \text{ in melt - } wt\%\ \text{Cl in melt})}{265}\right)\right]}{1 - X_{H_2O}^{melt}} \qquad \text{(V)}$$

This approach, however, requires the input of an initial estimate of the mass of H_2O in the melt (i.e., to estimate the *inputwt% H_2O in melt*) in order to solve equations (IV) and (V). It requires that this mass of H_2O in the melt be modified, iteratively, until its estimated equivalent concentration, i.e., ([mass of H_2O in melt/mass of melt]*100) ratio corresponds to the final H_2O concentration determined using the equation (V).

Always consult and cite the final, published document. See http:/www.minsocam.org or GeoscienceWorld

This is a preprint, the final version is subject to change, of the American Mineralogist (MSA)
Cite as Authors (Year) Title. American Mineralogist, in press.
(DOI will not work until issue is live.) DOI: http://dx.doi.org/10.2138/am-2017-5746

Figure 1

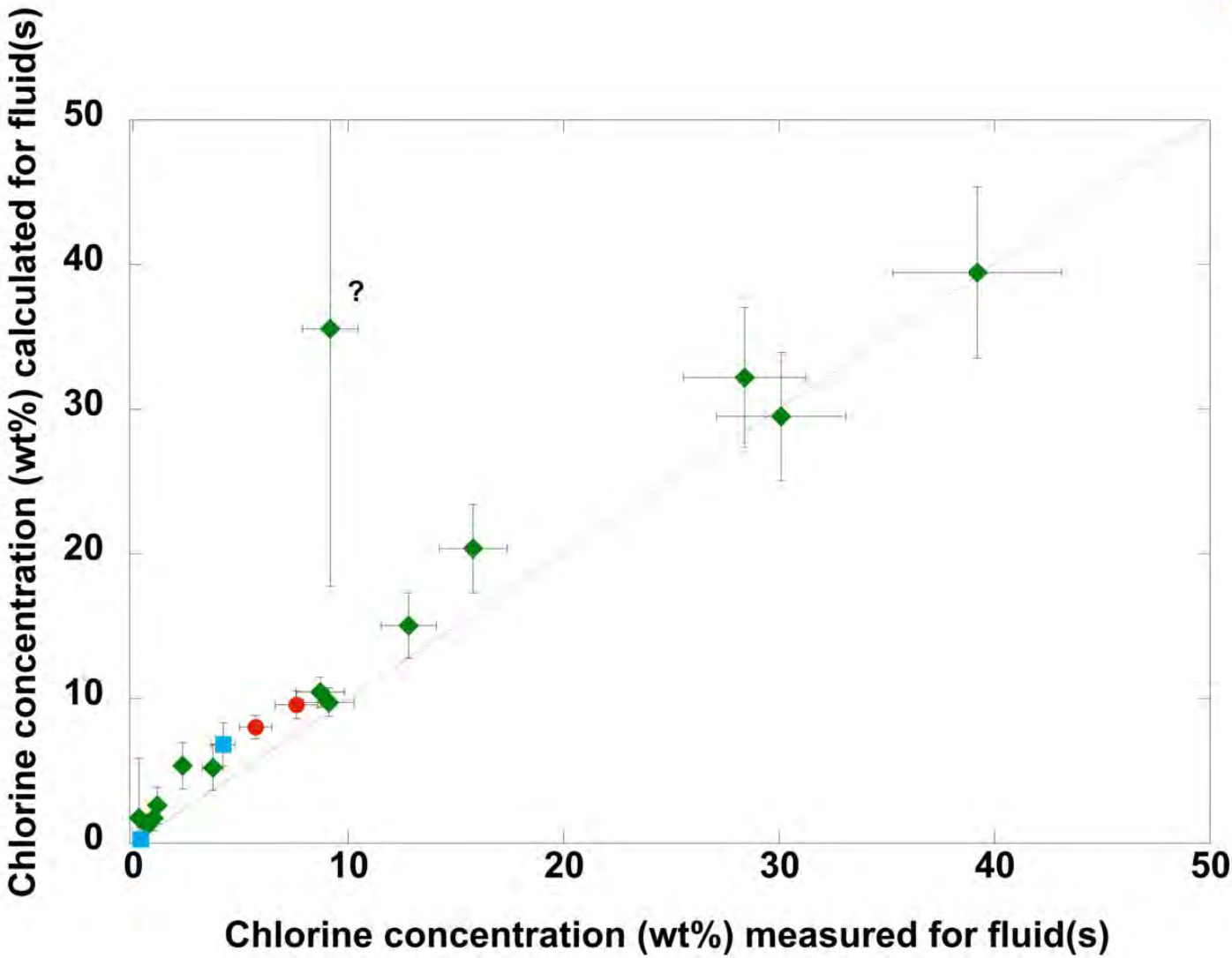

Always consult and cite the final, published document. See http:/www.minsocam.org or GeoscienceWorld

This is a preprint, the final version is subject to change, of the American Mineralogist (MSA)
Cite as Authors (Year) Title. American Mineralogist, in press.
(DOI will not work until issue is live.) DOI: http://dx.doi.org/10.2138/am-2017-5746

Figure 2A

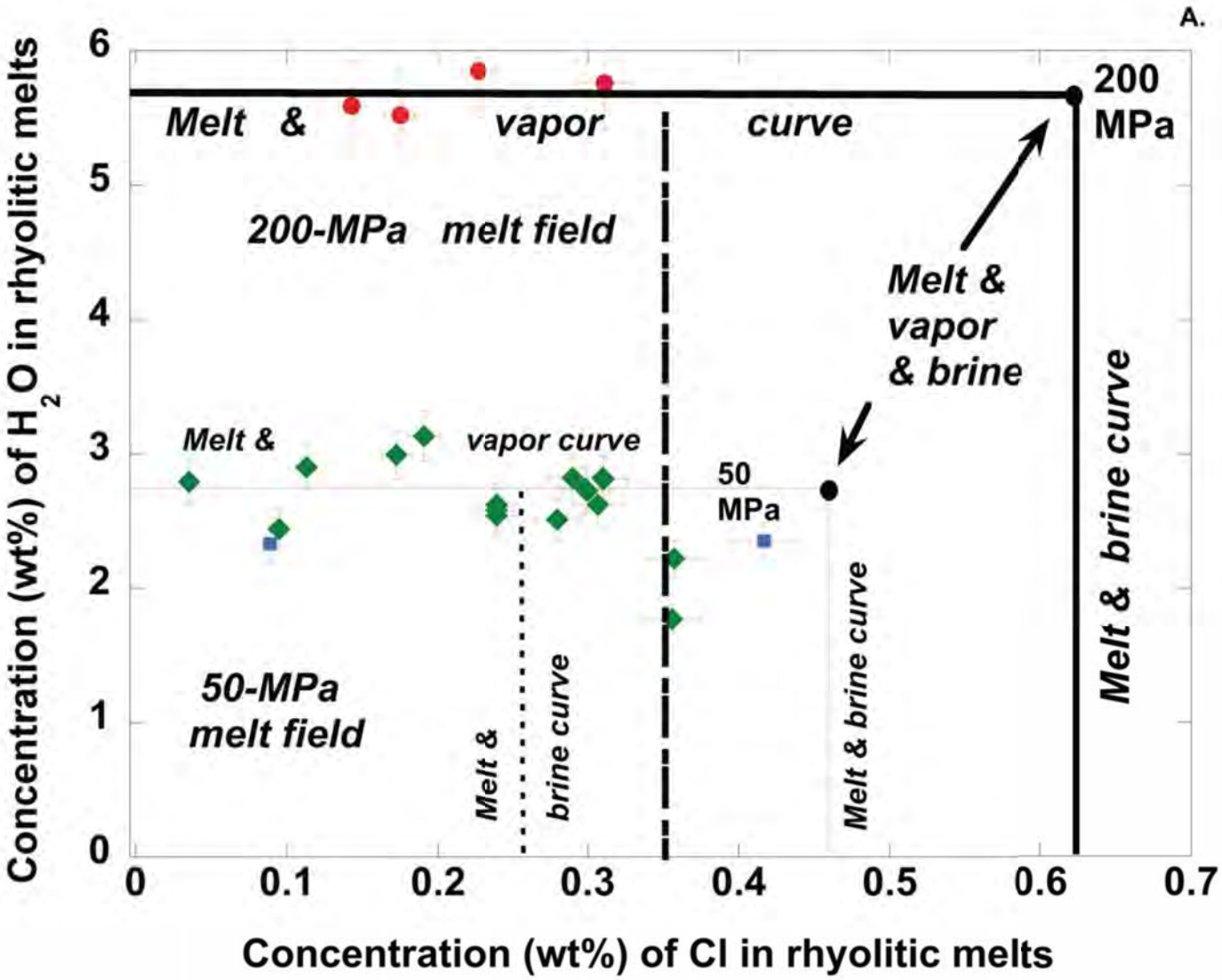

Always consult and cite the final, published document. See http:/www.minsocam.org or GeoscienceWorld

This is a preprint, the final version is subject to change, of the American Mineralogist (MSA)
Cite as Authors (Year) Title. American Mineralogist, in press.
(DOI will not work until issue is live.) DOI: http://dx.doi.org/10.2138/am-2017-5746

Figure 2B

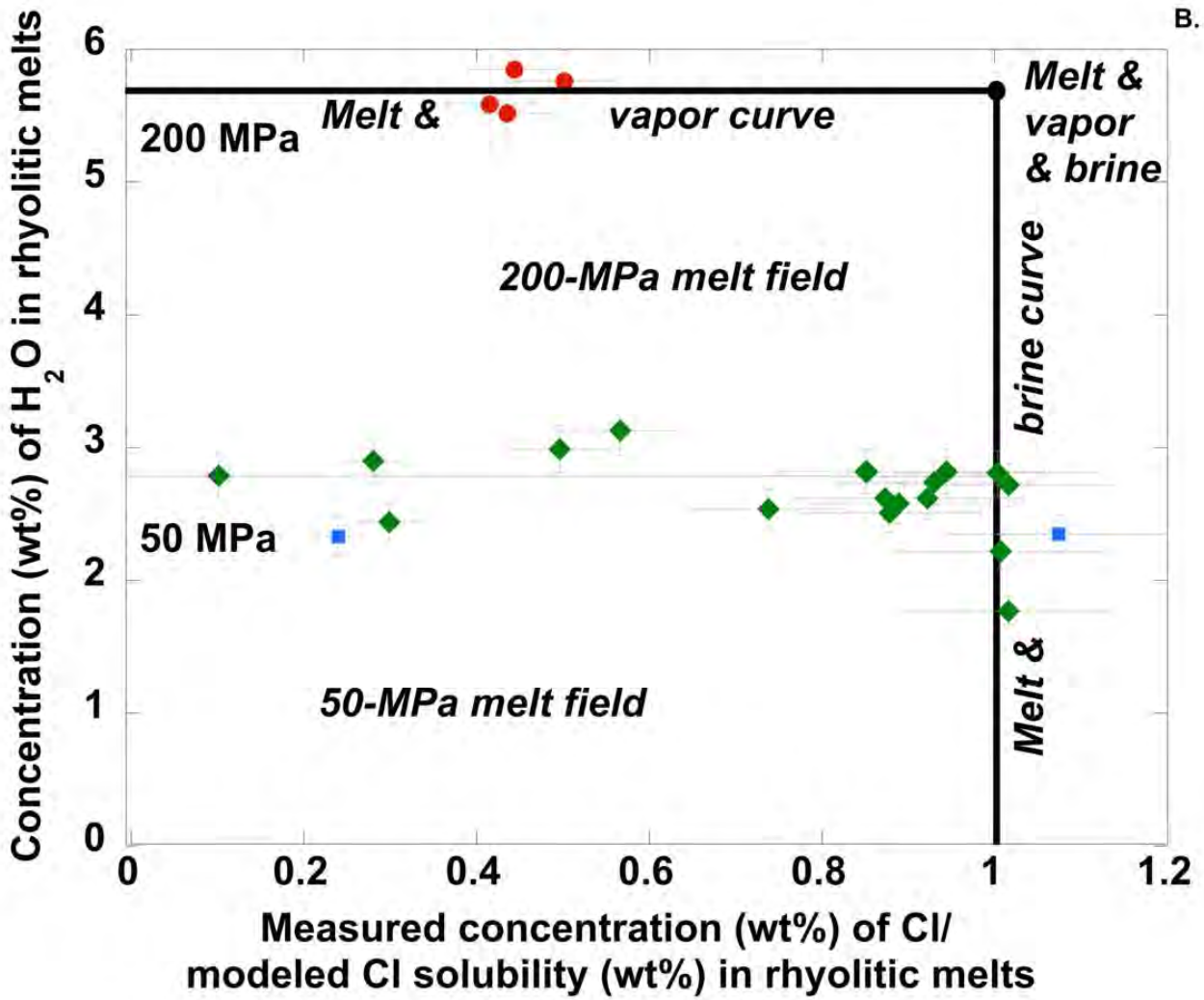

Always consult and cite the final, published document. See http:/www.minsocam.org or GeoscienceWorld

This is a preprint, the final version is subject to change, of the American Mineralogist (MSA)
Cite as Authors (Year) Title. American Mineralogist, in press.
(DOI will not work until issue is live.) DOI: http://dx.doi.org/10.2138/am-2017-5746

Figure 3A

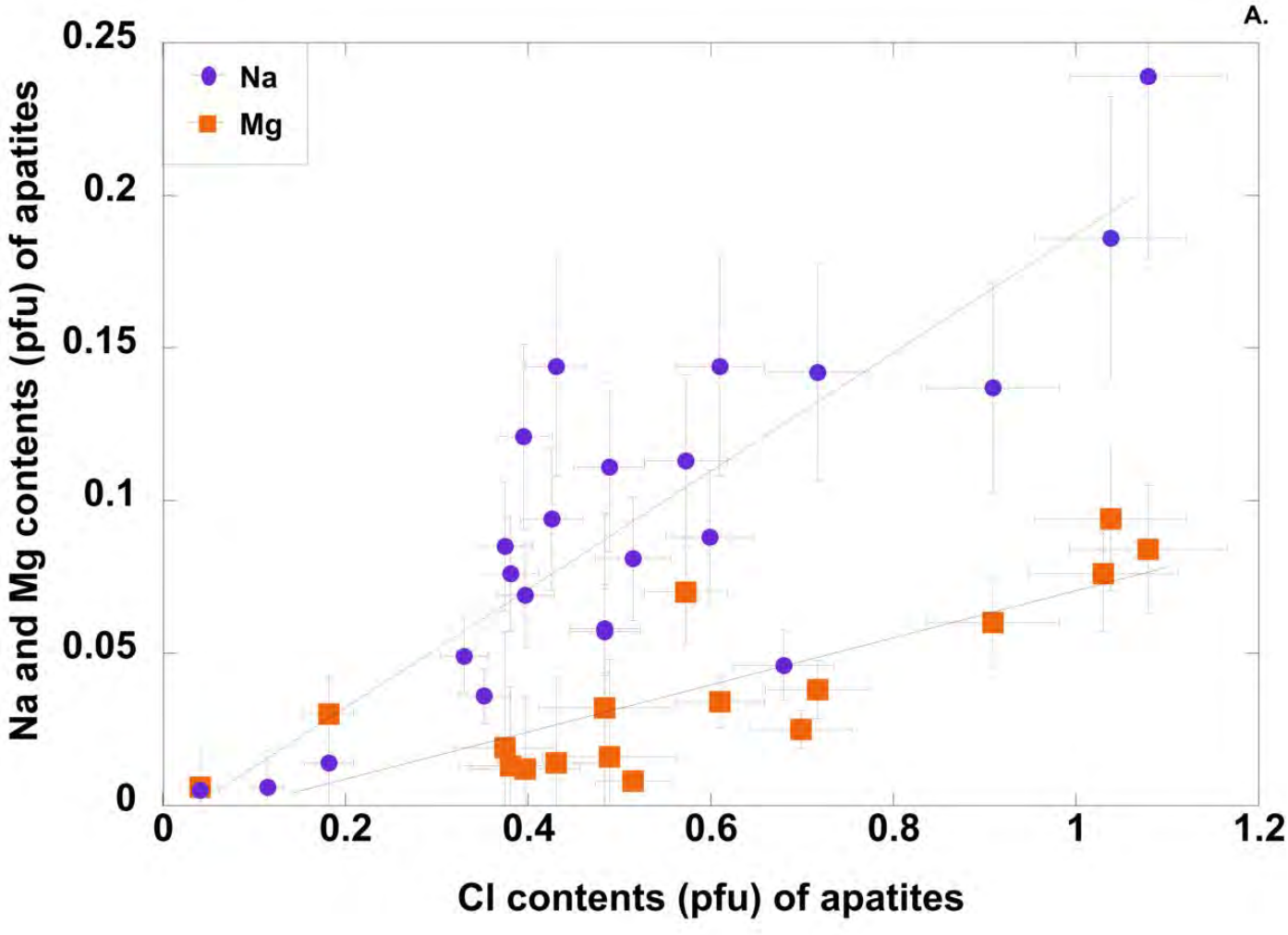

Always consult and cite the final, published document. See http:/www.minsocam.org or GeoscienceWorld

Figure 3B

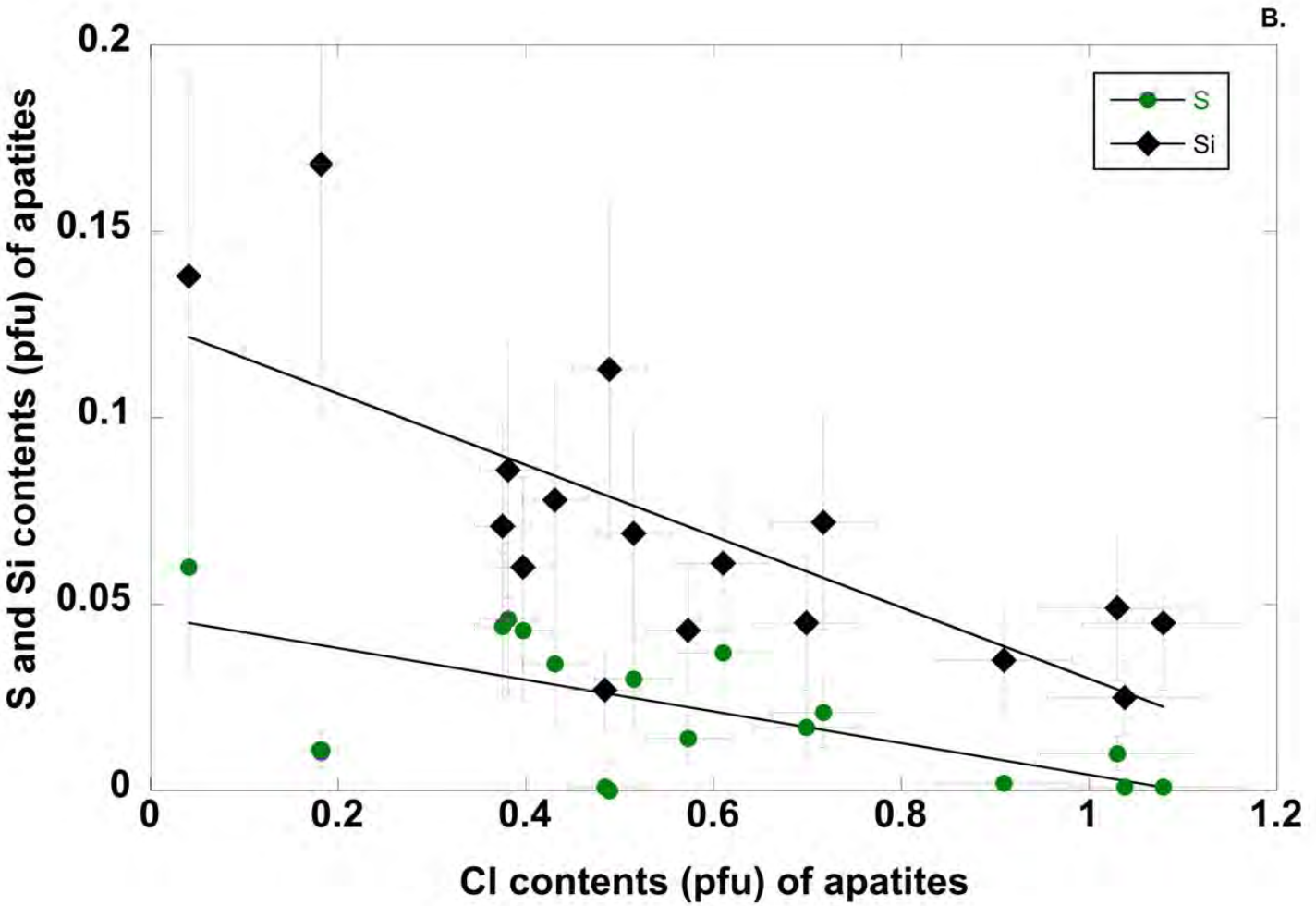
B.
S
Si
S and Si contents (pfu) of apatites
Cl contents (pfu) of apatites
0
0.05
0.1
0.15
0.2
0
0.2
0.4
0.6
0.8
1
1.2

This is a preprint, the final version is subject to change, of the American Mineralogist (MSA)
Cite as Authors (Year) Title. American Mineralogist, in press.
(DOI will not work until issue is live.) DOI: http://dx.doi.org/10.2138/am-2017-5746

Figure 3C

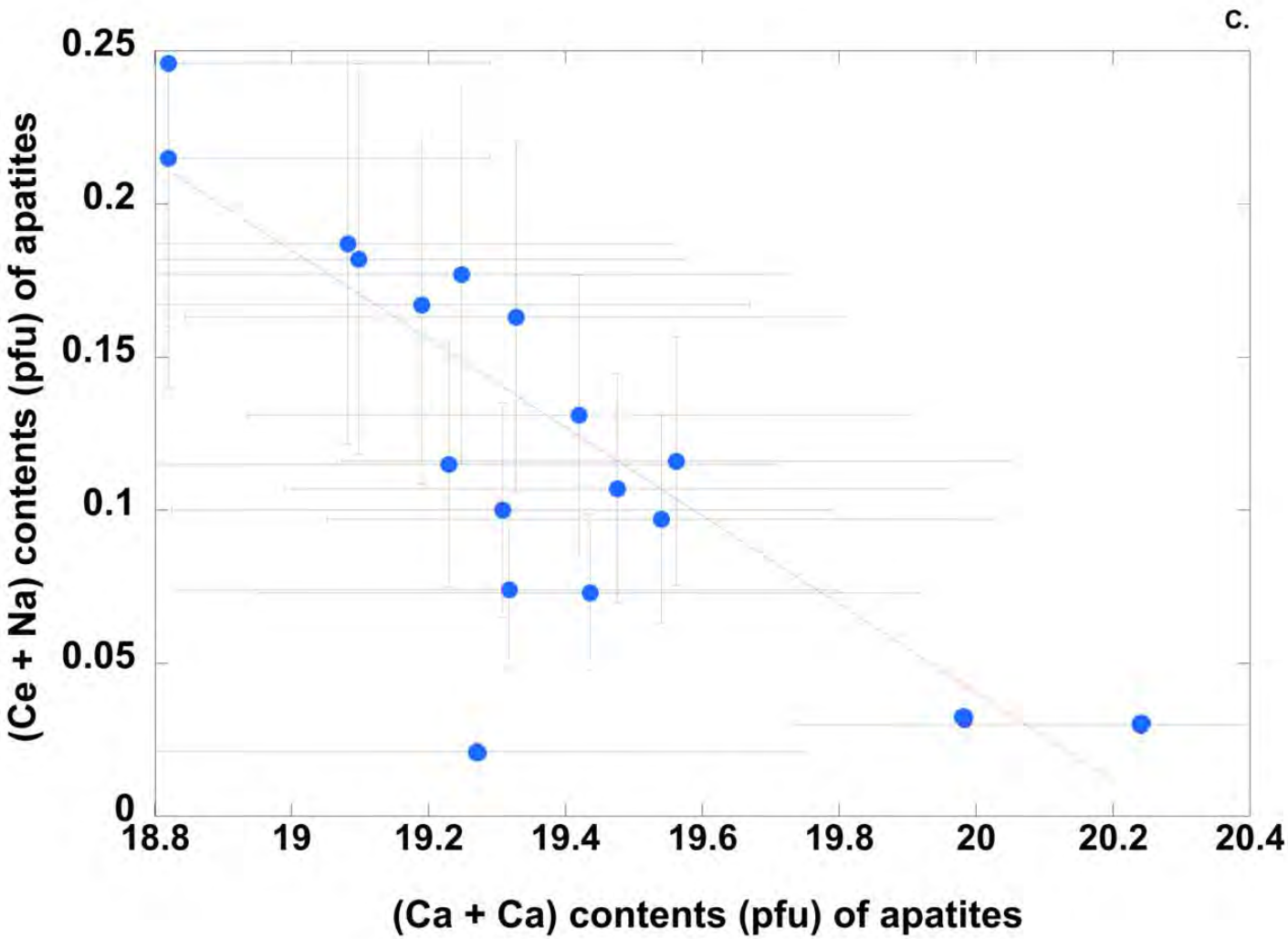

Always consult and cite the final, published document. See http:/www.minsocam.org or GeoscienceWorld

This is a preprint, the final version is subject to change, of the American Mineralogist (MSA)
Cite as Authors (Year) Title. American Mineralogist, in press.
(DOI will not work until issue is live.) DOI: http://dx.doi.org/10.2138/am-2017-5746

Figure 3D

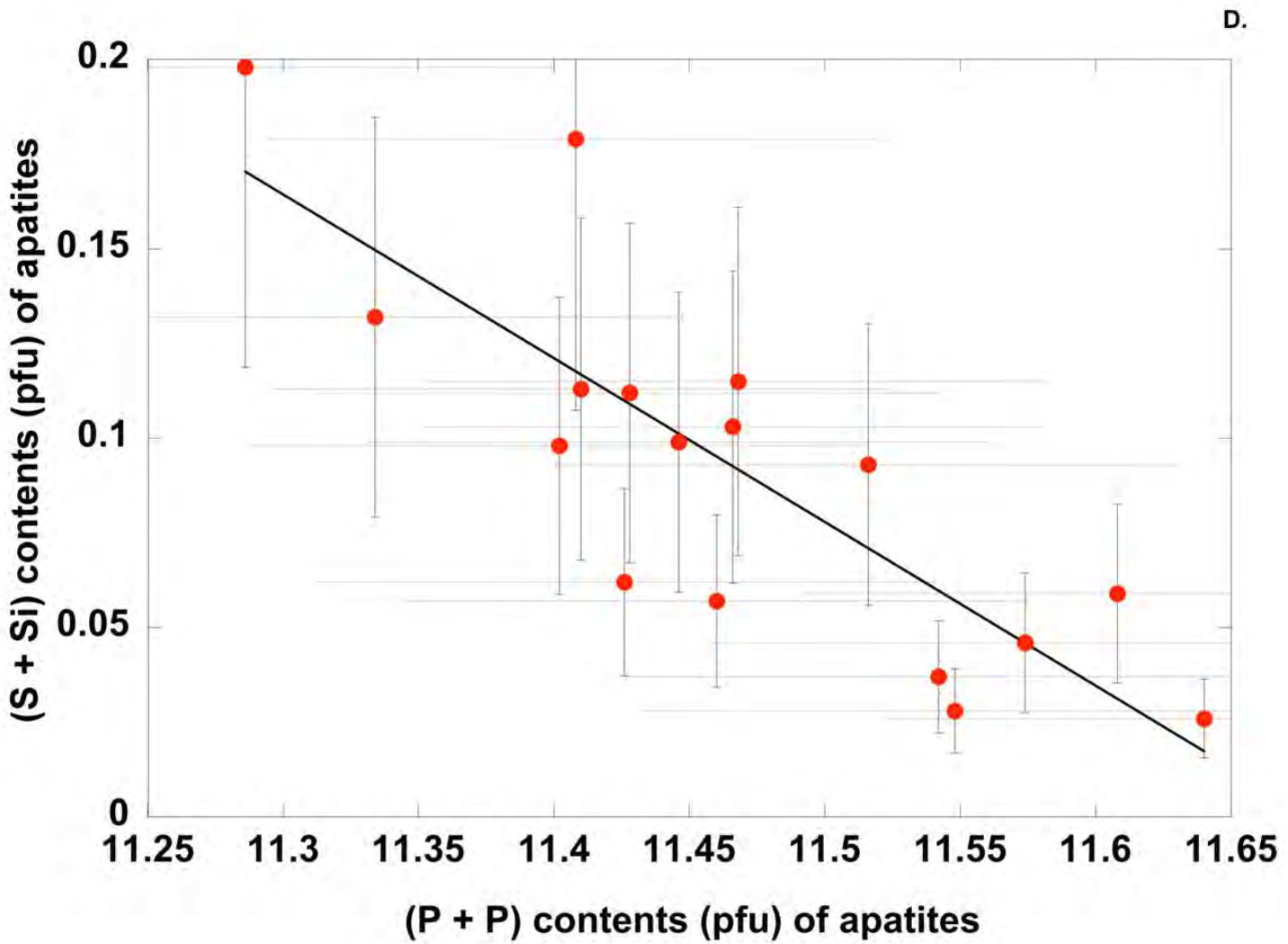

Always consult and cite the final, published document. See http:/www.minsocam.org or GeoscienceWorld

This is a preprint, the final version is subject to change, of the American Mineralogist (MSA)
Cite as Authors (Year) Title. American Mineralogist, in press.
(DOI will not work until issue is live.) DOI: http://dx.doi.org/10.2138/am-2017-5746

Figure 4A

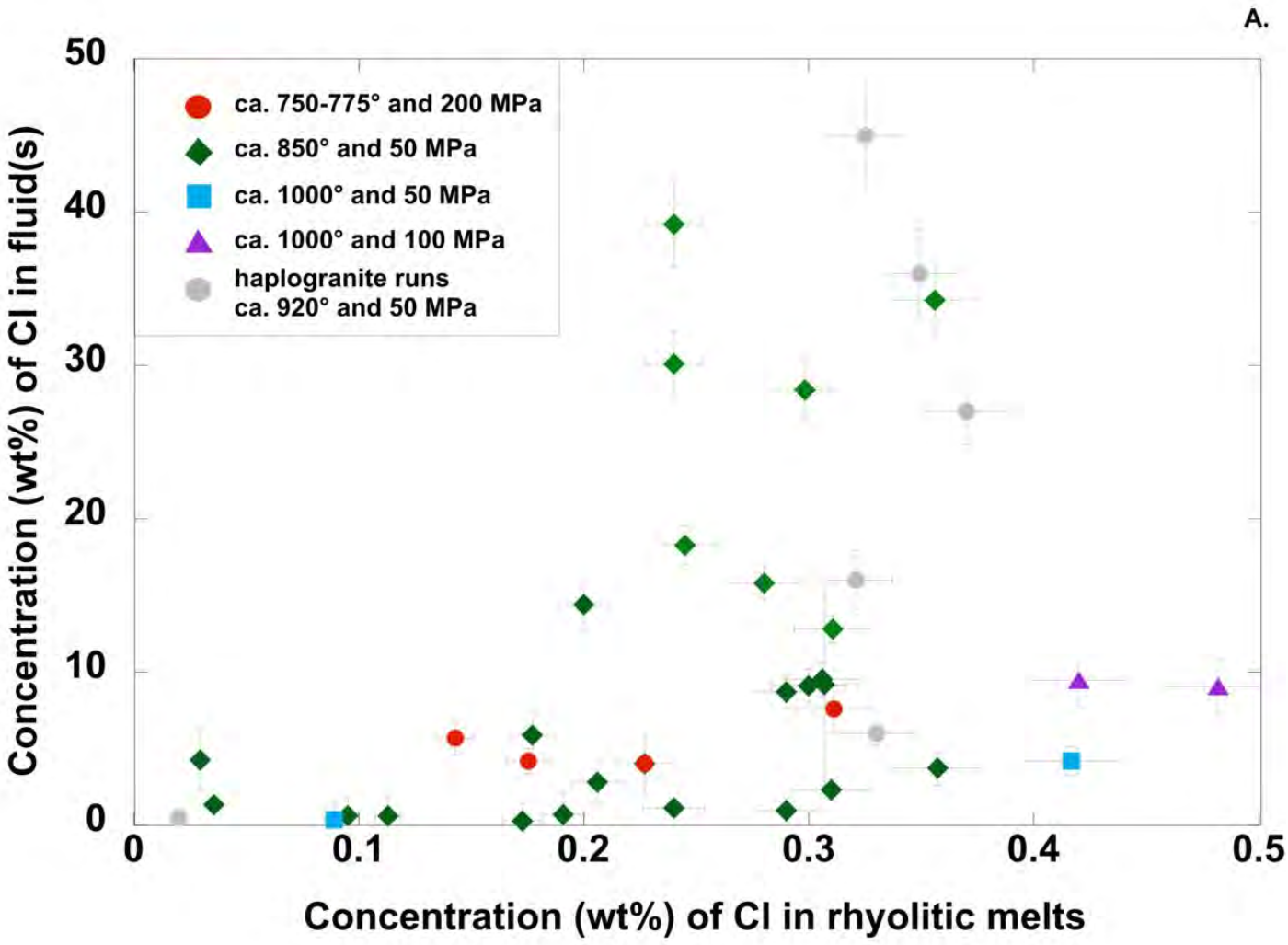

Always consult and cite the final, published document. See http:/www.minsocam.org or GeoscienceWorld

This is a preprint, the final version is subject to change, of the American Mineralogist (MSA)
Cite as Authors (Year) Title. American Mineralogist, in press.
(DOI will not work until issue is live.) DOI: http://dx.doi.org/10.2138/am-2017-5746

Figure 4B

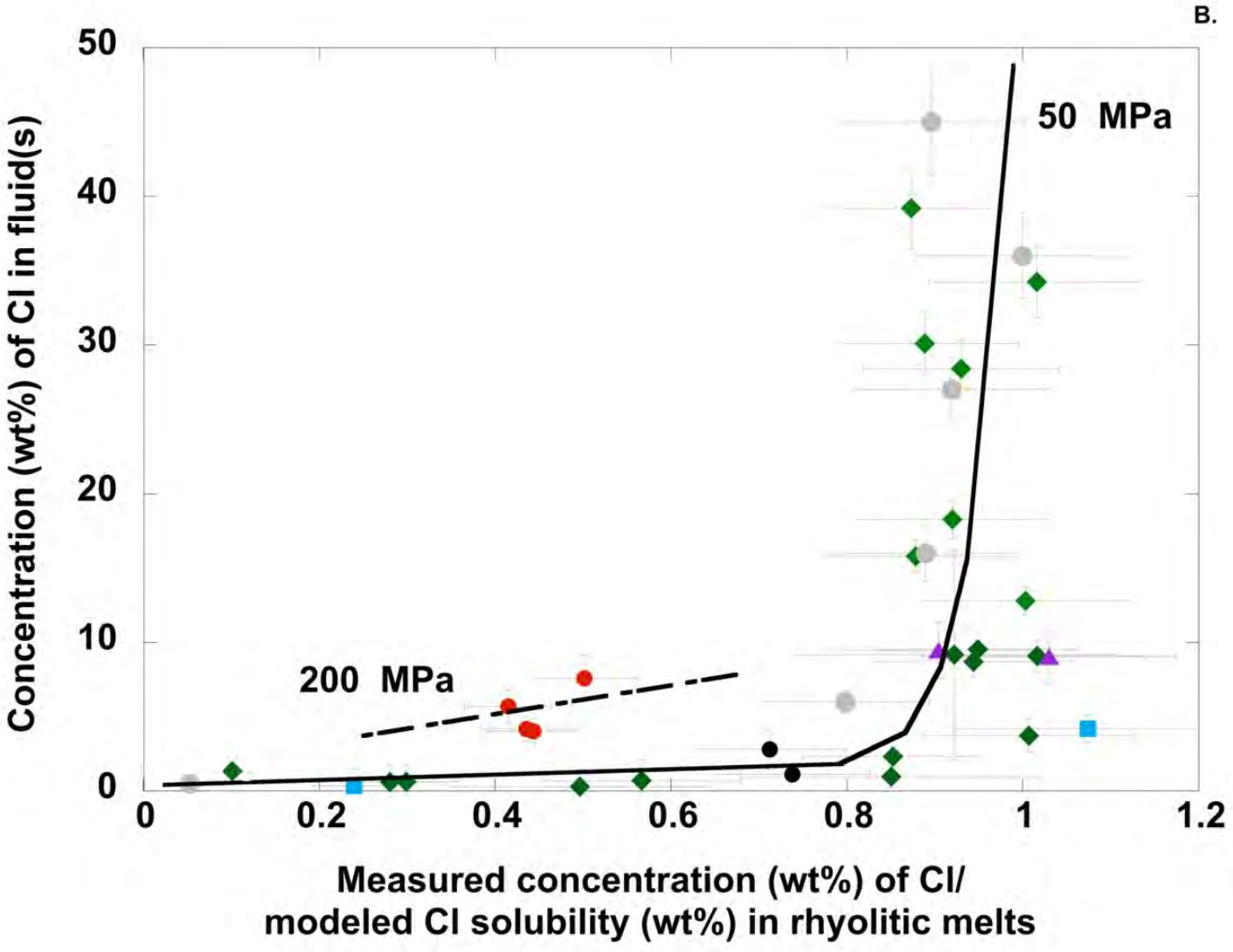

Always consult and cite the final, published document. See http:/www.minsocam.org or GeoscienceWorld

This is a preprint, the final version is subject to change, of the American Mineralogist (MSA)
Cite as Authors (Year) Title. American Mineralogist, in press.
(DOI will not work until issue is live.) DOI: http://dx.doi.org/10.2138/am-2017-5746

Figure 5A

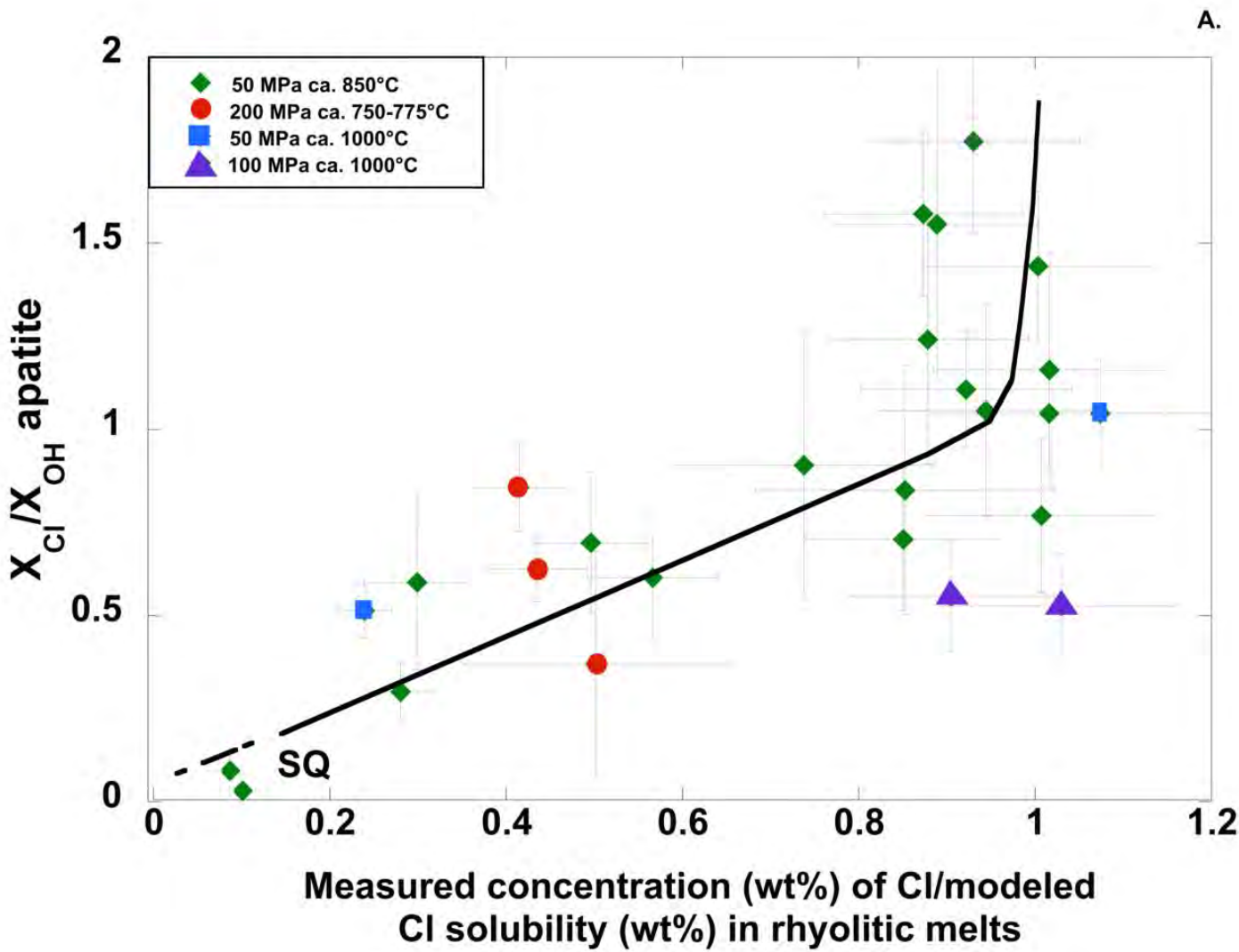

Always consult and cite the final, published document. See http:/www.minsocam.org or GeoscienceWorld

This is a preprint, the final version is subject to change, of the American Mineralogist (MSA)
Cite as Authors (Year) Title. American Mineralogist, in press.
(DOI will not work until issue is live.) DOI: http://dx.doi.org/10.2138/am-2017-5746

Figure 5B

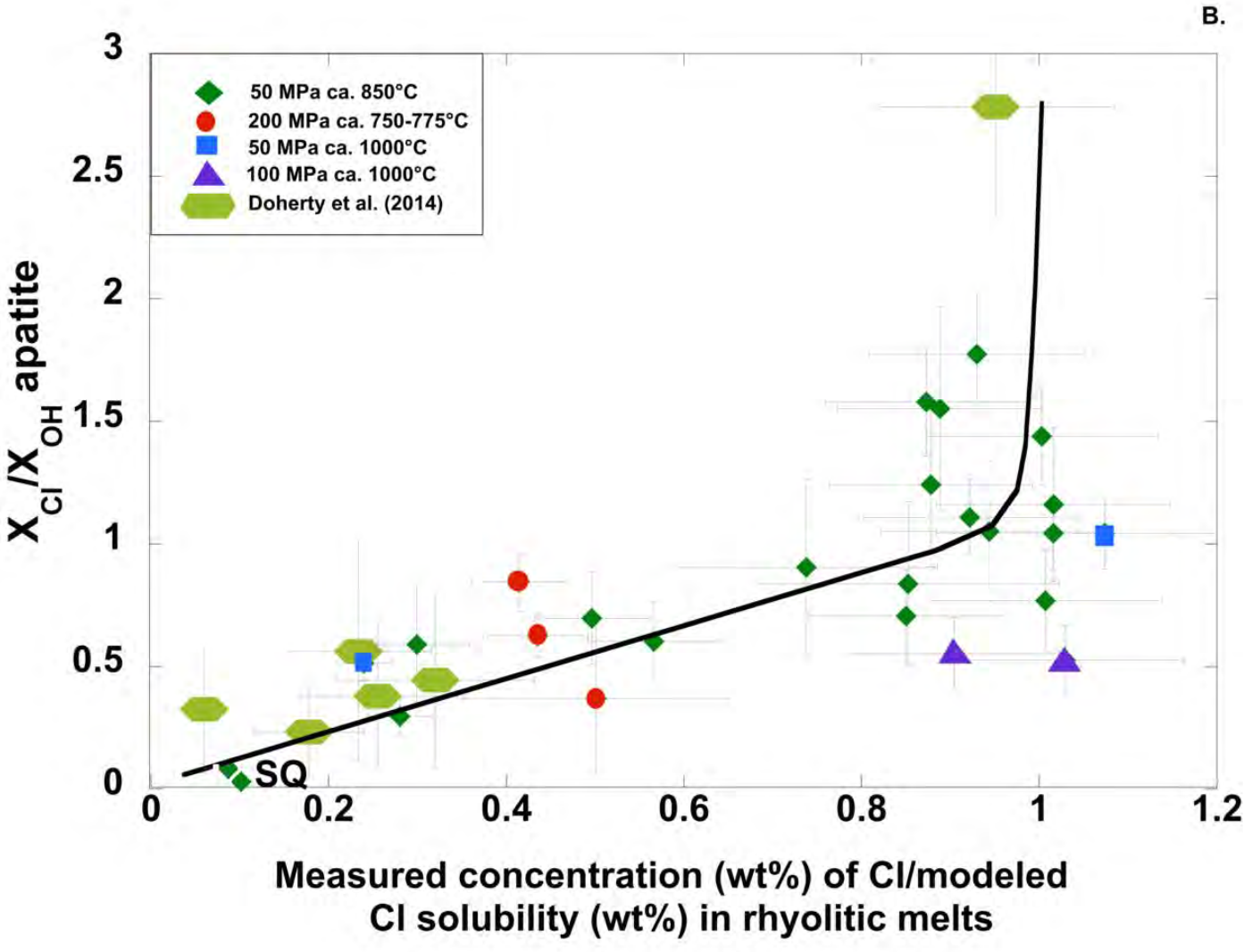

Always consult and cite the final, published document. See http:/www.minsocam.org or GeoscienceWorld

This is a preprint, the final version is subject to change, of the American Mineralogist (MSA)
Cite as Authors (Year) Title. American Mineralogist, in press.
(DOI will not work until issue is live.) DOI: http://dx.doi.org/10.2138/am-2017-5746

Figure 6

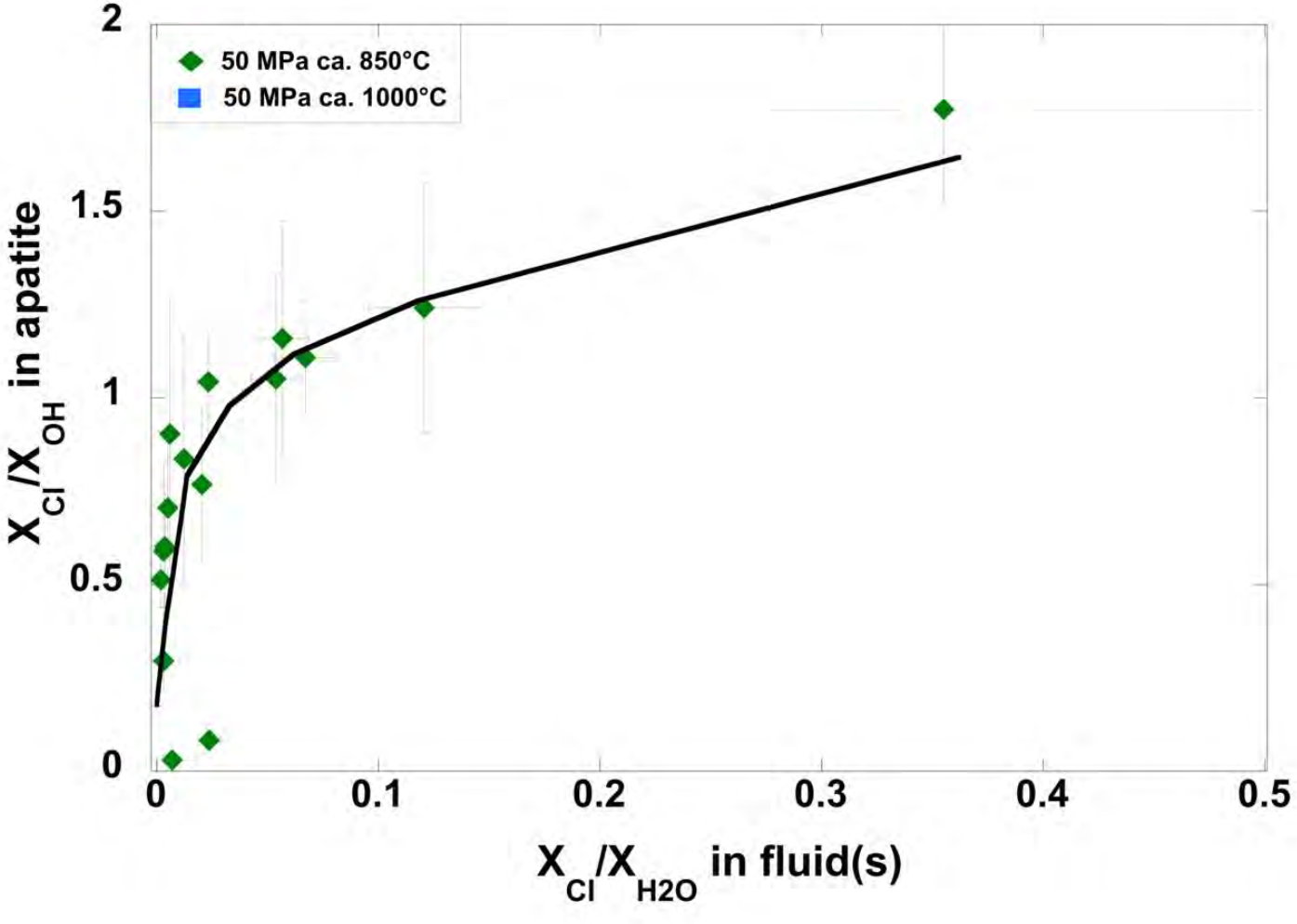

Always consult and cite the final, published document. See http:/www.minsocam.org or GeoscienceWorld

Figure 7

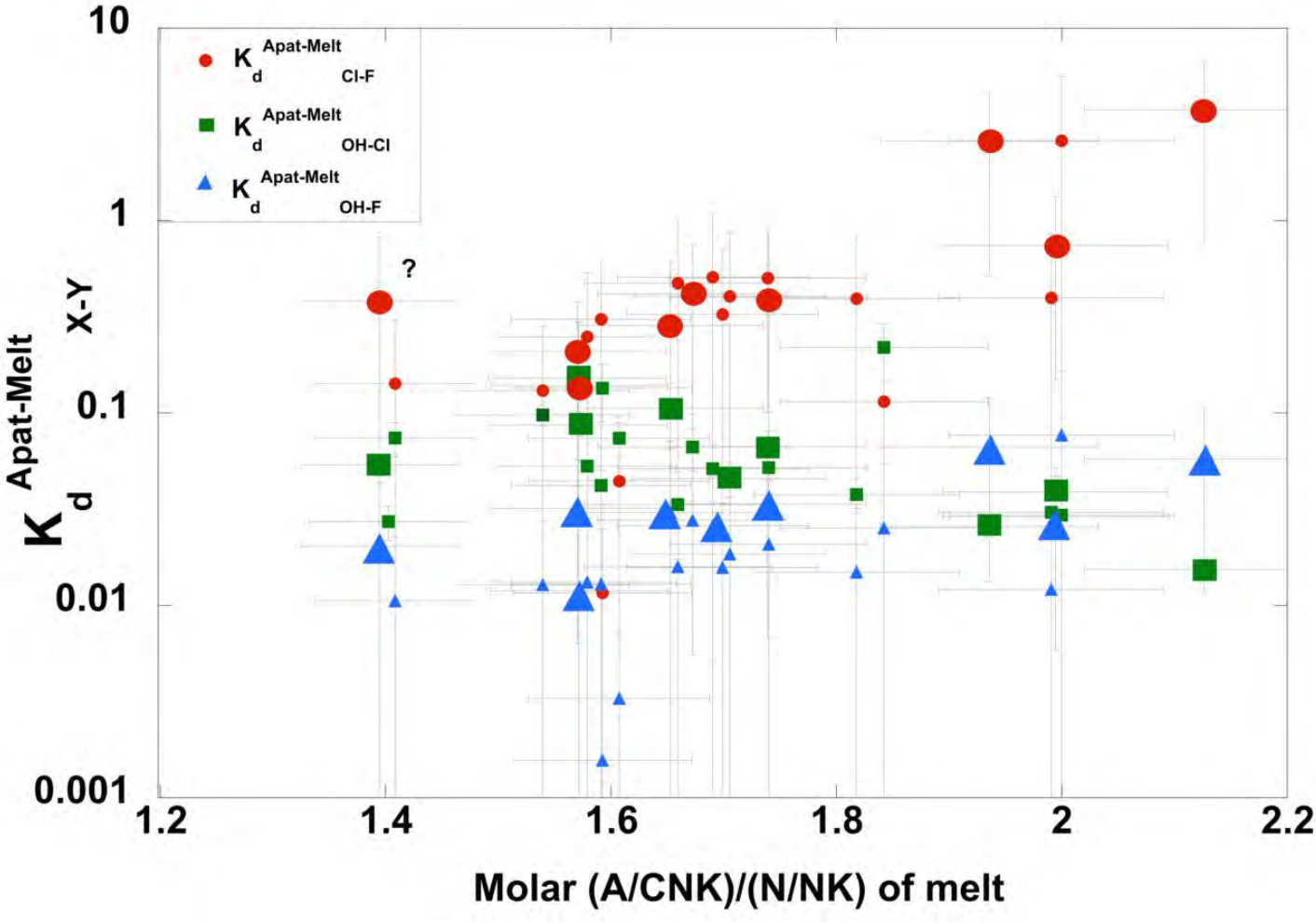
$K_d^{Apat-Melt}$ Cl-F
$K_d^{Apat-Melt}$ OH-Cl
$K_d^{Apat-Melt}$ OH-F
?
$K_d^{Apat-Melt}$ X-Y
10
1
0.1
0.01
0.001
1.2
1.4
1.6
1.8
2
2.2
Molar (A/CNK)/(N/NK) of melt

This is a preprint, the final version is subject to change, of the American Mineralogist (MSA)
Cite as Authors (Year) Title. American Mineralogist, in press.
(DOI will not work until issue is live.) DOI: http://dx.doi.org/10.2138/am-2017-5746

Figure 8A

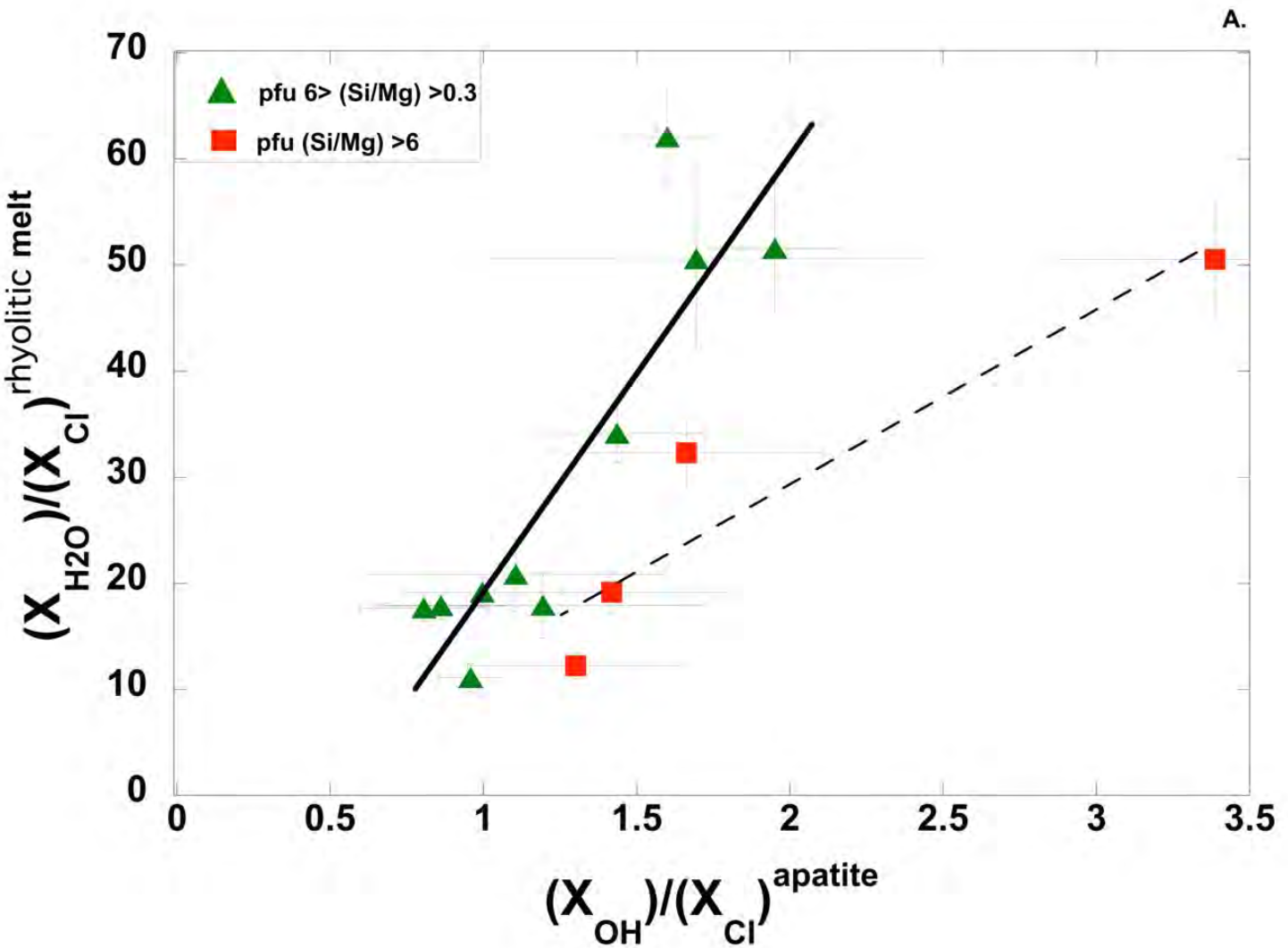

Always consult and cite the final, published document. See http:/www.minsocam.org or GeoscienceWorld

This is a preprint, the final version is subject to change, of the American Mineralogist (MSA)
Cite as Authors (Year) Title. American Mineralogist, in press.
(DOI will not work until issue is live.) DOI: http://dx.doi.org/10.2138/am-2017-5746

Figure 8B

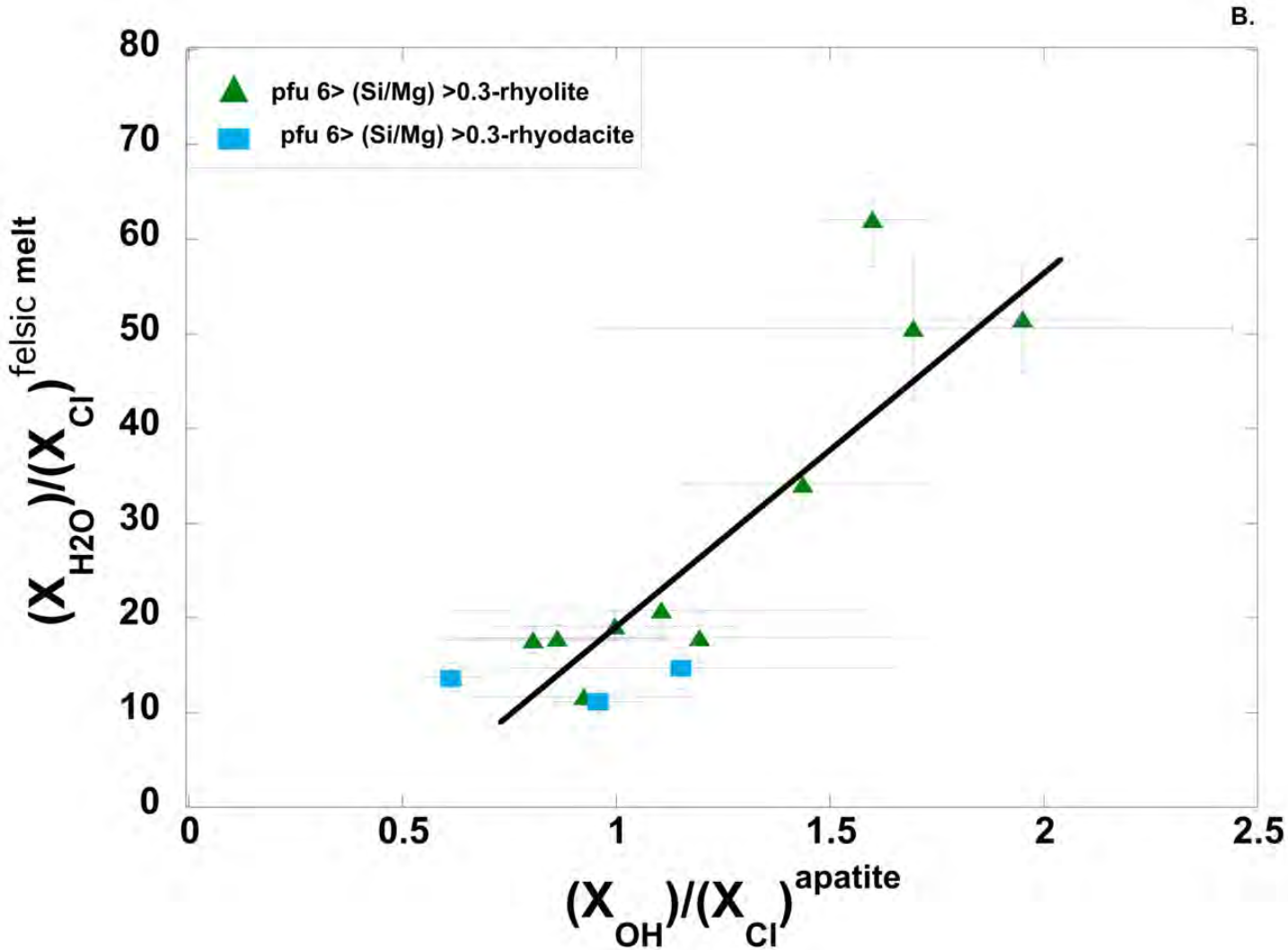

Always consult and cite the final, published document. See http:/www.minsocam.org or GeoscienceWorld

This is a preprint, the final version is subject to change, of the American Mineralogist (MSA)
Cite as Authors (Year) Title. American Mineralogist, in press.
(DOI will not work until issue is live.) DOI: http://dx.doi.org/10.2138/am-2017-5746

Figure 9A

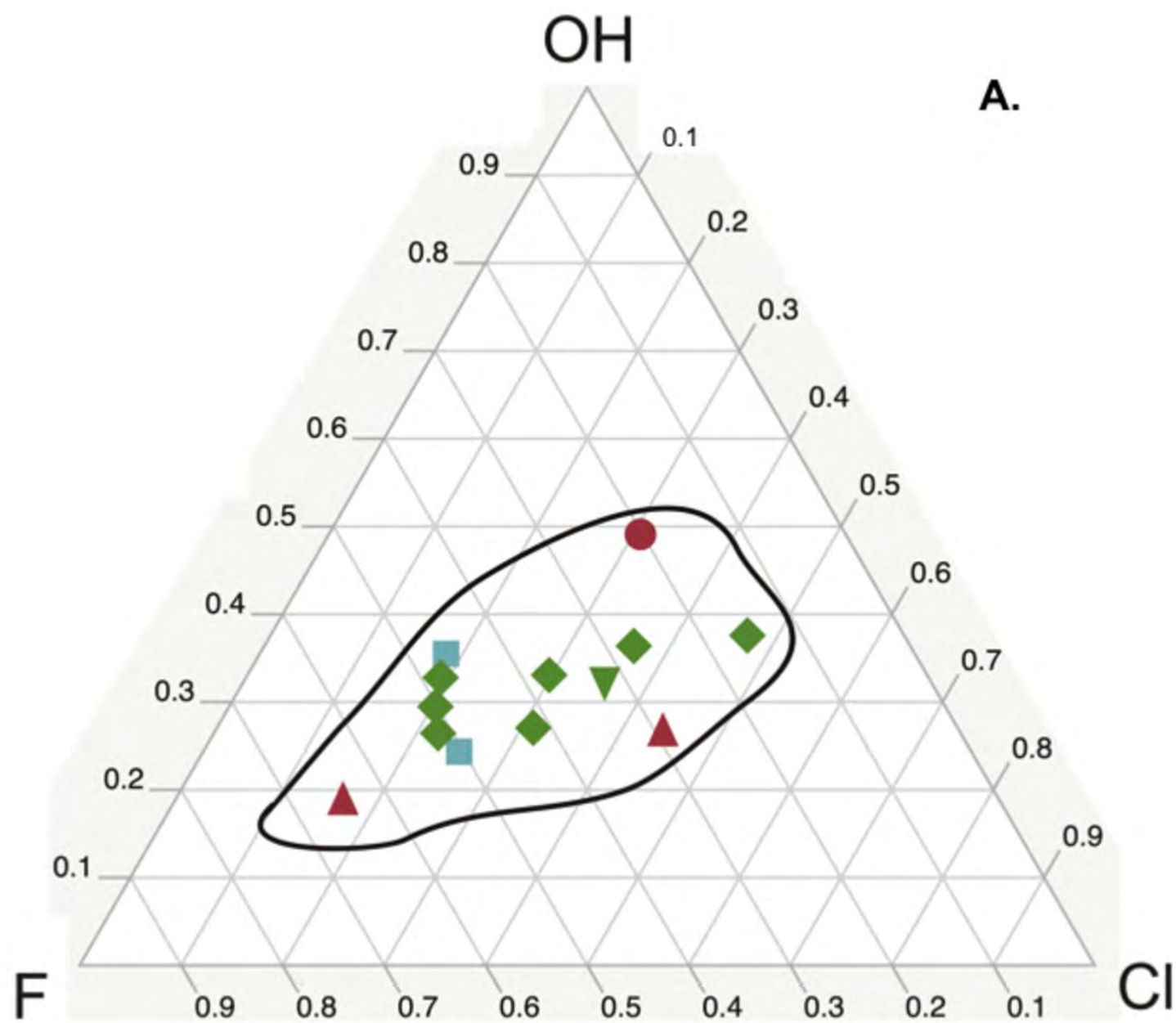

Always consult and cite the final, published document. See http:/www.minsocam.org or GeoscienceWorld

This is a preprint, the final version is subject to change, of the American Mineralogist (MSA)
Cite as Authors (Year) Title. American Mineralogist, in press.
(DOI will not work until issue is live.) DOI: http://dx.doi.org/10.2138/am-2017-5746

Figure 9B

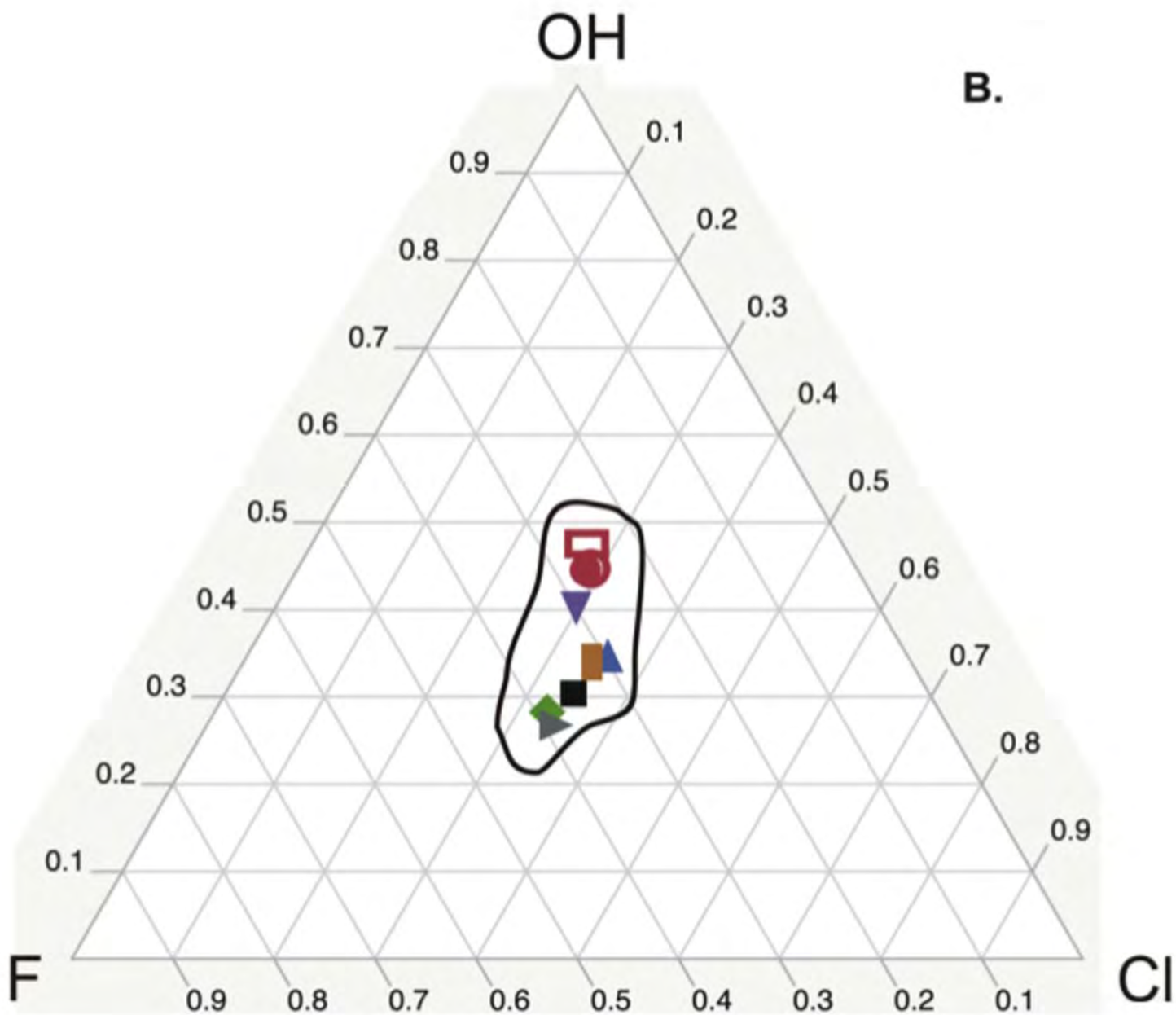

Always consult and cite the final, published document. See http:/www.minsocam.org or GeoscienceWorld

Figure 10

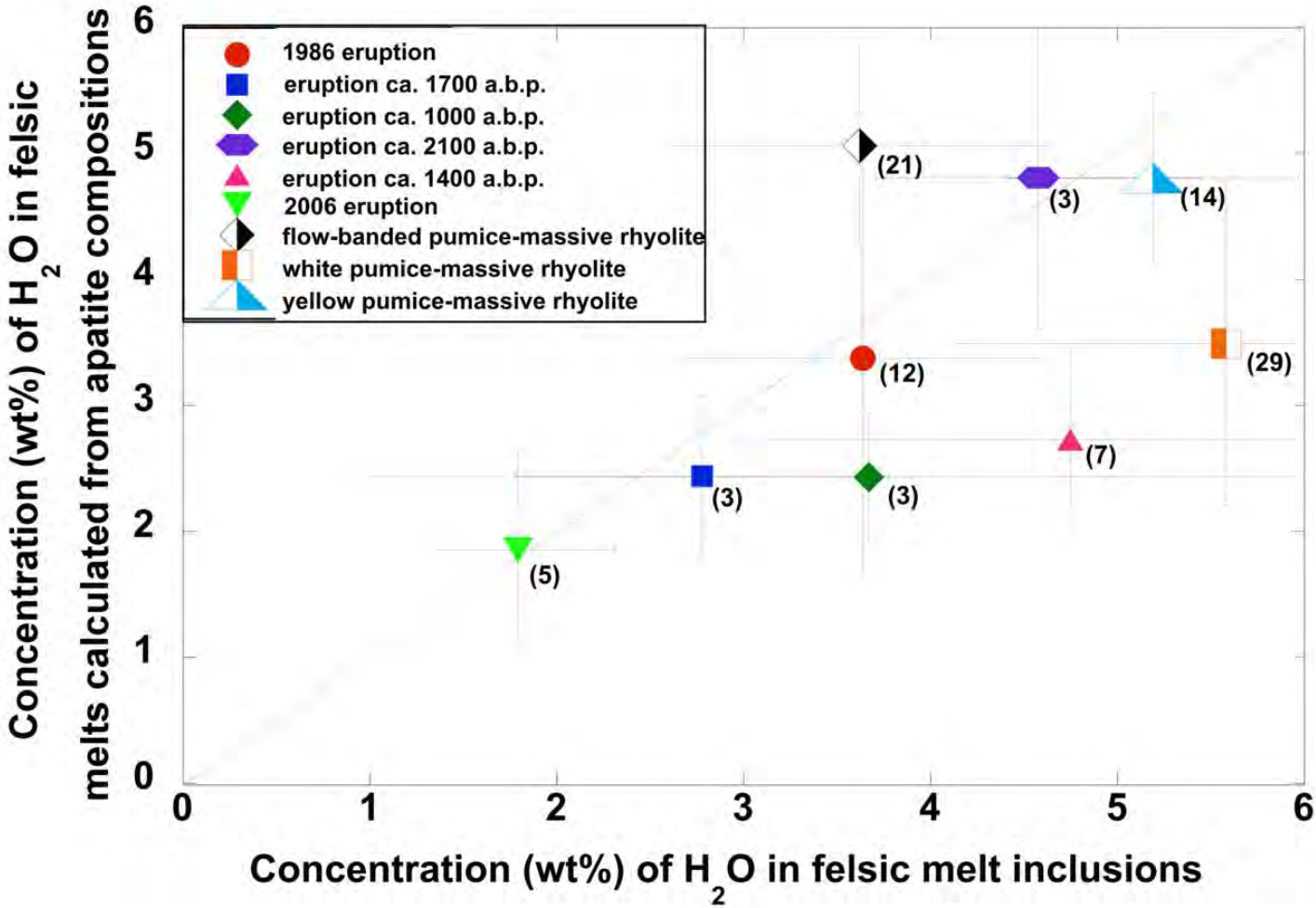
1986 eruption
eruption ca. 1700 a.b.p.
eruption ca. 1000 a.b.p.
eruption ca. 2100 a.b.p.
eruption ca. 1400 a.b.p.
2006 eruption
flow-banded pumice-massive rhyolite
white pumice-massive rhyolite
yellow pumice-massive rhyolite
(21)
(3)
(14)
(12)
(29)
(7)
(3)
(3)
(5)
0
1
2
3
4
5
6
Concentration (wt%) of H2O in felsic melts calculated from apatite compositions
Concentration (wt%) of H2O in felsic melt inclusions

Table 1

Compositions of rhyolitic starting obsidians, obsidian-apatite mixes, and natural apatite used in runs.

(wt%)	Los Posos Rhyolite (LPR)[a,b]	LPA-1 mix[c]	LPA-2 mix[d]	F-bearing rhyolite[e]	Durango apatite[f]
SiO_2	76.49	75.96	74.33	70.71	0.34
TiO_2	0.10	0.10	0.10	0.26	0.043
Al_2O_3	12.59	12.50	12.24	12.35	bd
MgO	0.06	0.06	0.06	0.17	0.01
MnO	0.06	0.06	0.06	0.04	0.01
CaO	0.31	0.68	1.83	0.77	54.02
FeO	0.88	0.87	0.85	1.01	0.06
Na_2O	4.34	4.31	4.22	3.28	0.23
K_2O	4.59	4.56	4.46	5.19	0.01
P_2O_5	0.01	0.29	1.16	0.02	40.78
SO_2	0.003	0.005	0.011	nd	0.30
BaO	0.05	0.05	0.05	0.01	0.0002
SrO	0.0005	0.001	0.002	nd	0.07
Ce_2O_3	0.011	0.015	0.026	0.02	0.52
F	0.08	0.10	0.18	0.18	3.53
Cl	0.12	0.12	0.13	0.065	0.41
Total	99.69	99.68	99.71	94.08	100.33
A/CNK[g]	0.99	0.94	0.81	0.99	nd
N/NK[h]	0.59	0.59	0.59	0.49	nd

[a]Analysis of natural Los Posos rhyolite powder by colorimetry, XRF, and INAA (Macdonald et al. 1992).
[b]Analysis of natural Los Posos rhyolite, fused to glass at elevated temperature and pressure prior to analysis by EPMA (this study).
[c]Mixture of 99.3 wt.% LPR and 0.69 wt% Durango apatite seeds.
[d]Mixture of 97.17 wt.% LPR and 2.83 wt% Durango apatite seeds.
[e]Sample TM-61a provided by Eric Christiansen and used for apatite-deficient runs.
[f]Bulk analysis by wet chemistry (Jarosewich et al. 1980); with TiO_2, BaO, and Ce_2O_3 by LA-ICPMS (Marks et al. 2012).
nd = data not determined; bd=below EPMA detection limit.
[g]Molar ($Al_2O_3/Na_2O+CaO+K_2O$).
[h]Molar (Na_2O/Na_2O+K_2O).

Table 2

Experimental run conditions, materials added to starting charges, and phases present at run conditions.

Run I.D.	T[a] (°C)	P (MPa)	Duration (hrs)	Starting silicates[b]	Added salts and solutions[c]	Stable phases at end of run[d]	Notes
1-12-05A	1000	101	286	LPA-1 + apat	NaCl:KCl + H_3PO_4 solution + $CaHPO_4$ + $Ca(OH)_2$ + DD H_2O	glass, apat, salts, aqliq, pyr	
1-12-05B	1000	101	286	LPA-1 + apat	NaCl:KCl + H_3PO_4 solution + $CaHPO_4$ + $Ca(OH)_2$ + DD H_2O	glass, apat, salts, aqliq, FeOx	
CS-14-18A	850	49	1008	LPA-1 + apat	HCl:NaCl:KCl solution + HCl solution + $CaHPO_4$ + $Ca(OH)_2$ + DD H_2O	glass, apat, salts, aqliq	
CS-14-18B	850	49	1008	LPA-1 + apat	NaCl:KCl + HCl solution + $CaHPO_4$ + $Ca(OH)_2$ +	glass, apat, salts, aqliq	
CS-14-18C	850	49	1008	LPA-1 + apat	HCl:NaCl:KCl solution + HCl solution + $CaHPO_4$ + $Ca(OH)_2$	glass, apat, salts, aqliq	
CS-14-18D	850	49	1008	LPA-1 + apat	HCl:NaCl:KCl solution + HCl solution + $CaHPO_4$ + $Ca(OH)_2$ + DD H_2O	glass, apat, salts, aqliq	
CS-15-01B[a]	702	49.5	767	LPA-1 + apat	NaCl:KCl + HCl:NaCl:KCl solution + HCl solution + $CaHPO_4$ + $Ca(OH)_2$	glass, apat, salts, aqliq, plag, qtz, FeOx	Trace glass
CS-15-02[a]	843	49.5	575	LPA-1 + apat	HCl:NaCl:KCl solution + HCl solution + $CaHPO_4$ + $Ca(OH)_2$ + DD H_2O	glass, apat, salts, aqliq, cpx	
CS-15-03[a]	844	49	844	LPA-1 + apat	HCl:NaCl:KCl solution + HCl solution + $CaHPO_4$ + $Ca(OH)_2$ + DD H_2O	glass, apat, salts, aqliq	
CS-15-04A[a]	844	49.5	579	LPA-1 + apat	NaCl:KCl + HCl:NaCl:KCl solution + HCl solution + $CaHPO_4$ + $Ca(OH)_2$ + DD H_2O	glass, apat, salts, aqliq, cpx, FeOx	
CS-15-04B[a]	844	49.5	579	LPA-1 + apat	NaCl:KCl + HCl:NaCl:KCl solution + HCl solution + $CaHPO_4$ + $Ca(OH)_2$ + DD H_2O	glass, apat, salts, aqliq, FeOx	
CS-15-04C[a]	844	49.5	579	LPA-1 + apat	NaCl:KCl + HCl:NaCl:KCl solution + HCl solution + $CaHPO_4$ + $Ca(OH)_2$	glass, apat, salts, aqliq, FeOx	
CS-15-05A[a]	862	51	858	LPA-1 + apat	HCl:NaCl:KCl solution + $CaHPO_4$ + $Ca(OH)_2$ + DD H_2O	glass, apat, salts, aqliq, qtz, FeOx	
CS-15-05B[a]	862	51	858	LPA-1 + apat	HCl:NaCl:KCl solution + HCl solution + $CaHPO_4$ + $Ca(OH)_2$ + DD H_2O	glass, apat, salts, aqliq, qtz	
CS-15-05C[a]	862	51	858	LPA-1 + apat	NaCl:KCl + HCl:NaCl:KCl solution + HCl solution + $CaHPO_4$ + $Ca(OH)_2$ + DD H_2O	glass, apat, salts, aqliq	
CS-15-05D[a]	862	51	858	LPA-1 + apat	HCl:NaCl:KCl solution + $CaHPO_4$ + $Ca(OH)_2$ + DD H_2O	glass, apat, salts, aqliq, qtz	
CS-15-06[a]	850	49.5	679	LPA-1 + apat	NaCl + HCl:NaCl:KCl solution + HCl solution + $CaHPO_4$ + $Ca(OH)_2$ + DD H_2O	glass, apat, salts, aqliq, FeOx	
CS-15-07[a]	844	49.5	795	LPA-1 + apat	NaCl + HCl:NaCl:KCl solution + HCl solution + $CaHPO_4$ + $Ca(OH)_2$	glass, apat, salts, aqliq, FeOx	
CS-15-09A[a,e]	850	49	670	LPA-1 + apat	$CaHPO_4$ + $Ca(OH)_2$ + DD H_2O	glass, apat, salts, aqliq, CaSi	Slow, non-isobaric quench
CS-15-09B[a,e]	850	49	670	LPA-1 + apat	$CaHPO_4$ + $Ca(OH)_2$ + DD H_2O	glass, apat, salts, aqliq, CaSi	Slow, non-isobaric quench
CS-15-16A[a]	853	50	936	LPA-2 + apat	$CaHPO_4$ + $Ca(OH)_2$ + DD H_2O	glass, apat, salts, aqliq, FeOx, CaSi	
1-15-14A[a]	995	50	792	LPA-2 + apat	NaCl + NaCl:KCl + HCl:NaCl:KCl solution + HCl solution + $CaHPO_4$ + $Ca(OH)_2$ + DD H_2O	glass, apat, salts, aqliq, FeOx	
1-15-14B[a]	995	50	792	LPA-2 + apat	HCl:NaCl:KCl solution + $CaHPO_4$ + $Ca(OH)_2$ + DD H_2O	glass, apat, salts, aqliq, FeOx	
CS-15-18[a]	722	49	1149	LPA-2 + apat	NaCl:KCl + HCl:NaCl:KCl solution + HCl solution + $CaHPO_4$ + $Ca(OH)_2$	glass, apat, salts, aqliq, FeOx	
1-15-10A[a]	775	203	478	LPA-2 + apat	HCl:NaCl:KCl solution + HCl solution + $CaHPO_4$ + $Ca(OH)_2$ + DD H_2O	glass, apat, salts, aqliq, cpx	
1-15-10B[a]	775	203	478	LPA-2 + apat	HCl:NaCl:KCl solution + HCl solution + $CaHPO_4$ + $Ca(OH)_2$ + DD H_2O	glass, apat, salts, aqliq, cpx	
1-15-13A[a]	748	202	603	LPA-2 + apat	HCl:NaCl:KCl solution + HCl solution + $CaHPO_4$ + $Ca(OH)_2$ + DD H_2O	glass, apat, salts, aqliq	
1-15-13B[a]	748	202	603	LPA-2 + apat	HCl:NaCl:KCl solution + HCl solution + $CaHPO_4$ + $Ca(OH)_2$ + DD H_2O	glass, apat, salts, aqliq	
CS-14-17B[f]	868	51	165	LPA-1 + apat	HCl:NaCl:KCl solution + HCl solution + $CaHPO_4$ + $Ca(OH)_2$	glass, salts, aqliq, plag, µm-sized apat	No analyzable apatite
CS-14-17C[f]	868	51	165	LPA-1 + apat	HCl:NaCl:KCl solution + HCl solution + $CaHPO_4$ + $Ca(OH)_2$ + DD H_2O	glass, salts, aqliq, cpx, µm-sized apat	No analyzable apatite
CS-14-17D[f]	868	51	165	LPA-1 + apat	NaCl:KCl + HCl solution + $CaHPO_4$ + $Ca(OH)_2$	glass, salts, aqliq, plag, µm-sized apat	No analyzable apatite
1-95-9E	930	50	624	TM-61a	NaCl:KCl + DD H_2O	glass, salts, aqliq, µm-sized apat	No analyzable apatite
1-95-9F	930	50	624	TM-61a	NaCl:KCl + DD H_2O	glass, salts, aqliq, µm-sized apat	No analyzable apatite
1-95-9B	930	50	624	TM-61a	NaCl:KCl	glass, salts, aqliq, µm-sized apat	No analyzable apatite
1-95-9D	930	50	624	TM-61a	NaCl:KCl + DD H_2O	glass, salts, aqliq, µm-sized apat	No analyzable apatite
1-95-9C	930	50	624	TM-61a	NaCl:KCl + DD H_2O	glass, salts, aqliq, µm-sized apat	No analyzable apatite
1-95-10F	901	49	288	TM-61a	NaCl:KCl + DD H_2O	glass, salts, aqliq, µm-sized apat	No analyzable apatite

Runs with "CS-" prefix were conducted in cold seal pressure vessels and runs with "1-" prefix in internally heated pressure vessel.
[a]Temperature held constant at run temperature for initial 72 hours, cycled ± 10-15°C daily afterward, and temperature held constant at run temperature for final 48-72 hours.
[b]Starting silicate glass or glass-apatite mixtures used (see Table 1 for compositions).
[c]LPA-1 mix, LPA-2 mix, apat = 1-3 µm-diameter Durango apatite seeds, DD H_2O = distilled and deionized H_2O. All solutions involved distilled and deionized H_2O.
[d]Phases in run product at conclusion of experiment: apat = apatite, plag = plagioclase, FeOx = iron (± titanium) oxides, cpx = clinopyroxene, CaSi – high-Ca aluminosilicate phase, salts = residual soluble salts, and aqliq = aqueous liquid.
[e]Run experienced slow, non-isobaric (uncontrolled) quench.
[f]Premature, slow, non isobaric quench and apatite too small to analyze

Table 3 – Compositions (in wt% and mole fraction) of melt (i.e., glass), bulk fluid, and apatite at run conditions.

Experimental Run Melt (wt%)	**1-12-05A**	**1-12-05B**	**CS-14-18A**	**CS-14-18B**	**CS-14-18C**
SiO_2	72.32 ± 1.12	72.98 ± 0.68	74.30 ± 0.32	74.00 ± 0.86	74.18 ± 0.52
TiO_2	0.11 ± 0.02	0.12 ± 0.02	0.09 ± 0.03	0.09 ± 0.03	0.12 ± 0.02
Al_2O_3	12.37 ± 0.24	12.13 ± 0.25	12.37 ± 0.08	12.35 ± 0.1	12.14 ± 0.12
MgO	0.07 ± 0.01	0.07 ± 0.01	0.05 ± 0.01	0.06 ± 0.01	0.05 ± 0.01
CaO	0.95 ± 0.24	1.03 ± 0.06	0.43 ± 0.14	0.27 ± 0.02	0.14 ± 0.02
MnO	0.04 ± 0.01	0.04 ± 0.03	0.02 ± 0.03	0.03 ± 0.02	0.02 ± 0.02
FeO	0.91 ± 0.12	0.80 ± 0.12	0.76 ± 0.14	0.47 ± 0.15	0.41 ± 0.07
Na_2O	4.18 ± 0.13	4.07 ± 0.12	4.27 ± 0.25	3.61 ± 0.14	4.25 ± 0.31
K_2O	5.72 ± 0.18	5.08 ± 0.15	4.39 ± 0.08	5.61 ± 0.14	4.41 ± 0.14
P_2O_5	0.01 ± 0.01	0.02 ± 0.01	0.01 ± 0.02	0.02 ± 0.02	0.07 ± 0.03
SO_2	0.002 ± 0.004	0.001 ± 0.002	0.001 ± 0.001	0.005 ± 0.004	0.009 ± 0.006
F	0.008 ± 0.01	0.11 ± 0.12	0.08 ± 0.01	0.15 ± 0.02	bdl
Cl	0.42 ± 0.02	0.48 ± 0.01	0.36 ± 0.01	0.31 ± 0.01	0.30 ± 0.01
Total	97.11	96.94	97.12	96.98	96.14
H_2O, FTIR	Nd	Nd	2.22	2.81	2.72
A/CNK[a]	0.84	0.86	0.99	0.99	1.01
N/NK[a]	0.53	0.55	0.60	0.49	0.59
Cl solubility in melt	0.46	0.47	0.35	0.30	0.29
Experimental Run Apatite (wt%)	**1-12-05A**	**1-12-05B**	**CS-14-18A**	**CS-14-18B**	**CS-14-18C**
SiO_2	0.51 ± 0.22	0.49 ± 0.12	0.41 ± 0.16	0.24 ± 0.18	0.45 ± 0.19
TiO_2	0.01 ± 0.01	0.01 ± 0.01	0	0.01 ± 0.01	0.01 ± 0.01
Al_2O_3	0.01 ± 0.01	0.02 ± 0.01	0.09 ± 0.08	0.03 ± 0.03	0.11 ± 0.11
MgO	0.01 ± 0.01	0.02 ± 0.01	0.03 ± 0.02	0.10 ± 0.03	0.13 ± 0.05
CaO	54.00 ± 0.38	53.60 ± 0.72	54.1 ± 0.3	54.2 ± 0.35	53.1 ± 0.54
MnO	0.03 ± 0.02	0.01 ± 0.01	0.03 ± 0.03	0.05 ± 0.03	0.07 ± 0.02
FeO	0.06 ± 0.02	0.07 ± 0.02	0.13 ± 0.07	0.09 ± 0.04	0.26 ± 0.06
Na_2O	0.15 ± 0.08	0.37 ± 0.33	0.25 ± 0.15	0.14 ± 0.12	0.44 ± 0.14
K_2O	0.05 ± 0.03	0.08 ± 0.02	0.09 ± 0.03	0.04 ± 0.06	0.09 ± 0.04
P_2O_5	40.48 ± 0.24	40.36 ± 0.35	40.24 ± 0.76	40.18 ± 0.35	39.83 ± 0.64
F	1.96 ± 0.29	1.55 ± 0.30	1.46 ± 0.37	1.49 ± 0.09	1.57 ± 0.19
Cl	1.16 ± 0.12	1.38 ± 0.25	1.81 ± 0.14	2.45 ± 0.23	2.13 ± 0.23
SO_2	0.01 ± 0.01	0.01 ± 0.01	0.19 ± 0.10	0.06 ± 0.10	0.23 ± 0.11
BaO	0.03 ± 0.03	0.03 ± 0.03	0.03 ± 0.03	0.02 ± 0.02	0.03 ± 0.03
Ce_2O_3	0.66 ± 0.09	0.43 ± 0.11	0.42 ± 0.21	0.21 ± 0.17	0.53 ± 0.08
SrO	Nd	Nd	Nd	Nd	Nd
Total	99.47	98.87	99.31	99.32	98.99
X_{Cl}^{apat}[b]	0.17	0.20	0.27	0.34	0.31
X_F^{apat}[b]	0.52	0.41	0.39	0.42	0.42
X_{OH}^{apat}[b]	0.31	0.39	0.34	0.24	0.27
Wt% Cl in fluid(s)	9.5	9.0	3.7	12.8	9.1
Exchange Coefficients					
$K_{dCl-F}^{apat-felsicmelt}$	0.012	0.21	0.29	0.74	0.33
$K_{dOH-Cl}^{apat-felsicmelt}$	0.13	0.15	0.11	0.039	0.048
$K_{dOH-F}^{apat-felsicmelt}$	0.0016	0.032	0.03	0.029	0.016
Partition Coefficients					
$D_{Cl}^{apat/mt}$	2.8	2.9	5.1	7.5	7.1
$D_{XOH}^{apat/mt}$	1.0	1.2	1.4	0.81	0.94
$D_{Cl}^{fluid(s)/mt}$	22.6	18.8	10.4	41.2	30.4
$D_{Cl}^{apat/fluid(s)}$	0.12	0.15	0.49	0.18	0.23
$D_F^{apat/mt}$	245	14.1	18.3	10.5	22.4

Table 3 continued.

Experimental Run Melt (wt%)	**CS-14-18D**	**CS-15-01B**	**CS-15-02**	**CS-15-03**	**CS-15-04A**
SiO_2	73.83 ± 0.56	Insufficient	74.5 ± 0.38	74.1 ± 0.26	74.90 ± 0.28
TiO_2	0.07 ± 0.02	Glass	0.06 ± 0.04	0.1 ± 0.04	0.09 ± 0.04
Al_2O_3	12.31 ± 0.19		12.20 ± 0.14	12.30 ± 0.14	12.20 ± 0.08
MgO	0.05 ± 0.005		0.05 ± 0.02	0.08 ± 0.02	0.08 ± 0.02
CaO	0.45 ± 0.09		0.10 ± 0.05	0.20 ± 0.08	0.08 ± 0.03
MnO	0.04 ± 0.03		0.02 ± 0.02	0.01 ± 0.01	0.01 ± 0.01
FeO	0.78 ± 0.08		0.77 ± 0.14	0.83 ± 0.14	0.75 ± 0.06
Na_2O	4.18 ± 0.12		4.63 ± 0.05	4.52 ± 0.12	4.30 ± 0.08
K_2O	4.44 ± 0.19		4.54 ± 0.15	4.60 ± 0.11	5.27 ± 0.23
P_2O_5	0.04 ± 0.03		0.02 ± 0.02	0.11 ± 0.26	0.05 ± 0.06
SO_2	0.008 ± 0.006		0.01 ± 0.01	0.01 ± 0.01	0.01 ± 0.01
F	0.16 ± 0.02		0.04 ± 0.02	0.01 ± 0.02	0.02 ± 0.02
Cl	0.31 ± 0.01		0.24 ± 0.01	0.29 ± 0.01	0.28 ± 0.01
Total	96.65		97.18	97.15	98.04
H_2O, FTIR	2.82		2.54	2.82	2.51
A/CNK[a]	0.98		0.96	0.96	0.94
N/NK[a]	0.59		0.61	0.60	0.55
Cl solubility in melt	0.36		0.33	0.34	0.32
Experimental Run Apatite (wt%)	**CS-14-18D**	**CS-15-01B**	**CS-15-02**	**CS-15-03**	**CS-15-04A**
SiO_2	0.46 ± 0.27	0.38 ± 0.16	0.26 ± 0.13	0.32 ± 0.25	0.21 ± 0.04
TiO_2	0.01 ± 0.01	0.01 ± 0.01	0.01 ± 0.01	0.01 ± 0.01	0.01 ± 0.01
Al_2O_3	0.04 ± 0.05	0.04 ± 0.06	0.01 ± 0.01	0.03 ± 0.05	0.01 ± 0.01
MgO	0.06 ± 0.03	0.04 ± 0.05	0.28 ± 0.05	0.21 ± 0.10	0.24 ± 0.09
CaO	53.7 ± 0.61	54.80 ± 0.25	54.41 ± 0.97	54.50 ± 1.86	53.66 ± 1.21
MnO	0.06 ± 0.07	0.01 ± 0.02	0.05 ± 0.05	0.28 ± 0.12	0.16 ± 0.17
FeO	0.12 ± 0.07	0.21 ± 0.30	0.19 ± 0.01	0.38 ± 0.22	0.24 ± 0.13
Na_2O	0.28 ± 0.17	0.29 ± 0.12	0.35 ± 0.08	0.40 ± 0.28	0.42 ± 0.16
K_2O	0.13 ± 0.13	0.14 ± 0.06	0.14 ± 0.03	0.09 ± 0.01	0.11 ± 0.02
P_2O_5	40.02 ± 0.48	40.52 ± 0.25	40.64 ± 0.57	39.83 ± 1.57	40.55 ± 0.38
F	1.93 ± 0.35	2.38 ± 0.23	1.40 ± 0.29	1.41 ± 0.29	0.58 ± 0.18
Cl	1.51 ± 0.35	1.52 ± 0.58	2.03 ± 0.56	1.76 ± 0.25	3.19 ± 0.41
SO_2	0.22 ± 0.12	0.19 ± 0.15	0.09 ± 0.11	0.03 ± 0.05	0.01 ± 0.01
BaO	0.01 ± 0.03	0.02 ± 0.03	0.01 ± 0.01	0.03 ± 0.03	0.02 ± 0.03
Ce_2O_3	0.37 ± 0.27	0.12 ± 0.16	0.30 ± 0.23	0.08 ± 0.12	0.42 ± 0.25
SrO	Nd	Nd	Nd	Nd	Nd
Total	99.30	100.93	100.74	99.36	99.75
X_{Cl}^{apat}[b]	0.22	0.22	0.30	0.26	0.47
X_F^{apat}[b]	0.51	0.63	0.37	0.38	0.15
X_{OH}^{apat}[b]	0.27	0.15	0.33	0.36	0.38
Wt% Cl in fluid(s)	2.3	14.4	1.1	0.97	15.8
Exchange Coefficients					
$K_{dCl\text{-}F}^{apat\text{-}felsicmelt}$	0.42	Nd	0.25	0.044	0.40
$K_{dOH\text{-}Cl}^{apat\text{-}felsicmelt}$	0.07	Nd	0.053	0.074	0.045
$K_{dOH\text{-}F}^{apat\text{-}felsicmelt}$	0.03	Nd	0.013	0.0033	0.018
Partition Coefficients					
$D_{Cl}^{apat/mt}$	4.9	Nd	8.5	6.1	11.4
$D_{XOH}^{apat/mt}$	0.89	Nd	1.2	1.2	1.4
$D_{Cl}^{fluid(s)/mt}$	7.5	Nd	4.8	3.3	56.4
$D_{Cl}^{apat\ /fluid(s)}$	0.65	0.11	1.8	1.8	0.20
$D_F^{apat/mt}$	12.1	Nd	35	141	29

Table 3 continued.

Experimental Run	**CS-15-04B**	**CS-15-04C**	**CS-15-05A**	**CS-15-05B**	**CS-15-05C**
Melt (wt%)					
SiO_2	74.3 ± 0.38	75.20 ± 0.53	74.63 ± 0.29	75.04 ± 0.11	74.77 ± 0.15
TiO_2	0.08 ± 0.05	0.07 ± 0.03	0.09 ± 0.03	0.10 ± 0.02	0.06 ± 0.02
Al_2O_3	12.20 ± 0.23	11.80 ± 0.19	12.06 ± 0.09	12.22 ± 0.13	11.98 ± 0.09
MgO	0.04 ± 0.02	0.04 ± 0.01	0.05 ± 0.01	0.06 ± 0.02	0.05 ± 0.01
CaO	0.03 ± 0.01	0.07 ± 0.06	0.28 ± 0.15	0.28 ± 0.08	0.09 ± 0.02
MnO	0.02 ± 0.02	0.02 ± 0.01	0.02 ± 0.02	Bdl	0.02 ± 0.01
FeO	0.45 ± 0.20	0.21 ± 0.08	0.76 ± 0.05	0.75 ± 0.15	0.75 ± 0.11
Na_2O	3.71 ± 0.43	3.45 ± 0.16	4.16 ± 0.21	4.48 ± 0.07	4.13 ± 0.26
K_2O	5.97 ± 0.48	5.75 ± 0.17	4.52 ± 0.08	4.57 ± 0.10	4.99 ± 0.05
P_2O_5	0.16 ± 0.02	0.11 ± 0.03	0.04 ± 0.02	0.04 ± 0.02	0.05 ± 0.03
SO_2	0.01 ± 0.02	0.01 ± 0.01	0.009 ± 0.004	0.008 ± 0.007	0.008 ± 0.005
F	0.01 ± 0.01	0.05 ± 0.03	0.13 ± 0.04	0.07 ± 0.03	0.05 ± 0.01
Cl	0.24 ± 0.02	0.24 ± 0.02	0.19 ± 0.02	0.17 ± 0.01	0.29 ± 0.01
Total	97.28	97.21	96.95	97.78	97.22
H_2O, FTIR	2.58	2.62	3.11	2.99	2.82
A/CNK[a]	0.97	0.95	0.99	0.95	0.97
N/NK[a]	0.49	0.48	0.58	0.60	0.56
Cl solubility in melt	0.27	0.27	0.34	0.35	0.30
Apatite (wt%)					
Experimental Run	**CS-15-04B**	**CS-15-04C**	**CS-15-05A**	**CS-15-05B**	**CS-15-05C**
SiO_2	0.15 ± 0.09	0.27 ± 0.18	0.51 ± 0.15	0.36 ± 0.06	0.42 ± 0.07
TiO_2	0.01 ± 0.01	0.01 ± 0.01	0.01 ± 0.01	0.01 ± 0.01	0.002 ± 0.003
Al_2O_3	0.03 ± 0.03	0.02 ± 0.01	0.03 ± 0.02	0.003 ± 0.003	0.02 ± 0.03
MgO	0.38 ± 0.04	0.34 ± 0.05	0.05 ± 0.01	0.05 ± 0.03	0.15 ± 0.07
CaO	53.82 ± 0.79	52.70 ± 0.79	53.53 ± 0.47	53.48 ± 0.35	52.28 ± 0.99
MnO	0.06 ± 0.02	0.18 ± 0.02	0.05 ± 0.01	0.03 ± 0.02	0.10 ± 0.08
FeO	0.21 ± 0.05	1.20 ± 0.23	0.19 ± 0.16	0.12 ± 0.06	0.21 ± 0.09
Na_2O	0.59 ± 0.04	0.74 ± 0.24	0.23 ± 0.07	0.21 ± 0.03	0.43 ± 0.25
K_2O	0.11 ± 0.05	0.09 ± 0.04	0.13 ± 0.03	0.08 ± 0.01	0.12 ± 0.05
P_2O_5	41.55 ± 0.41	41.02 ± 0.79	39.29 ± 0.37	40.20 ± 0.27	39.89 ± 1.01
F	0.40 ± 0.07	0.32 ± 0.05	1.82 ± 0.18	1.89 ± 0.15	1.03 ± 0.20
Cl	3.70 ± 0.48	3.82 ± 0.33	1.32 ± 0.28	1.39 ± 0.17	2.48 ± 0.40
SO_2	0.01 ± 0.01	0.01 ± 0.01	0.29 ± 0.10	0.30 ± 0.04	0.13 ± 0.11
BaO	0.01 ± 0.01	0.02 ± 0.04	0.02 ± 0.03	0.02 ± 0.03	0.01 ± 0.01
Ce_2O_3	0.02 ± 0.02	0.11 ± 0.14	0.53 ± 0.06	0.51 ± 0.06	0.64 ± 0.18
SrO	Nd	Nd	0.05 ± 0.04	0.03 ± 0.02	0.05 ± 0.02
Total	101.20	101.73	97.69	98.55	98.00
X_{Cl}^{apat}[b]	0.54	0.56	0.19	0.20	0.36
X_F^{apat}[b]	0.11	0.08	0.48	0.50	0.27
Apparent X_{OH}^{apat}[b]	0.36	0.36	0.32	0.30	0.36
Wt% Cl in fluid(s)	30.1	39.2	0.7	0.3	8.7
Exchange Coefficients					
$K_{dCl-F}^{apat-felsicmelt}$	0.40	2.6	0.51	0.31	0.40
$K_{dOH-Cl}^{apat-felsicmelt}$	0.03	0.029	0.051	0.042	0.052
$K_{dOH-F}^{apat-felsicmelt}$	0.012	0.077	0.026	0.013	0.021
Partition Coefficients					
$D_{Cl}^{apat/mt}$	15.4	15.9	6.9	8.1	8.5
$D_{XOH}^{apat/mt}$	1.3	1.3	1.0	0.95	1.2
$D_{Cl}^{fluid(s)/mt}$	125	163	3.7	1.7	30
$D_{Cl}^{apat/fluid(s)}$	0.12	0.097	1.9	4.8	0.28
$D_F^{apat/mt}$	40	6.3	14	27	22

Table 3 continued.

Experimental Run Melt (wt%)	**CS-15-05D**	**CS-15-06**	**CS-15-07**	**CS-15-09A**	**CS-15-09B**
SiO_2	75.11 ± 0.26	74.96 ± 0.67	74.75 ± 0.40	74.55 ± 0.66	74.38 ± 0.43
TiO_2	0.06 ± 0.03	0.08 ± 0.03	0.07 ± 0.03	0.02 ± 0.01	0.05 ± 0.03
Al_2O_3	12.06 ± 0.15	12.17 ± 0.17	12.15 ± 0.12	11.91 ± 0.15	12.06 ± 0.10
MgO	0.05 ± 0.01	0.04 ± 0.02	0.05 ± 0.01	0.06 ± 0.01	0.05 ± 0.01
CaO	0.10 ± 0.03	0.04 ± 0.04	0.16 ± 0.05	0.62 ± 0.04	0.35 ± 0.06
MnO	0.01 ± 0.01	0.01 ± 0.01	0.01 ± 0.02	0.02 ± 0.02	0.01 ± 0.02
FeO	0.82 ± 0.08	0.30 ± 0.07	0.43 ± 0.12	0.79 ± 0.09	0.80 ± 0.07
Na_2O	4.35 ± 0.13	5.25 ± 0.13	5.17 ± 0.15	3.56 ± 0.27	4.05 ± 0.16
K_2O	4.45 ± 0.07	3.78 ± 0.07	3.71 ± 0.02	4.67 ± 0.04	4.97 ± 0.12
P_2O_5	0.03 ± 0.03	0.26 ± 0.08	0.03 ± 0.03	0.02 ± 0.01	0.03 ± 0.03
SO_2	0.003 ± 0.004	0.006 ± 0.01	0.01 ± 0.01	0.009 ± 0.007	0.005 ± 0.006
F	0.06 ± 0.03	0.11 ± 0.02	0.09 ± 0.02	0.03 ± 0.04	0.04 ± 0.02
Cl	0.10 ± 0.01	0.30 ± 0.02	0.31 ± 0.01	0.04 ± 0.01	0.03 ± 0.01
Total	97.21	97.31	96.92	96.33	96.86
H_2O, FTIR	2.44	2.74	2.62	3.7	3.2
A/CNK[a]	0.99	0.95	0.95	0.99	0.95
N/NK[a]	0.60	0.68	0.68	0.54	0.55
Cl solubility in melt	0.32	0.32	0.33	0.35	0.34
Experimental Run Apatite (wt%)	**CS-15-05D**	**CS-15-06**	**CS-15-07**	**CS-15-09A**	**CS-15-09B**
SiO_2	0.42 ± 0.05	0.29 ± 0.11	0.47 ± 0.27	0.80 ± 0.23	0.84 ± 0.13
TiO_2	0.01 ± 0.01	0.004 ± 0.003	0.003 ± 0.006	0.01 ± 0.01	0.01 ± 0.01
Al_2O_3	0.01 ± 0.01	0.01 ± 0.01	0.03 ± 0.04	0.19 ± 0.04	0.001 ± 0.001
MgO	0.08 ± 0.06	0.30 ± 0.06	0.12 ± 0.03	0.03 ± 0.02	0.10 ± 0.05
CaO	53.19 ± 0.59	52.03 ± 0.69	53.27 ± 0.39	54.96 ± 0.88	55.86 ± 0.17
MnO	0.07 ± 0.06	0.13 ± 0.04	0.02 ± 0.01	0.01 ± 0.01	0.02 ± 0.02
FeO	0.22 ± 0.17	0.27 ± 0.04	0.08 ± 0.02	0.12 ± 0.06	0.03 ± 0.03
Na_2O	0.26 ± 0.06	0.55 ± 0.10	0.31 ± 0.05	0.02 ± 0.02	0.02 ± 0.02
K_2O	0.10 ± 0.03	0.08 ± 0.01	0.09 ± 0.05	0.003 ± 0.004	0.01 ± 0.01
P_2O_5	40.14 ± 0.65	40.60 ± 0.41	40.17 ± 0.81	38.78 ± 1.50	39.40 ± 0.01
F	1.80 ± 0.50	0.66 ± 0.12	1.62 ± 0.04	1.06 ± 0.26	0.89 ± 0.13
Cl	1.31 ± 0.30	3.60 ± 0.09	2.04 ± 0.11	0.14 ± 0.03	0.40 ± 0.07
SO_2	0.28 ± 0.04	0.06 ± 0.08	0.23 ± 0.12	0.37 ± 0.06	0.05 ± 0.02
BaO	0.01 ± 0.02	0.01 ± 0.01	0.06 ± 0.05	0.03 ± 0.03	0.01 ± 0.01
Ce_2O_3	0.49 ± 0.05	0.56 ± 0.13	0.49 ± 0.07	0.39 ± 0.27	0.02 ± 0.03
SrO	0.05 ± 0.03	0.04 ± 0.02	0.03 ± 0.02	0.03 ± 0.03	0.02 ± 0.01
Total	98.33	99.09	98.91	96.74	97.66
X_{Cl}^{apat}[b]	0.19	0.53	0.30	0.02	0.06
X_F^{apat}[b]	0.48	0.18	0.43	0.28	0.24
Apparent X_{OH}^{apat}[b]	0.33	0.29	0.27	0.70	0.70
Wt% Cl in fluid(s)	0.6	28.4	9.2	1.4	4.3
Exchange Coefficients					
$K_{dCl\text{-}F}^{apat\text{-}felsicmelt}$	0.47	2.07	0.38	0.11	0.63
$K_{dOH\text{-}Cl}^{apat\text{-}felsicmelt}$	0.033	0.031	0.054	0.22	0.076
$K_{dOH\text{-}F}^{apat\text{-}felsicmelt}$	0.016	0.064	0.02	0.025	0.048
Partition Coefficients					
$D_{Cl}^{apat/mt}$	13.8	12.0	6.6	3.9	13.6
$D_{XOH}^{apat/mt}$	1.2	1.03	0.96	2.4	2.7
$D_{Cl}^{fluid(s)/mt}$	6.5	95.2	29.9	38	145
$D_{Cl}^{apat/fluid(s)}$	2.1	0.13	0.22	0.1	0.09
$D_F^{apat/mt}$	30	6	18	35.3	22.2

Table 3 continued.

Experimental Run Melt (wt%)	**CS-15-16A**	**1-15-14A**	**1-15-14B**	**CS-15-18**	**1-15-10A[c]**
SiO_2	74.81 ± 0.13	74.06 ± 0.83	75.33 ± 0.33	73.7 ± 0.23	71.68 ± 0.12
TiO_2	0.04 ± 0.04	0.06 ± 0.03	0.06 ± 0.05	0.07 ± 0.01	0.07 ± 0.02
Al_2O_3	12.36 ± 0.08	12.40 ± 0.15	12.57 ± 0.08	12.22 ± 0.27	11.72 ± 0.07
MgO	0.05 ± 0.01	0.06 ± 0.01	0.05 ± 0.01	0.06 ± 0.01	0.03 ± 0.01
CaO	0.70 ± 0.12	0.48 ± 0.11	0.54 ± 0.03	0.23 ± 0.15	2.07 ± 0.04
MnO	0.03 ± 0.03	0.04 ± 0.02	0.04 ± 0.02	0.03 ± 0.01	0.02 ± 0.02
FeO	0.99 ± 0.14	1.02 ± 0.02	1.02 ± 0.13	0.7 ± 0.05	0.64 ± 0.09
Na_2O	3.89 ± 0.09	4.47 ± 0.37	3.86 ± 0.14	4.68 ± 0.22	3.63 ± 0.10
K_2O	4.66 ± 0.05	4.34 ± 0.18	4.42 ± 0.08	5.35 ± 0.14	3.38 ± 0.04
P_2O_5	0.03 ± 0.03	0.10 ± 0.03	0.17 ± 0.03	0.06 ± 0.07	0.08 ± 0.06
SO_2	0.004 ± 0.002	0.003 ± 0.005	0.004 ± 0.002	0.005 ± 0.004	0.003 ± 0.004
F	0.19 ± 0.07	0.06 ± 0.04	0.05 ± 0.07	0.05 ± 0.04	0.10 ± 0.02
Cl	0.11 ± 0.01	0.42 ± 0.01	0.09 ± 0.01	0.36 ± 0.01	0.32 ± 0.01
Total	97.86	97.50	98.20	97.46	93.74
H_2O, FTIR	2.9	2.35	2.3	2.54	5.76
A/CNK[a]	0.97	0.96	1.04	0.88	0.87
N/NK[a]	0.56	0.61	0.57	0.57	0.62
Cl solubility in melt	0.40	0.39	0.37	0.35	0.62
Experimental Run Apatite (wt%)	**CS-15-16A**	**1-15-14A**	**1-15-14B**	**CS-15-18**	**1-15-10A[c]**
SiO_2	1.02 ± 0.31	0.26 ± 0.14	0.18 ± 0.02	0.16 ± 0.07	1.53 ± 0.16
TiO_2	0.01 ± 0.01	0.003 ± 0.005	0.01 ± 0.01	0.003 ± 0.007	0.01 ± 0.005
Al_2O_3	0.05 ± 0.03	0.003 ± 0.01	0.12 ± 0.1	0.003 ± 0.004	0.27 ± 0.10
MgO	0.12 ± 0.01	0.13 ± 0.01	0.18 ± 0.02	0.13 ± 0.03	0.09 ± 0.06
CaO	53.67 ± 0.79	54.33 ± 0.73	54.72 ± 1.3	54.33 ± 0.30	53.40 ± 0.36
MnO	0.01 ± 0.02	0.03 ± 0.03	0.22 ± 0.03	0.03 ± 0.03	0.03 ± 0.02
FeO	0.19 ± 0.15	0.13 ± 0.03	0.39 ± 0.07	0.13 ± 0.04	0.26 ± 0.06
Na_2O	0.07 ± 0.04	0.18 ± 0.08	0.11 ± 0.05	0.18 ± 0.04	0.20 ± 0.06
K_2O	0.03 ± 0.02	0.09 ± 0.03	0.05 ± 0.02	0.09 ± 0.03	0.13 ± 0.03
P_2O_5	40.21 ± 0.77	41.10 ± 0.40	40.48 ± 1.12	41.10 ± 0.25	39.80 ± 0.61
F	2.21 ± 0.11	1.90 ± 0.06	1.74 ± 0.15	1.90 ± 0.07	2.00 ± 0.09
Cl	0.64 ± 0.09	1.72 ± 0.09	1.24 ± 0.04	1.72 ± 0.15	0.86 ± 0.27
SO_2	0.07 ± 0.10	0.006 ± 0.01	0.001 ± 0.01	0.006 ± 0.004	0.03 ± 0.004
BaO	0.01 ± 0.01	0.01 ± 0.01	0.02 ± 0.03	0.01 ± 0.02	0.01 ± 0.03
Ce_2O_3	0.02 ± 0.02	0.26 ± 0.23	0.03 ± 0.07	0.26 ± 0.08	0.05 ± 0.03
SrO	0.04 ± 0.02	0.03 ± 0.02	0.05 ± 0.02	0.03 ± 0.02	0.02 ± 0.01
Total	98.29	100.00	99.36	99.99	98.29
X_{Cl}^{apat}[b]	0.09	0.25	0.18	0.25	0.13
X_F^{apat}[b]	0.59	0.51	0.46	0.51	0.53
Apparent X_{OH}^{apat}[b]	0.32	0.24	0.36	0.24	0.34
Wt% Cl in fluid(s)	0.62	4.2	0.40	34.2	7.6
Exchange Coefficients					
$K_{dCl-F}^{apat-felsicmelt}$	0.50	0.14	0.39	0.13	0.14
$K_{dOH-Cl}^{apat-felsicmelt}$	0.067	0.086	0.038	0.098	0.074
$K_{dOH-F}^{apat-felsicmelt}$	0.034	0.012	0.015	0.013	0.010
Partition Coefficientsß					
$D_{Cl}^{apat/mt}$	5.7	4.1	13.9	4.8	2.8
$D_{XOH}^{apat/mt}$	1.0	0.9	1.4	1.2	0.7
$D_{Cl}^{fluid(s)/mt}$	5.5	10.0	4.0	96.2	17.8
$D_{Cl}^{apat/fluid(s)}$	1.04	0.41	3.4	0.05	0.09
$D_F^{apat/mt}$	11.6	30.7	36.4	38	20

Table 3 continued.

Experimental Run Melt (wt%)	**1-15-10B**	**1-15-13A**	**1-15-13B**	**CS-14-17B[c]**	**CS-14-17C[c]**
SiO_2	71.89 ± 0.18	73.32 ± 0.68	73.87 ± 0.30	74.01 ± 0.92	73.25 ± 0.68
TiO_2	0.08 ± 0.01	0.08 ± 0.04	0.08 ± 0.05	0.08 ± 0.04	0.07 ± 0.01
Al_2O_3	11.70 ± 0.02	12.29 ± 0.17	12.25 ± 0.21	11.90 ± 0.36	11.60 ± 0.23
MgO	0.04 ± 0.01	0.06 ± 0.01	0.09 ± 0.01	0.06 ± 0.01	0.02 ± 0.01
CaO	1.17 ± 0.05	0.29 ± 0.03	0.45 ± 0.11	0.32 ± 0.03	0.02 ± 0.02
MnO	0.04 ± 0.01	0.01 ± 0.01	0.01 ± 0.01	0.02 ± 0.02	0.02 ± 0.03
FeO	0.77 ± 0.06	0.39 ± 0.06	0.70 ± 0.11	0.52 ± 0.03	0.70 ± 0.06
Na_2O	3.78 ± 0.02	3.34 ± 0.18	3.56 ± 0.05	4.32 ± 0.16	4.01 ± 0.30
K_2O	3.91 ± 0.06	4.00 ± 0.06	4.01 ± 0.03	4.33 ± 0.10	4.88 ± 0.07
P_2O_5	0.005 ± 0.006	0.11 ± 0.10	0.09 ± 0.08	0.02 ± 0.03	0.35 ± 0.04
SO_2	bdl	0.004 ± 0.01	0.002 ± 0.001	0.002 ± 0.004	0.005 ± 0.006
F	0.18 ± 0.02	0.19 ± 0.07	0.16 ± 0.04	0.02 ± 0.04	0.03 ± 0.01
Cl	0.23 ± 0.01	0.14 ± 0.01	0.18 ± 0.01	0.31 ± 0.01	0.21 ± 0.02
Total	93.79	94.23	95.45	95.91	95.15
H_2O, FTIR	5.85	5.59	5.52	Nd	Nd
A/CNK[a]	0.93	1.19	1.11	0.99	0.97
N/NK[a]	0.60	0.56	0.57	0.59	0.55
Cl solubility in melt	0.51	0.34	0.40	0.32	0.29
Experimental Run Apatite (wt%)	**1-15-10B**	**1-15-13A**	**1-15-13B**	**CS-14-17B[c]**	**CS-14-17C[c]**
SiO_2		0.20 ± 0.20	0.12 ± 0.01		
TiO_2		0.01 ± 0.01	bdl		
Al_2O_3		0.01 ± 0.01	0.02 ± 0.03		
MgO		0.50 ± 0.26	0.14 ± 0.02		
CaO		52.60 ± 1.06	53.30 ± 0.36		
MnO		0.23 ± 0.08	0.25 ± 0.04		
FeO		1.1 ± 0.48	0.81 ± 0.10		
Na_2O		0.14 ± 0.05	0.14 ± 0.07		
K_2O		0.04 ± 0.04	0.04 ± 0.01		
P_2O_5		40.80 ± 0.30	41.50 ± 0.20		
F		0.89 ± 0.05	0.76 ± 0.04		
Cl		2.38 ± 0.22	2.09 ± 0.15		
SO_2		0.01 ± 0.01	0.01 ± 0.01		
BaO		0.01 ± 0.01	0.02 ± 0.02		
Ce_2O_3		0.04 ± 0.04	0.07 ± 0.02		
SrO		0.10 ± 0.03	0.06 ± 0.02		
Total		99.01	99.27		
X_{Cl}^{apat}[b]		0.35	0.31		
X_F^{apat}[b]		0.24	0.20		
Apparent X_{OH}^{apat}[b]		0.41	0.49		
Wt% Cl in fluid(s)	4.0	5.7	4.2	9.5	2.8
Exchange Coefficients					
$K_{dCl-F}^{apat-felsicmelt}$	Nd	3.77	2.6	Nd	Nd
$K_{dOH-Cl}^{apat-felsicmelt}$	Nd	0.015	0.026	Nd	Nd
$K_{dOH-F}^{apat-felsicmelt}$	Nd	0.058	0.067	Nd	Nd
Partition Coefficients					
$D_{Cl}^{apat/mt}$	Nd	16.7	11.9	Nd	Nd
$D_{XOH}^{apat/mt}$	Nd	0.89	1.1	Nd	Nd
$D_{Cl}^{fluid(s)/mt}$	17.8	39.9	23.9	31.1	13.7
$D_{Cl}^{apat/fluid(s)}$	Nd	0.42	0.50	Nd	Nd
$D_F^{apat/mt}$	Nd	4.6	4.8	Nd	Nd

Table 3 continued.

Experimental Run Melt (wt%)	**CS-14-17D[c]**	**1-95-9E[d]**	**1-95-9F[d]**	**1-95-9B[d]**	**1-95-9D[d]**
SiO_2	74.57 ± 0.16	74.59	72.34	75.23	73.2
TiO_2	0.12 ± 0.02	0.22	0.24	0.31	0.25
Al_2O_3	11.94 ± 0.22	12.49	12.3	12.74	12.24
MgO	0.04 ± 0.02	0.14	0.15	0.13	0.14
CaO	0.15 ± 0.11	0.71	0.33	0.62	0.32
MnO	0.03 ± 0.02	0.05	0.03	0.08	0.02
FeO	0.34 ± 0.08	1.1	0.81	0.97	0.81
Na_2O	3.45 ± 0.18	3.53	3.33	3.27	3.44
K_2O	5.74 ± 0.09	5.32	7.63	5.24	6.89
P_2O_5	0.09 ± 0.02	0.02	0.01	0.01	0.01
SO_2	0.005 ± 0.009	Nd	Nd	Nd	Nd
F	0.03 ± 0.02	0.13	0.14	0.08	0.10
Cl	0.25 ± 0.01	0.33 ± 0.02	0.32 ± 0.04	0.02 ± 0.01	0.35 ± 0.01
Total	96.75	98.63	97.63	98.72	97.76
H_2O, FTIR	Nd	Nd	Nd	Nd	Nd
A/CNK[a]	0.98	0.97	0.86	1.05	0.89
N/NK[a]	0.48	0.50	0.40	0.49	0.43
Cl solubility in melt	0.27	0.36	0.41	0.36	0.38
Experimental Run Apatite (wt%)	**CS-14-17D[c]**	**1-95-9E[d]**	**1-95-9F[d]**	**1-95-9B[d]**	**1-95-9D[d]**
SiO_2		No apatite	No apatite	No apatite	No apatite
TiO_2					
Al_2O_3					
MgO					
CaO					
MnO					
FeO					
Na_2O					
K_2O					
P_2O_5					
F					
Cl					
SO_2					
BaO					
Ce_2O_3					
SrO					
Total					
X_{Cl}^{apat}[b]	Nd				
X_F^{apat}[b]	Nd				
Apparent X_{OH}^{apat}[b]	Nd				
Wt% Cl in fluid(s)	18.3	45	6	16	0.5
Partition Coefficient					
$D_{Cl}^{fluid(s)/mt}$	74.6	138.5	18.2	49.8	25

Table 3 continued.

Experimental Run Melt (wt%)	**1-95-9C[d]**	**1-95-10F[d]**
SiO_2	73.2	72.63
TiO_2	0.25	0.22
Al_2O_3	12.24	12.11
MgO	0.13	0.14
CaO	0.32	0.66
MnO	0.02	0.03
FeO	0.81	1.01
Na_2O	3.44	3.45
K_2O	6.89	5.54
P_2O_5	0.01	0.01
SO_2	Nd	Nd
F	0.10	0.18
Cl	0.35± 0.03	0.37 ± 0.01
Total	97.76	96.35
H_2O, FTIR	Nd	Nd
A/CNK[a]	0.89	0.94
N/NK[a]	0.43	0.49
Cl solubility in melt	0.35	0.40
Experimental Run Apatite (wt%)	**1-95-9C[d]**	**1-95-10F[d]**
SiO_2	No apatite	No apatite
TiO_2		
Al_2O_3		
MgO		
CaO		
MnO		
FeO		
Na_2O		
K_2O		
P_2O_5		
F		
Cl		
SO_2		
BaO		
Ce_2O_3		
SrO		
Total		
X_{Cl}^{apat}[b]		
X_F^{apat}[b]		
Apparent X_{OH}^{apat}[b]		
Wt% Cl in fluid(s)	36	27
Partition Coefficient		
$D_{Cl}^{fluid(s)/mt}$	103	73

Note: Runs with "CS-" prefix were conducted in cold seal vessels and runs with "1-" prefix involved internally heated pressure vessel. D_{XOH} = partition coefficient for OH ion on molar basis; all other partition coefficients D_i calculated on a wt% basis. Exchange coefficients defined in text. Reported errors are 1 sigma deviations.
Nd = data not determined; bdl = below detection limit.
[a]Molar ratios of ($Al_2O_3/Na_2O+CaO+K_2O$) and (Na_2O/Na_2O+K_2O) of melt.
[b]Mole fractions of volatile components in apatite determined via Piccoli and Candela (2002) (apparent X_{OH}^{apat} computed by difference).
[c]Apatite grains too small for accurate EMPA.
[d]Low-phosphorus, apatite-deficient runs.

Table 4.
Average compositions of Augustine volcano, Alaska, apatites.

Apatite Constituent (wt%)	**Yellow Pleistocene rhyolite** [a] (15)[b]	**White Pleistocene rhyolite** (25)	**Flow-banded Pleistocene rhyolite** (49)	**2100 a.b.p.**[c] (16)	**1700 a.b.p.** (9)	**1400 a.b.p.** (11)	**1000 a.b.p.** (4)	**1986** (2)	**2016 sample JW004** (6)
SiO_2	0.13±0.03	0.15±0.10	0.18±0.10	0.18±0.08	0.18±0.12	0.09±0.05	0.11±0.09	0.19±0.11	0.28±0.11
TiO_2	0.01±0.02	0.01±0.01	0.01±0.01	0.01±0.02	0.01±0.02	0.01±0.02	0.03±0.02	0.002±0.003	0.07±0.09
Al_2O_3	0	0.006±0.02	0.002±0.009	0.001±0.002	0.01±0.01	0.01±0.02	0.02±0.05	0.04±0.05	0.005±0.008
MgO	0.23±0.01	0.22±0.01	0.22±0.01	0.22±0.08	0.20±0.04	0.21±0.02	0.27±0.06	0.20±0.01	0.24±0.02
CaO	53.71±0.33	53.78±0.71	53.99±0.51	53.22±0.84	53.36±0.78	53.79±0.74	53.12±0.29	51.92±0.51	53.17±0.69
MnO	0.39±0.02	0.38±0.03	0.36±0.06	0.17±0.04	0.16±0.05	0.16±0.07	0.15±0.06	0.14±0.02	0.12±0.02
FeO	0.50±0.08	0.52±0.09	0.52±0.13	0.99±0.27	0.68±0.26	0.62±0.23	1.19±0.35	0.76±0.65	0.98±0.40
Na_2O	0.14±0.06	0.13±0.05	0.16±0.17	0.16±0.05	0.16±0.05	0.10±0.06	0.15±0.03	0.19±0.08	0.18±0.04
P_2O_5	41.14±0.31	40.98±0.75	41.20±0.33	40.41±0.52	40.19±0.62	40.74±0.28	40.43±1.0	39.53±0.53	40.15±0.34
F	1.01±0.15	0.99±0.16	0.96±0.16	1.12±0.17	1.11±0.14	1.19±0.30	1.32±0.09	1.46±0.03	1.42±0.17
Cl	1.94±0.09	1.98±0.10	1.87±0.20	2.03±0.38	2.44±0.22	2.34±0.17	2.34±0.22	2.24±0.08	2.18±0.09
SO_2	0.22±0.05	0.25±0.18	0.23±0.08	0.20±0.10	0.27±0.10	0.20±0.05	0.27±0.05	0.35±0.19	0.27±0.11
TOTAL	99.43	99.41	99.70	98.71	98.77	99.46	99.40	97.02	100.91
[d]X_{Cl}^{apat}	0.28±0.01	0.29±0.01	0.27±0.03	0.30±0.06	0.35±0.03	0.34±0.02	0.34±0.03	0.33±0.03	0.32±0.01
[d]X_{F}^{apat}	0.27±0.04	0.26±0.04	0.25±0.04	0.30±0.08	0.30±0.04	0.32±0.08	0.35±0.02	0.39±0.02	0.38±0.05
[d]X_{OH}^{apat}	0.45±0.05	0.45±0.05	0.47±0.07	0.40±0.08	0.35±0.4	0.34±0.08	0.31±0.03	0.28±0.03	0.32±0.06
(Si/Mg)[e]	0.38	0.46	0.55	0.56	0.6	0.31	0.32	0.67	0.77

[a]Age (a.b.p. = approximate years before present) or year of eruption.
[b]Number of analyzed apatites (n).
[c]a.b.p. = approximate years since eruption.
[d]X_i^{apat} calculated with method of Piccoli and Candela (2002).
[e]Per formula unit cation ratio of Si to Mg.